MIMO and Relay Systems Based on Multi-Amplitude Minimum Shift Keying

A thesis submitted in partial fulfilment

of the requirements for the degree of

Master of Engineering

in

Electrical and Computer Engineering

at the

UNIVERSITY OF CANTERBURY

Christchurch, New Zealand

By

Sarhad Basharati, B.E. (Hons)

Tuesday, 15 October 2013

ii

Abstract

This thesis describes the use of a multi-amplitude minimum shift keying (MAMSK) signal in various types of wireless communication system. A MAMSK signal is a bandwidth efficient modulation scheme obtained by superimposing M minimum shift keying (MSK) signals with unequal amplitudes. The overall phase of a MAMSK signal is controlled by the phase of the largest component MSK signal which allows the use of a low-complexity differential detector. A closed form expression for the average bit error rate (BER) for coherent detection of an MAMSK in AWGN is derived and is shown to achieve the same BER as that of square constellation quadrature amplitude modulation (QAM) with the same average transmit power.

We describe the design and implementation of a STBC-based MIMO radio system in conjunction with MAMSK modulation. The proposed system provides high capacity data transmission by carrying information not only in the phases but also in the amplitude. Despite using a simple MAMSK differential receiver the system achieves performance within 1 dB of coherent detection. The existing MSK modems in conjunction with STBC could easily be modified to construct the proposed system.

The MAMSK modulation scheme is extended to a multiuser relaying network where two nodes cooperate in a half-duplex environment to achieve diversity gain. The cooperative scheme is based on superposition modulation using a decode-and-forward (DF) strategy. In the proposed scheme, each node simultaneously transmits its own and the relayed signals by superimposing one on the other. A MAMSK signal is an excellent choice for this type of cooperative communication due its being obtained by a

superposition technique. The proposed system exploits the overall phase of a MAMSK signal which allows differential detection and as a result it provides the lowest decoding complexity and memory requirements among the existing superposition based cooperation schemes. The performance of the system is evaluated by simulation, where it is shown that the MAMSK cooperative system outperforms a conventional DF scheme in terms of both power and bandwidth efficiency.

Acknowledgements

I would like to thank my supervisor Professor Desmond Taylor for his valuable advice and guidance throughout this research. I am very fortunate to have him as my supervisor; obviously, this thesis would not have been possible without his thoughtful reviews, comments and suggestions. Also, I would like to thank Des for allowing me to switch to part-time study.

I would also like to thank Associate Professor Philippa Martin for her occasional reviews of my documents and kind guidance during my study.

Thank you also to my current and past colleagues in the Comms Lab at University of Canterbury for their friendly conversations and discussions.

Many thanks to my parents, family and friends for their love and for the confidence that they had in me during all these years. My special thanks go to my wife Hafsa and my little son Kamyar for their kindness, encouragements, sacrifices and patience.

The University of Canterbury   *Sarhad Basharati*

April 2013

Contents

List of Figures

Chapter 1

Introduction

In recent years, the use of wireless and mobile technologies has become increasingly important to both individuals and organisations. This is because of lower costs, better mobility, increasing availability and elimination of wires. However, demand for the available shared radio frequency spectrum continues to grow. The increasing congestion in the spectrum has inspired research to find more efficient signalling techniques using the same bandwidth.

Multi-amplitude minimum shift keying (MAMSK) is a bandwidth efficient modulation [1, 2] scheme that doubles the data rate of conventional minimum shift keying (MSK). Superimposing two MSK signals with different amplitudes provides the same throughput as 16-level quadrature amplitude modulation (16-QAM) but with the advantage of having continuous phase and sharper spectral sidelobe roll-off. Despite slightly wider main spectral lobe, MAMSK provides an efficient alternative to the currently used QAM formats.

Furthermore, significant improvement in spectral efficiency achieved by deploying multiple antennas at both ends of the communication link [3, 4]. Specifically, these works show that the achievable spectral efficiency increases linearly with increasing numbers of antennas. Space-time block

codes (STBCs) use both spatial and temporal diversity and are used in systems with multiple transmit and receive antennas. In [5] it has been shown that multiple input multiple output (MIMO) systems with STBCs can improve the performance of the communication link without consuming more bandwidth and/or power. The thesis concentrates on the design and implementation of an Alamouti STBC [6] in conjunction with a MAMSK modulation scheme. This is with the intention of combining the benefits of MAMSK signals and wireless MIMO systems to achieve high data rate wireless links. The idea is then further developed to include cooperative communications through the use of virtual MIMO systems.

The rest of the chapter is organised as follows. In the next section, we provide a short overview of a communication system utilising single antennas at both ends of the link. The mathematical modelling and characterisation of the communication channels are discussed, focusing on two different types of channels: the additive white Gaussian noise (AWGN) channel and the Rayleigh flat fading channel. We then move on to more advanced systems, which are equipped with multiple transmit and receive antennas or which form a virtual MIMO system through relaying nodes. The chapter concludes with a description of the thesis contributions and an outline of the thesis.

1.1 Overview of Digital Communication systems

The fundamental components of any digital wireless communication system [7, 8] are the modulator, channel, demodulator, amplifiers and antennas as illustrated in Figure 1-1. The simplest of all configurations is the point-to-point link [9]. It consists of two connected nodes and in its most basic form, contains a single antenna at each end of the link.

The information to be transmitted can be from either an analogue or a digital source. In a digital communication system, the source messages are converted into a stream of discrete (usually binary) numbers [7]. Digital

modulation schemes translate the sequence of binary digits into signal waveforms that are appropriate for transmission. In general, wireless communication is a passband transmission and up-conversion to a higher frequency band is required [8]. The primary purpose of the up-convertor is to shift the intermediate frequency (IF) or baseband signal to a higher frequency sinusoidal carrier signal. At the transmitter, the last stage of the operation is to amplify the radio frequency (RF) signal and transmit it from the antenna.
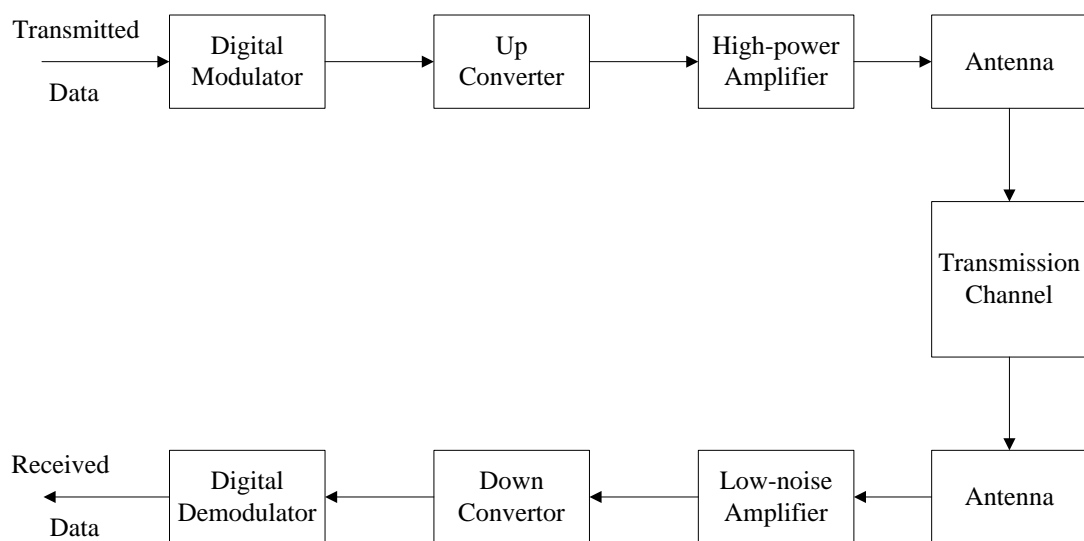
Figure 1-1 Basic model of a digital communication system

The channel is the only element of the model that is independent of the other communication subsystems [10]. Channel attributes, such as fading and dispersion play a significant part in designing digital transmission schemes [8]. The transmitted RF signal propagates though the channel in multiple directions over different paths. These signals suffer different attenuations and path delays [8, 11]. In consequence, the received signal is the superposition of multiple versions of the transmitted signal which arrive at the receiver's antenna at slightly different times [11-13]. The resulting multipath fading may cause intersymbol interference, amplitude fluctuations and phase variations of the received signal. All of these factors degrade system reliability and performance [11, 12, 14].

At the receiving end of a digital communication system, ideally the reverse signal processing happens. The first step is to amplify the received weak signal to a much higher level [8, 9]. The amplified RF signal is then down-converted to baseband for further processing. As a final step, the digital demodulator block processes the channel corrupted received signal in order to reconstruct the original transmitted data sequence with as few errors as possible.

1.2   Communication Channels

Channel characteristics play an important role in studying, selecting, and designing transmission schemes. The design and performance analysis of systems is usually based on a statistical model of the channel rather than a specific physical channel. The most common form of signal degradation is additive noise, which is generated at the front end of the receiver [7-10, 13]. Another form of signal degradation is multipath fading, which is a result of propagation effects such as reflection, refraction and scattering [8, 11, 12, 14]. Such signal distortion is characterised as a non-additive signal disturbance. Both additive and non-additive signal distortions are usually characterised as random phenomena and described in statistical terms. In this section, we discuss two important channel models, the AWGN channel and the Rayleigh flat fading channel.

1.2.1 Additive White Gaussian Noise Channel

The AWGN channel as shown in Figure 1-2 is the simplest model for a communication channel [7].
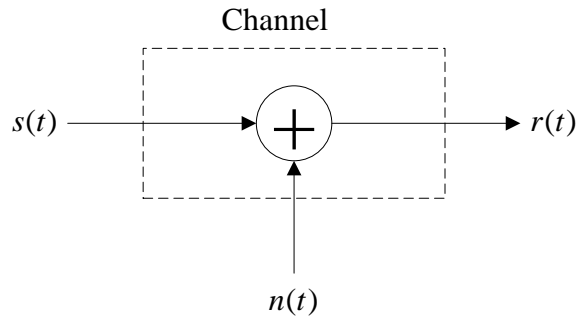
Figure 1-2 A model of AWGN channel

Under this model, the transmitted signal, $s(t)$ is corrupted only by additive white Gaussian noise, $n(t)$. This implies that fading does not exist and the modulated signals propagate without any amplitude loss and/or phase distortion. Therefore, the received signal, $r(t)$ is simplified to the form,

$$r(t) = s(t) + n(t), \qquad (1.1)$$

where $n(t)$ is the white noise, represented as a zero mean, stationary Gaussian random process with a constant power spectral density [8, 15, 16].

1.2.2 Frequency-Flat Fading Channel

Flat or frequency non-selective fading is the term used when the signal bandwidth, B_s is much smaller than the channel coherence bandwidth, B_c. The later is the bandwidth over which the channel transfer function remains virtually constant. If a wireless channel has a constant gain and linear phase response, then all frequencies of the transmitted signal will experience the same fading [8, 12]. In a flat fading channel, the strength of the received signal changes with time, due to the variation of the gain of the channel

caused by multipath. On the other hand, the spectral characteristics of the transmitted signal are preserved at the receiver.

Typically, signals that undergo non-selective fading are narrowband where each channel is modelled by a complex Gaussian random variable with mean zero. Based on the central limit theorem the envelope of the random Gaussian channel will follow the statistical characteristics of a Rayleigh distribution [17]. Rayleigh fading is a useful model in situations where there is no line of sight (LOS) path between transmitter and receiver. There are several methods [18-21] available to generate the Rayleigh fading process for simulation purposes. The well known Jakes' model [18] based on summing sinusoids is widely used to realise Rayleigh fading characteristics. Figure 1-3 illustrates the mathematical representation of a flat fading channel with a single multiplicative channel coefficient [7, 8].
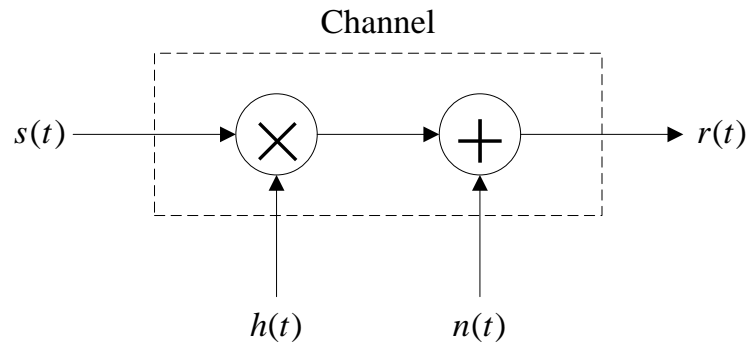
Figure 1-3   Flat fading channel with additive noise

Based on this model, the received baseband signal, $r(t)$ over a Rayleigh flat fading channel can be represented as [14, 15, 22],

$$r(t) = h(t)\, s(t) + \, n(t), \tag{1.2}$$

where $h(t)$ is a zero-mean complex Gaussian random process which is assumed to be constant during one symbol duration and to change from symbol to symbol, $s(t)$ is the transmitted signal and $n(t)$ is additive white Gaussian noise.

In addition to multipath effects and thermal noise the received signal can experience another phenomenon, known as a Doppler shift in frequency [23]. The change in frequency of the multipath waves is due to the relative motion between the transmitter and the receiver. Furthermore, a time-varying Doppler shift on different multipath components is observed if the surrounding objects are in motion. The effect of such time variations can be neglected if the surrounding objects move at a much lower speed than the mobile receiver.

In [11, 23], the magnitude of the Doppler shift in frequency defined in terms of the speed of the mobile is given by,

$$f_d = \frac{f_c\, v}{c}\, \cos\theta \qquad\qquad (1.3)$$

Where, f_c is the carrier frequency, v is the mobile speed, c is the speed of light and θ is the arrival angle of the received signal with respect to the direction of the receiver's motion. The rate of fading in a Rayleigh channel is often characterised by the value of the normalised Doppler frequency, $f_d T$, where f_d represents the maximum Doppler shift arising from the motion of the mobile and $1/T$ is the symbol rate. For a slow fading channel the value of $f_d T$ is considered to be ≤ 0.00001, whereas a value of 0.01 indicates a very fast fading channel [24].

Figure 1-4 illustrates simulated Rayleigh flat fading with a normalised Doppler frequency of $f_d T = 0.001$. Flat fading channels often experience deep fades of more than $20\,\text{dB}$ as shown in Figure 1-4. The occasional deep fade can cause severe error propagation in wireless communication systems. In a slow fading environment, the fading process has a strong correlation, which means long bursts of errors. Conversely, for a fast fading channel, the fading process has a weak correlation. Throughout this thesis, we shall assume a quasi-static Rayleigh flat fading channel, where the channel coefficients are constant during each transmission block and vary independently from one block to another. Such channels are classified in [5] as slow fading.
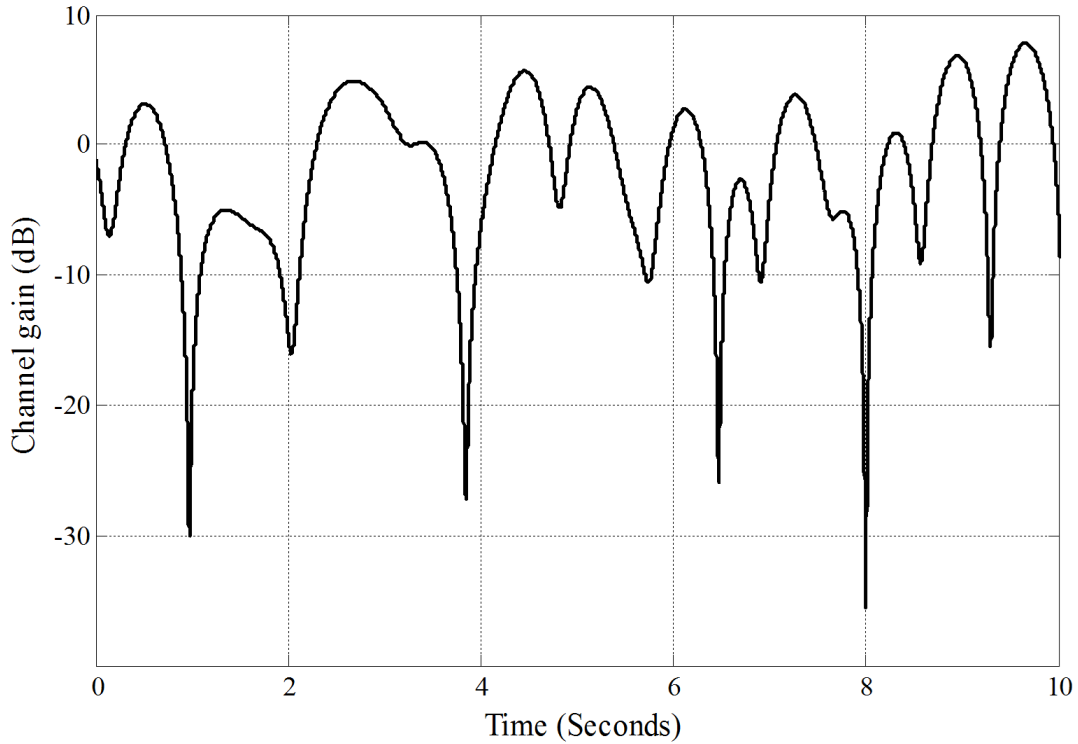
Figure 1-4 Rayleigh fading channel with a normalised Doppler frequency of 0.001

1.3 Multi-Input Multi-Output Systems

A typical single user MIMO system equipped with M transmit antennas and N receive antennas is illustrated in Figure 1-5. MIMO systems [25, 26] have been employed to counter the effects of random fading and to achieve diversity gain. In most MIMO systems, multiple antennas are used to transmit and to receive several versions of the same signal over independent fading paths in order to increase the possibility that at least one of the received signals is not subject to deep fading. These independent paths are combined in some way such that the fading of the resultant signal is reduced [11] and hence the quality, data rate and capacity of the system [3, 12, 27] are improved.
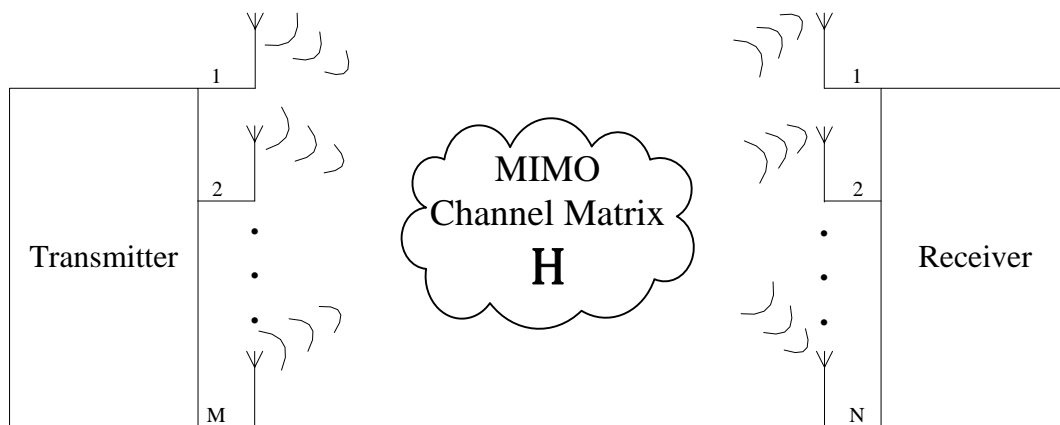
Figure 1-5   Block Diagram of a MIMO communication link

MIMO systems can be realised using various schemes such as space-time block codes (STBCs), space-time trellis codes (STTCs) and the Vertical Bell Laboratories Layered Space-Time (V-BLAST) architecture. In general, STBCs can be classified into two categories: Orthogonal STBCs (OSTBCs) and non-orthogonal STBCs (NOSTBCs). The advantage of OSTBCs is that the system can achieve maximum diversity gain with simple linear processing at the receiver. Their shortcoming is that they do not provide full rate, as the number of transmit antennas is increased. NOSTBCs offer an effective way to increase the data rate but at the cost of greater decoding complexity.

In a space-time block coded MIMO system the channel is required to remain essentially constant over the duration of a STBC code word. STBCs are used to exploit diversity by generating and combining multiple versions of the same signal and mapping the transmitted symbols into a structured matrix code.

Another possible approach to overcome the effect of multipath fading is to group multiple single antenna systems to create a virtual MIMO (VMIMO) system [28, 29]. This technique is often known as cooperative communication [30]. The idea of cooperation is attractive in wireless networks where nodes are constrained in size and power. Cooperative diversity as shown in Figure 1-6 can be realised with either a single relay or

9

multiple relays where each relaying node acts as a virtual antenna and cooperatively transmits data to a destination. The model, in its most basic form, consists of a single source, destination and relay node. This fundamental concept known as the relay channel, was first proposed by Meulen in [31] and later analysed in [32].
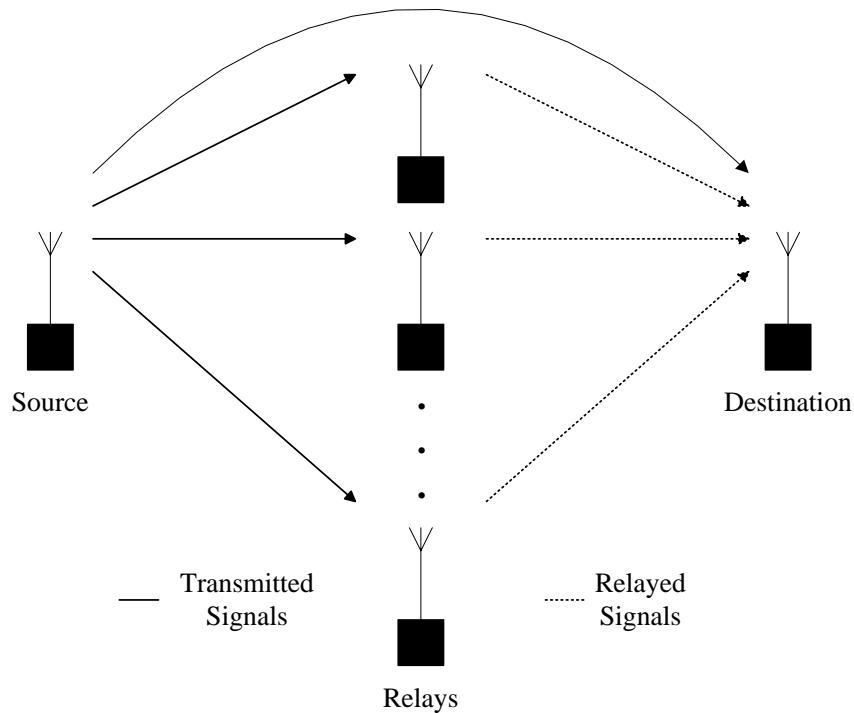
Figure 1-6 Model of cooperative communications with multiple relay nodes

There are several cooperation strategies available for the relaying network shown in Figure 1-6. Two of the most significant schemes [33-35] are amplify-and-forward (AF) and decode-and-forward (DF). In AF cooperative diversity each relay node simply amplifies and forwards the received signal towards the destination. On the other hand, in a DF scheme, cooperative nodes decode the received signal, re-encode it, and then retransmit it to the destination.

The above two cooperation strategies can outperform each other depending on the channel condition of the source-relay link and the relaying capabilities [36-38]. For example, the AF scheme is preferable in situations where the received signal power is weak (low SNR) at the relaying node

[39]. Moreover, the AF relaying strategy is of low complexity and the relay terminal does not require channel state information (CSI), however, it suffers from noise amplification. The advantage of DF over AF is more significant [40] if the source-relay channel quality is high. This is because the source-relay link noise effect is eliminated at the relay terminal and not forwarded to the destination. The major weaknesses associated with the DF strategy are high complexity and error propagation, due to incorrect decoding at the relay node [41].

In general, the transmission protocol for both cooperative strategies requires two phases. In phase one, the source broadcasts its information to the relay nodes and the destination (solid lines in Figure 1-6). In the second phase, the relays process the received signal according to the cooperative strategy employed before forwarding it to the destination node (dotted lines in Figure 1-6). Finally, the destination receives multiple copies of the source's signal with different magnitudes and phases. There are different methods available to combine signals received from multiple diversity branches. The optimal combining scheme maximises the overall signal to noise ratio and is known as maximum ratio combining [9, 11, 14].

1.4 Literature Review

The idea of MAMSK modulation scheme can be traced back four decades, to when Simon [1] demonstrated that an offset quadrature amplitude shift keying (QASK) signal with half-cycle sinusoidal symbol shaping can be represented as an n-component version of a minimum shift keying (MSK) signal. The spectral advantage of such signals over conventional offset QASK with rectangular pulses follows directly from the advantage of MSK over offset quadrature phase shift keying (QPSK). The result showed that a signal set obtained by summing two MSK signals with 6 dB difference in power is spectrally equivalent to an offset QASK signal set composed of 16 signals. Two years later, in a laboratory environment Weber et al. [2] constructed a physical bandwidth compressive modem making use of

MAMSK signals. The entire system operated at 1 Mbits/s and achieved a measured bit error rate (BER) performance within 0.5 dB of the theoretical value for an AWGN channel.

The effect of imperfect phase synchronisation on the coherent detection of MAMSK signals is analysed in [42], where it is shown that MAMSK schemes are less sensitive to imperfect carrier recovery than the corresponding quadrature amplitude modulation (QAM) schemes. The work of [7] pointed out that the phase change in a MAMSK modulated signal is determined by the phase of the MSK component with the larger amplitude. The work of [43] has exploited this property and proposed a differential MAMSK receiver based on the regeneration of the larger MSK signal component. The proposed receiver structure is relatively simple, does not require carrier phase recovery and requires an additional 1 dB of received signal power to achieve the BER performance of coherent detection. In [44], it has been shown that a MAMSK signal can outperform a QAM modulated signal when used with orthogonal frequency division multiplexing (OFDM) due to its low peak to average power ratio (PAR).

Transmit diversity in conjunction with continuous phase modulation (CPM) has attracted the attention of researchers [45-49]. To overcome the effect of multipath fading, an early transmit diversity scheme employing MSK signals with two-bit differential detection was proposed by Ogose et al. [46]. The proposed system provides an improvement in BER performance over a fading channel but at the cost of increased bandwidth. More recently, the work of [49] employed simple delay diversity to present a space-time coded scheme using MSK. The performance of iterative non-coherent decoding in a fast fading channel for a serial concatenated MSK modulated STBC is simulated and analysed in [50]. In a quasi-static fading channel, 4-state and 8-state STTC schemes with MSK have been presented in [51] for two transmit and N receive antennas. The proposed space-time MSK codes provide full rate, full diversity, high coding gain and are based on a technique similar to the [52, 53] super orthogonal STTCs. An MSK signal sampled at the symbol rate with a two transmit antenna STBC based

on the Alamouti STBC is investigated in [54]. The scheme takes advantage of the block-wise differential encoding and guarantees a diversity order of two.

To date, the majority of research on space-time coded signals is based on linear modulations such as QAM and QPSK. Moreover, there is a few papers (for example [47, 55-59]) on space-time coding that make use of CPM signals. Most of the STC-CPM schemes proposed in the literature employ coherent demodulation that requires expensive and complex receivers. In [58, 60-63] simplified and non-coherent detectors have been developed. The reduced complexity receiver [60] requires the number of receive antennas to be greater than or equal to the number of transmit antennas. In fact, as far as we are aware, there has been no research done on space-time coding with MAMSK or multi-amplitude CPM (MACPM) signals. The focus of this thesis is on design and implementation of STBCs in conjunction with a MAMSK modulation scheme (STBC-MAMSK).

1.5 Thesis Contributions and Outline

The electromagnetic radio spectrum is a natural resource, finite, very valuable and demand for spectrum appears virtually limitless. One approach to mitigating demand is the use of bandwidth efficient modulation schemes such as MSK. A MAMSK modulation scheme is a superposition of multi level (M) MSK signals and thus its spectral efficiency is M times that of an MSK signal [2, 44]. Furthermore, a MAMSK signal envelope never reaches zero [44] because the constituent signals have unequal but constant amplitude. This enables MAMSK modulated signals to utilize low cost and power efficient amplifiers operating in their nonlinear regions [64] with only a small signal distortion. Of course, this is under the assumption that we generate and amplify each MSK component signal independently prior to summation [42, 65].

MAMSK modulation provides a remarkable number of benefits such as continuous phase, bandwidth efficient and sharper spectral sidelobe roll-off and there has not been much work done to explore all the properties of the MAMSK signals. The first contribution of the thesis is to reveal new characteristics of MAMSK modulation schemes and to analytically prove some simulation results that have been claimed by others [2, 7, 43]. A novel approach to analytically evaluate the bit error probability for coherent detection of a M-level MAMSK (M-MAMSK) transmission through an AWGN is presented. The performance of the differential receiver proposed in [43] is simulated in MATLAB and compared to that of coherent detection.

Recent wireless applications demand higher data rates, greater system capacity and low bit error rate. These strict requirements pose a great challenge to wireless system designers. The work of [3, 5] confirmed that a MIMO system can increase system capacity in proportion to the number of transmit and receive antennas employed. Combining MIMO systems with bandwidth efficient modulation schemes as an application of spatial diversity can transmit more data over the same allocated spectrum. The second contribution of the thesis is to design and develop STBC-based MIMO radio systems in conjunction with a 2-MAMSK modulation scheme to achieve high capacity data transmission and to improve bit error performance.

Extending what we have discussed in the previous section, cooperative communication has been shown to provide the network with higher throughput, reduced energy requirements and extended coverage [32, 35, 66, 67]. The final contribution of the thesis is to merge the benefits of MAMSK signals and virtual MIMO systems in a relaying wireless network with two users that communicate data packets to a common destination. Cooperative transmit diversity based on superposition modulation [68] is considered with the MAMSK signal. Furthermore, we focus on the DF relay strategy in a half-duplex environment.

The rest of the thesis is organised in the following manner. Chapter 2 presents some relevant modulation schemes and their properties. The MAMSK modulator and the performance of the differential detector in an AWGN channel are described. The optimum maximum likelihood detector is described as well as some important performance measures in wireless communication systems. The chapter ends with a brief review of STBCs that have been developed for frequency-flat fading channels, in particular, the Alamouti scheme. The primary objective of this chapter is to provide the reader with all the necessary terminology and background materials that are used throughout the thesis. In chapter 3, we present characteristics of MAMSK signals, including a closed form expression for the minimum squared Euclidean distance of a M-level MAMSK signal, power spectral density of MAMSK, analysis of its phase tree and trellis, MAMSK signal trajectory and explicitly showing that the larger MSK signal is dominant in determining the overall phase of a MAMSK signal. Chapter 4 describes the design and implementation of an orthogonal STBC in conjunction with a 2-MAMSK modulated signal. In chapter 5, a multiuser cooperation system based on superposition modulation utilizing DF transmission strategy is presented. The thesis is concluded in Chapter 6, with a summary of the main results and a list of suggestions for further research.

Chapter 2

Background

2.1 Basic Modulation Schemes

Modulation schemes use a sequence of digital symbols to vary parameters such as amplitude, phase or frequency of a high frequency sinusoidal carrier signal. The choice of modulation is crucial to the design of wireless communication systems. Each type has its own advantages and disadvantages depending on many factors such as system complexity, available power and bandwidth resources. In general, all digital modulation schemes may be classified into two main categories: constant envelope and non-constant envelope.

There are three major schemes of carrier modulation as shown in Figure 2-1. One scheme conveys the information in carrier amplitude variations and is known as amplitude shift keying (ASK). The other two carry the information in carrier phase or frequency variations and are known as phase shift keying (PSK) and frequency shift keying (FSK), respectively. Using these basic ideas as a foundation, a variety of modulation schemes can be derived from their combinations. As an example, QPSK is generated by combining two binary PSK (BPSK) signals with orthogonal carriers. More advanced digital modulation schemes include MSK, CPM, QAM, MAMSK and so forth.
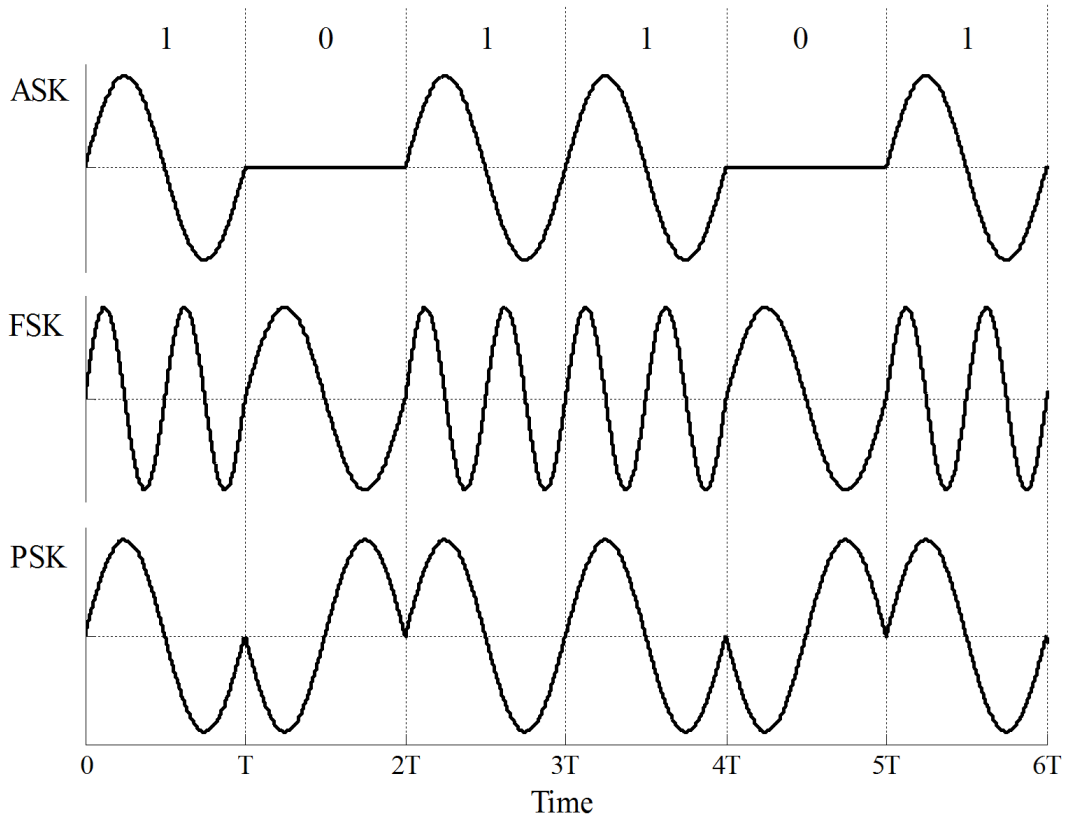
Figure 2-1　Basic binary carrier modulation schemes

In many digital transmitters, it is desirable to operate power amplifiers at or near saturation to achieve maximum power efficiency. Signals with constant envelope and continuous phase are well suited to this type of wireless application. Multilevel amplitude modulation techniques such as M-ary QAM (M-QAM) offer higher transmission rates for a given signal bandwidth. The penalty paid for this improvement is the requirement to use less efficient and more expensive linear amplifiers. In the next sections, we briefly review some modulation schemes which are relevant to the thesis. For more detailed information on modulation schemes and their characteristics, see references [7, 8, 11].

2.2　Quaternary Phase Shift Keying

In QPSK, the input binary data stream is split into in-phase (I) and quadrature (Q) components. These are then independently modulated onto

two orthogonal basis functions. The bit rate in either the I or the Q channel is equal to one-half of the input data rate. As a result, phase changes over intervals of $2T_b$, where T_b is the duration of each bit. Accordingly, a maximum phase transition of $\pm\pi$ radians can occur, such phase transitions causes the signal envelope to go to zero momentarily. The nonlinear behaviour of power amplifiers can distort such signals, which leads to undesirable spectral regrowth.

QPSK is a special case of M-ary PSK (M-PSK) with $M = 4$, and we can define its signal set for $i = 1, 2, 3, 4$ as

$$s_i(t) = \sqrt{\frac{2E}{T}} \cos\left(2\pi f_c t + (2i - 1)\frac{\pi}{4}\right), \qquad 0 \le t \le T \qquad (2.1)$$

here, E is the signal energy per symbol interval, T is the duration of a symbol and f_c is the signal carrier frequency. From this it can be seen that the phase of the carrier takes on one of four equally spaced values from the set $\left\{\pi/4, \, 3\pi/4, \, 5\pi/4, \, 7\pi/4\right\}$, where each value from the set corresponds to a unique pair of information bits. Normally, the carrier frequency is chosen as an integer multiple of the symbol rate, as $f_c = k/T$, where k is an integer.

Equation (2.1) equivalently can be written as

$$s_i(t) = \sqrt{E} \, \cos\left((2i - 1)\frac{\pi}{4}\right) \phi_1(t) + \sqrt{E} \, \sin\left((2i - 1)\frac{\pi}{4}\right) \phi_2(t) \qquad (2.2)$$

where, $\phi_1(t)$ and $\phi_2(t)$ are orthonormal basis functions, defined over the interval $0 \le t \le T$ as

$$\phi_1(t) = \sqrt{\frac{2}{T}} \, \cos 2\pi f_c t \qquad (2.3)$$

$$\phi_2(t) = -\sqrt{\frac{2}{T}} \sin 2\pi f_c t \qquad (2.4)$$

The message signals with respect to the coordinate axes, $\phi_1(t)$ and $\phi_2(t)$ can be expressed as a two-dimensional vector given by,

$$\mathbf{s}_i = \left(\sqrt{E}\ \cos\left[(2i-1)\frac{\pi}{4}\right],\ \sqrt{E}\ \sin\left[(2i-1)\frac{\pi}{4}\right]\right), \qquad i = 1,2,3,4 \qquad (2.5)$$

In this representation, a QPSK signal can be depicted using a two-dimensional signal space diagram with four points as shown in Figure 2-2. It should be noted that different QPSK signal sets can be obtained by simply rotating the constellation points [69].
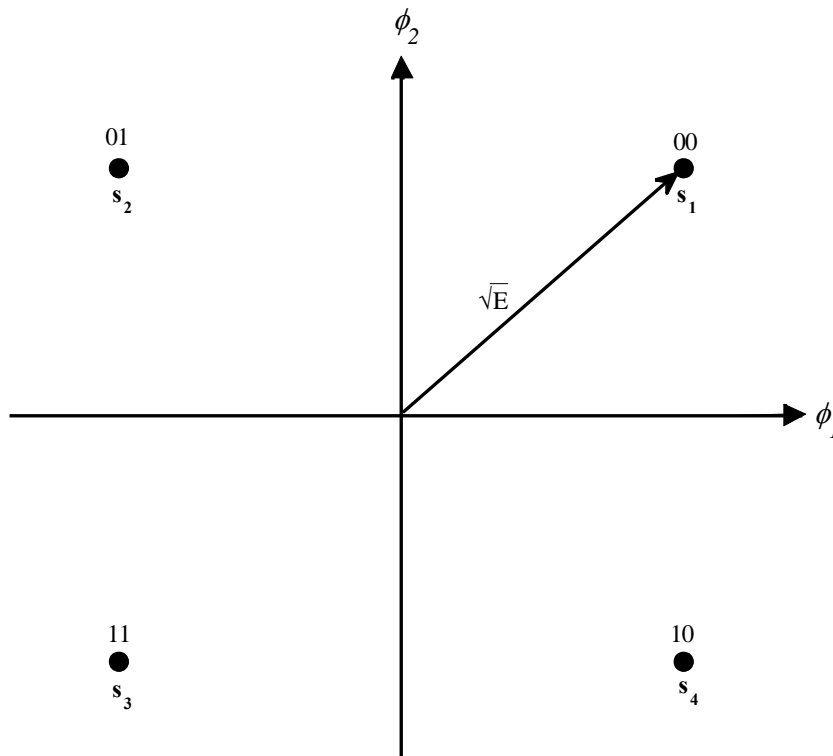
Figure 2-2 QPSK signal constellation with Gray coding

Offset QPSK (OQPSK) is a modified form of QPSK, where the I and Q channels are offset from each other by half a symbol period, so at any transition, only one of them changes, and therefore the maximum phase

transition allowed is $\pm\pi/2$ radians. This modification to QPSK prevents the signal envelope from passing through the origin which makes it less susceptible to distortion in nonlinear amplifiers.

2.3   Minimum Shift Keying

Minimum shift keying [70] is a continuous phase modulation scheme with constant envelope signal and excellent spectral roll-off characteristics [71-73]. It can be derived from offset QPSK [71, 74] by shaping the pulses with half sinusoidal waveforms, or can be derived as a special case of continuous phase frequency shift keying (CPFSK) [75, 76]. In this section, we review both methods of obtaining MSK signals.

2.3.1   Generating MSK Signals From OQPSK

In the OQPSK modulation scheme, the staggered data streams of the I and Q channels are directly modulated onto two orthogonal carriers. To obtain an MSK signal, each I or Q bit is weighted with a half cycle cosine pulse shaping function, $A\cos\left(\frac{\pi t}{2T}\right)$. The outcome is then modulated onto one of the two orthogonal carriers, $\sin(2\pi f_c t)$ and $\cos(2\pi f_c t)$. MSK signals can mathematically be expressed as [8, 71]

$$s(t) = \sqrt{\frac{2E}{T}}\left(a_I(t)\cos\left(\frac{\pi t}{2T}\right)\cos 2\pi f_c t + a_Q(t)\sin\left(\frac{\pi t}{2T}\right)\sin 2\pi f_c t\right), \quad (2.6)$$

where, E is the energy per information bit, T is the bit period of the data streams, $a_I(t)$ and $a_Q(t)$ encode the even and odd information respectively with a sequence of square pulses of duration $2T$ and f_c is the carrier frequency.

In the kth bit period of T seconds, $a_I(t)$ and $a_Q(t)$ take the values ± 1. Consequently, MSK signals can also be expressed in the form [8],

$$s(t) = \sqrt{\frac{2E}{T}} \cos\left[2\pi\left(f_c + d_k \frac{1}{4T}\right)t + \Phi_k\right], \qquad kT \leq t \leq (k+1)T \quad (2.7)$$

where d_k is -1 if $a_I(t)$ and $a_Q(t)$ have the same sign and $+1$ otherwise [8], or equivalently $d_k = -a_I(t)\,a_Q(t)$. In [8] also shown that, $\Phi_k = 0$ or π corresponding to $a_I(t) = 1$ or -1, or equally

$$\Phi_k = \frac{\pi}{2}\bigl(1 - a_I(t)\bigr). \qquad (2.8)$$

From Equation (2.7), it can be noted that the signal is binary FSK signal with the two frequencies $\left(f_c + \frac{1}{4T}\right.$ and $\left.f_c - \frac{1}{4T}\right)$ and with a symbol period of $2T$, where each symbol is 2 bits. Also, both d_k and Φ_k are continuous over a bit duration of T seconds, since $a_I(t)$ and $a_Q(t)$ are constant over T seconds.

2.3.2   Generating MSK Signals From CPFSK

Alternatively, MSK signals can be derived as a special case of continuous phase frequency shift keying (CPFSK) [72, 75], defined over the interval $kT \leq t \leq (k+1)T$ as

$$s(t) = \sqrt{\frac{2E}{T}} \cos\left(2\pi f_c t + \frac{\pi h d_k(t - kT)}{T} + \pi h \sum_{i=0}^{k-1} d_i\right). \qquad (2.9)$$

This can be simplified to the form,

$$s(t) = \sqrt{\frac{2E}{T}} \cos\left[2\pi f_c t + h d_k \frac{\pi t}{T} + \Phi_k\right], \qquad kT \leq t \leq (k+1)T \quad (2.10)$$

where, E is the energy per information bit, T is the bit period of the data streams, f_c is the carrier frequency, d_k is the input data with the values of ±1 transmitted at rate $R = 1/T$ and h is the modulation index. The term Φ_k

represents the excess phase which is constant in the bit interval, and defined as [7, 8, 11],

$$\Phi_k = \pi h \left(\sum_{i=0}^{k-1} d_i - k d_k \right). \qquad (2.11)$$

In MSK, the frequency separation between the two tones $f_c + \frac{1}{4T}$ and $f_c - \frac{1}{4T}$ is $\Delta f = {}^1\!/_{2T}$. This is the minimum frequency spacing that allows two FSK signals to be coherently orthogonal and corresponds to $h = 0.5$, thus the modulated signal becomes,

$$s(t) = \sqrt{\frac{2E}{T}} \cos\left[2\pi f_c t + d_k \frac{\pi t}{2T} + \Phi_k \right], \quad kT \leq t \leq (k+1)T \quad (2.12)$$

It is exactly what we had before. The MSK signal formed in this case is also known as fast frequency shift keying (FFSK) [77-80].

2.3.3   MSK Modulator

In this subsection, we discuss the I-Q implementation of MSK. The MSK modulator [81, 82] shown in Figure 2-3 is only one among several possible configurations. The offset QPSK realisation of MSK suggested here is a direct implementation of Equation (2.6). After the serial to parallel conversion, the input data stream, $a(t)$ is split into an even bit stream, $a_I(t)$ and an odd bit stream, $a_Q(t)$, taking values from the set $\{-1, +1\}$.

As in offset QPSK, $a_Q(t)$ is delayed by T relative to $a_I(t)$ and the duration of each bit of the sequences is extended from the original duration of T, to $2T$ seconds. Each bit of the two data streams is converted into a signal amplitude of $+A$ and a signal amplitude of $-A$ corresponding to $+1$ and -1, respectively. Typically, the amplitude, A is expressed in terms of bit energy, E and bit duration, T, and is given by, $A = \sqrt{(2E\,/\,T)}$.

The two local oscillators generate $\cos(2\pi f_c t)$ and $\cos\left(\frac{\pi t}{2T}\right)$, which are transformed to $\sin(2\pi f_c t)$ and $\sin\left(\frac{\pi t}{2T}\right)$ respectively by the $\pi/2$ phase shifters. The mixers multiply the two orthogonal carriers with the half cycle sinusoidal shaped I and Q waveforms. Finally, the summer adds the outputs of the two mixers together to produce an MSK signal.
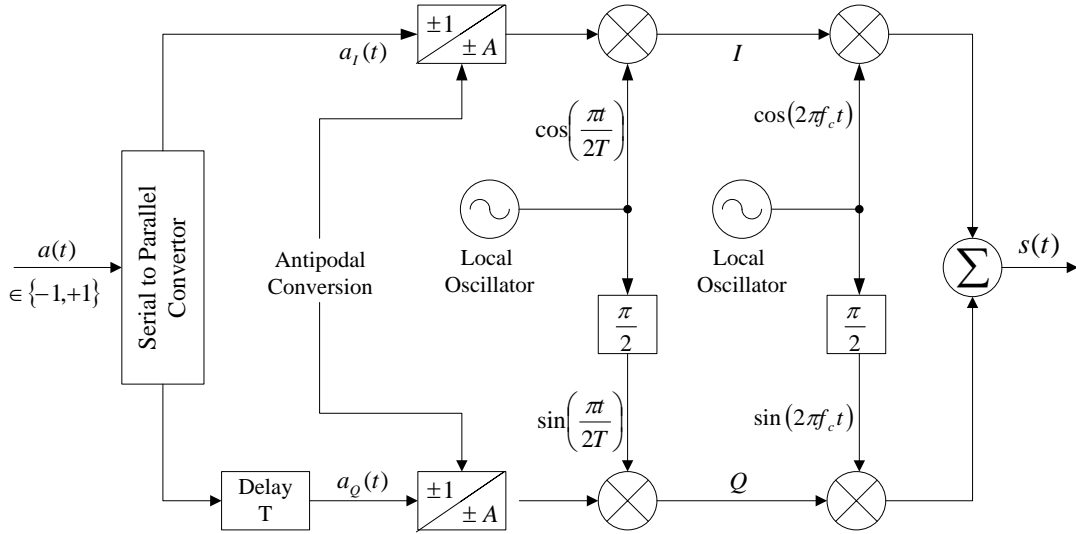
Figure 2-3 Block diagram of MSK modulator

2.4   Multi-Amplitude Minimum Shift Keying

As described in the previous sections, MSK is a bandwidth efficient modulation scheme that has properties such as, continuous phase, sharp spectral sidelobe roll-off and constant envelope. The same properties hold for multi level (M) multi-amplitude minimum shift keying (M-MAMSK) except that it has a non-constant envelope but with the advantage of increased spectral efficiency. According to [1, 2, 42-44, 83] M-MAMSK signals can be generated by the superposition of MSK component signals. In [84], it is proposed that an M-MAMSK signal can also be represented in term of orthogonal frequency division multiplexing (OFDM). In the following subsections, we discuss these two representations of M-MAMSK signals.

2.4.1 Generating M-MAMSK Signal From MSK

M-MAMSK is a generalisation of conventional MSK in which the signal amplitude is allowed to vary over a set of $M > 2$ amplitude values while the phase is constrained to be continuous. M-MAMSK signals may be formed as the superposition of multiple MSK signals with different amplitudes. For M-MAMSK signals there is no requirement for the MSK constituent signals to be orthogonal, in fact, they are co-phased [44]. In addition, the amplitudes of the MSK components are not equal and this prevents the phase track backing to the previous one.

For example, a two level MAMSK (i.e. 2-MAMSK[1]) signal is obtained by summing two MSK signals with different amplitudes (6 dB difference in power) and can be expressed as

$$s_{2-MAMSK}(t) = s_{MSK\,1}(t) + s_{MSK\,2}(t) \tag{2.13}$$

Using the results from the previous sections, we may define a two level MAMSK signal as

$$s(t, \alpha, \beta) = A\, s_{MSK}(t, \alpha) + 2A\, s_{MSK}(t, \beta)$$

$$= A\cos\big(2\pi f_c t + \phi(t, \alpha)\big) + 2\,A\cos\big(2\pi f_c t + \phi(t, \beta)\big) \tag{2.14}$$

where, $s_{MSK}(t, \alpha)$ is the MSK component with the smaller amplitude, $s_{MSK}(t, \beta)$ is the MSK component with the larger amplitude, f_c is the signal carrier frequency, and A is the amplitude which is defined in [43, 73] as

$$A = \sqrt{\frac{2E}{5T}}, \tag{2.15}$$

here, E is the average signal energy per symbol interval, T is the duration of a symbol interval and the sequences α and β represent input data with

---

[1] A 2-MAMSK signal is usually referred to in the literature as "Multi-Amplitude Minimum Shift Keying", or MAMSK for short.

values ± 1. $\phi(t, \alpha)$ and $\phi(t, \beta)$ are the information carrying parts of the MSK signal phases and may be expressed as

$$\phi(t, \alpha) = \frac{\pi}{2} \sum_{k=-\infty}^{n-1} \alpha_k + \frac{\pi}{2T} \alpha_n (t - nT), \qquad nT \le t \le (n+1)T \qquad (2.16)$$

$$\phi(t, \beta) = \frac{\pi}{2} \sum_{k=-\infty}^{n-1} \beta_k + \frac{\pi}{2T} \beta_n (t - nT), \qquad nT \le t \le (n+1)T \qquad (2.17)$$

To find the value of A, recall that energy of a signal of amplitude, A is equal to

$$E = \frac{T}{2} A^2 \qquad (2.18)$$

Now, consider that the amplitude of the larger MSK component is twice that of the MSK component with the smaller amplitude, then E becomes

$$E = \frac{T}{2}(A^2 + (2A)^2) = \frac{5A^2 T}{2} \qquad (2.19)$$

Rearranging to solve for A and we obtain

$$A = \sqrt{\frac{2E}{5T}}. \qquad (2.20)$$

As a generalisation, an MAMSK signal with $M > 2$ component MSK signals (i.e. M-MAMSK[2]) is defined in [64] as

$$s_{M-MAMSK}(t, \alpha_1, \alpha_2, \dots, \alpha_M) = \frac{1}{\sum_{i=1}^{M} 2^{2(i-1)}} \sum_{i=1}^{M} s(t, \alpha_i) \qquad (2.21)$$

---

[2] Several authors use the notation N-MSK in place of M-MAMSK.

where, $s(t, \alpha_i)$ is the ith MSK component of the M-MAMSK signal, given by,

$$s(t, \alpha_i) = 2^{(i-1)} \left(\sqrt{\frac{2E}{T}} \cos(2\pi f_c t + \phi(t, \alpha_i)) \right), \qquad (2.22)$$

and $\phi(t, \alpha_i)$ is the phase of the ith MSK component signal, expressed as

$$\phi(t, \alpha_i) = \frac{\pi}{2} \sum_{k=-\infty}^{n-1} \alpha_{ik} + \frac{\pi}{2T} \alpha_{in} (t - nT), \qquad nT \leq t \leq (n+1)T \quad (2.23)$$

The sequences $\{\alpha_i\}$ for $i = 1, 2, 3, \dots, M$ are statistically independent, binary valued sequences that take values from the set $\{+1, -1\}$ and all other terms are defined as before.

From Equation (2.22), we observe that each MSK component in the sum has a constant envelope. A number of authors [42, 64, 65, 85] point out that this aspect allows an efficient high-power M-MAMSK signal with $M \geq 2$ to be obtained by combining M nonlinearly amplified MSK signals. An attractive feature of this is that despite being a non-constant envelope modulation, it can be used in systems with efficient nonlinear power amplifiers. This is useful in cases where power resources are limited.

2.4.2 Representation of M-MAMSK Signal in Terms of OFDM

M-MAMSK signals can also be represented in term of OFDM [84]. The nth symbol interval of the complex signal of baseband M-MAMSK can be expressed as

$$s_{M-MAMSK}(t) = \sum_{k=1}^{N} C_k(t) \cdot e^{j\frac{2\pi kt}{NT}}, \qquad 0 < t < NT \qquad (2.24)$$

where, k is the index of the sub-carrier, N is the total number of the sub-carriers, T is the time duration of every symbol and $C_k(t)$ is the M-MAMSK modulated information symbol in the kth sub-carrier, defined as

$$C_k(t) = \sum_{i=1}^{M} A_i \cdot e^{j\theta_{ik} + j\alpha_{ik}\frac{\pi t}{2NT}} \qquad (2.25)$$

here, α_{ik} is the input binary data sequences with values of ± 1, θ_{ik} is the phase state and A_i is the amplitude of the i th component inside the M-MAMSK signal.

As an example, if we consider a 2-MAMSK signal (i.e. $M = 2$), then the transmitted signal, $s_{2-MAMSK}(t)$ can be written in the form,

$$s_{2-MAMSK}(t) = \sum_{k=1}^{N} \left(A_1 e^{j\theta_{1k} + j\alpha_{1k}\frac{\pi t}{2NT}} + A_2 e^{j\theta_{2k} + j\alpha_{2k}\frac{\pi t}{2NT}} \right) \cdot e^{j\frac{2\pi kt}{NT}} \qquad (2.26)$$

From the above equation, we can see that when the constituent signals have unequal amplitudes (when $A_1 \neq A_2$), the 2-MAMSK signal never reaches zero signal energy. This should improve the performance of the signal as it is less sensitive to nonlinear power amplifiers [44]. From this result one can conclude that a MAMSK modulated signal is both power and bandwidth efficient. Hence, it is an appealing modulation scheme for systems with limited power and bandwidth resources.

2.5　2-MAMSK Modulator

A simplified block diagram of a 2-MAMSK modulator is illustrated in Figure 2-4.
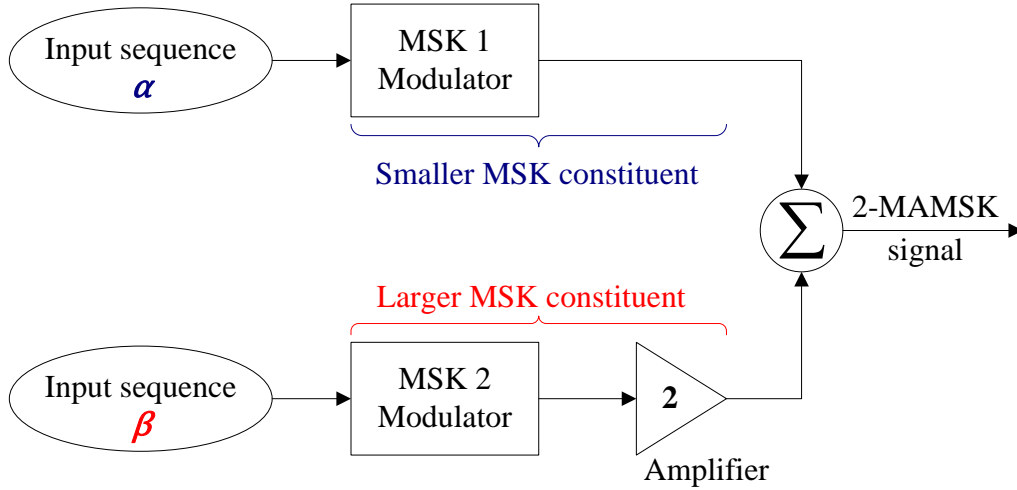
Figure 2-4 Block diagram of a 2-MAMSK modulator

Let us define the terms and explain the operation of each block briefly. α, is the information sequence that is carried by the MSK constituent with smaller amplitude. β, is the information sequence that is carried by the MSK constituent with larger amplitude. Both α and β are independent and identically distributed binary random variables, each taking values from the set $\{-1, +1\}$.

The MSK Modulator block (described in section 2.3) takes the input sequence and generates a continuous phase modulated signal based on minimum shift keying and its output in general given by,

$$s_{MSK}(t, I) = A \cos\big(2\pi f_c t + \phi(t, I)\big) \qquad (2.27)$$

where A is the amplitude, I is the input sequence and $\phi(t, I)$ is the information carrying part of the MSK signal phase and expressed mathematically as

$$\phi(t, I) = \frac{\pi}{2} \sum_{k=-\infty}^{n-1} I_k + \frac{\pi}{2T} I_n (t - nT), \qquad nT \leq t \leq (n+1)T \quad (2.28)$$

where T is the duration of one symbol interval.

To get a better understanding of the above equation, let us plot the MSK signal phase for a given input data sequence,

$$I = \{-1, -1, +1, +1, +1, +1, -1\}$$

The MSK signal phase for the above information sequence is shown in Figure 2-5.
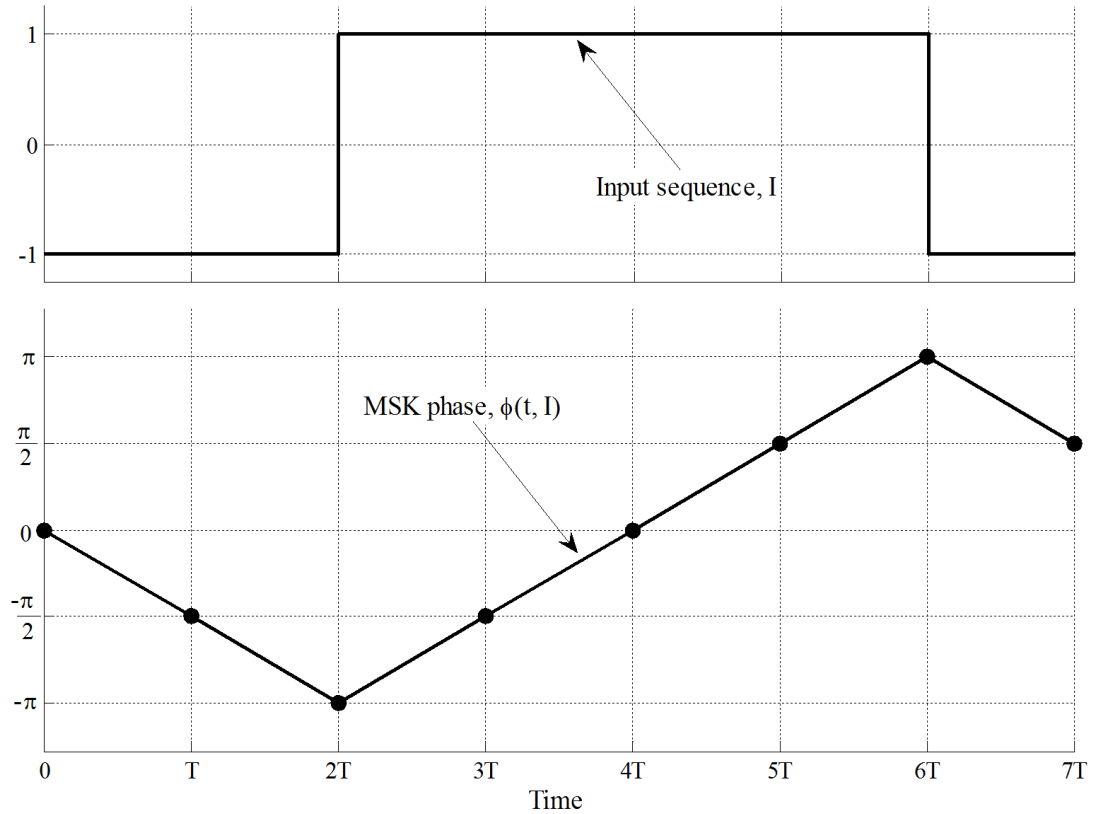
Figure 2-5   MSK signal phase for some particular information sequence

The phase values at the time instants $t = nT$ are represented in the figure as small circles. From the above figure, we observe that the MSK signal phase is a piecewise linear function of time and the input data sequence. Clearly, we can see that the MSK signal phase change within the symbol interval depends on the input data, I. $I_n = +1$, causes the MSK signal phase to increase by $\pi / 2$ while $I_n = -1$, causes the phase to decrease by $-\pi / 2$, over a of T-sec interval.

From these observations, we can define the difference in phase, $\Delta\phi$ between symbol intervals as,

$$\Delta\phi = \phi\big((n+1)T, I\big) - \phi(nT, I) = \frac{\pi}{2}I_n \qquad (2.29)$$

The above result is important because it allows symbol-by-symbol differential detection of an MSK signal [86, 87], which is significantly less complex to implement than coherent detection. In [43], this idea is extended to differential detection of MAMSK signal, as we shall see later on in the chapter.

Now using the above results, the output of the MSK 1 and MSK 2 modulator blocks as a function of time and the data sequences, α and β can be defined in the form,

$$s_{MSK\,1}(t, \alpha) = A\,\cos\big(2\pi f_c t + \phi(t, \alpha)\big), \qquad nT \leq t \leq (n+1)T \qquad (2.30)$$

$$s_{MSK\,2}(t, \beta) = 2A\,\cos\big(2\pi f_c t + \phi(t, \beta)\big), \qquad nT \leq t \leq (n+1)T \qquad (2.31)$$

where $s_{MSK\,1}(t, \alpha)$ is the MSK component with the smaller amplitude and $s_{MSK\,2}(t, \beta)$ is the MSK component with the larger amplitude. $\phi(t, \alpha)$ and $\phi(t, \beta)$ are information carrying phase functions, which are defined in Equations (2.16) and (2.17), respectively.

It can be noted from the above equations that the amplitude of the larger MSK constituent is twice that of the smaller MSK constituent. As illustrated in Figure 2-4, a 2-MAMSK modulated signal is a superposition of the two MSK components. The output of the 2-MAMSK modulator defined over the interval $nT \leq t \leq (n+1)T$ can be written as

$$s(t, \alpha, \beta) = s_{MSK\,1}(t, \alpha) + s_{MSK\,2}(t, \beta)$$

$$(2.32)$$

$$= A\cos\big(2\pi f_c t + \phi(t, \alpha)\big) + 2\,A\cos\big(2\pi f_c t + \phi(t, \beta)\big)$$

Figure 2-6 illustrates a 2-MAMSK modulated signal with carrier frequency of 2 Hz[3] , for the information sequences,

$$\alpha = \{+1, +1, -1, -1, +1, -1, -1, -1\}$$

$$\beta = \{-1, +1, -1, +1, +1, -1, +1, -1\}$$
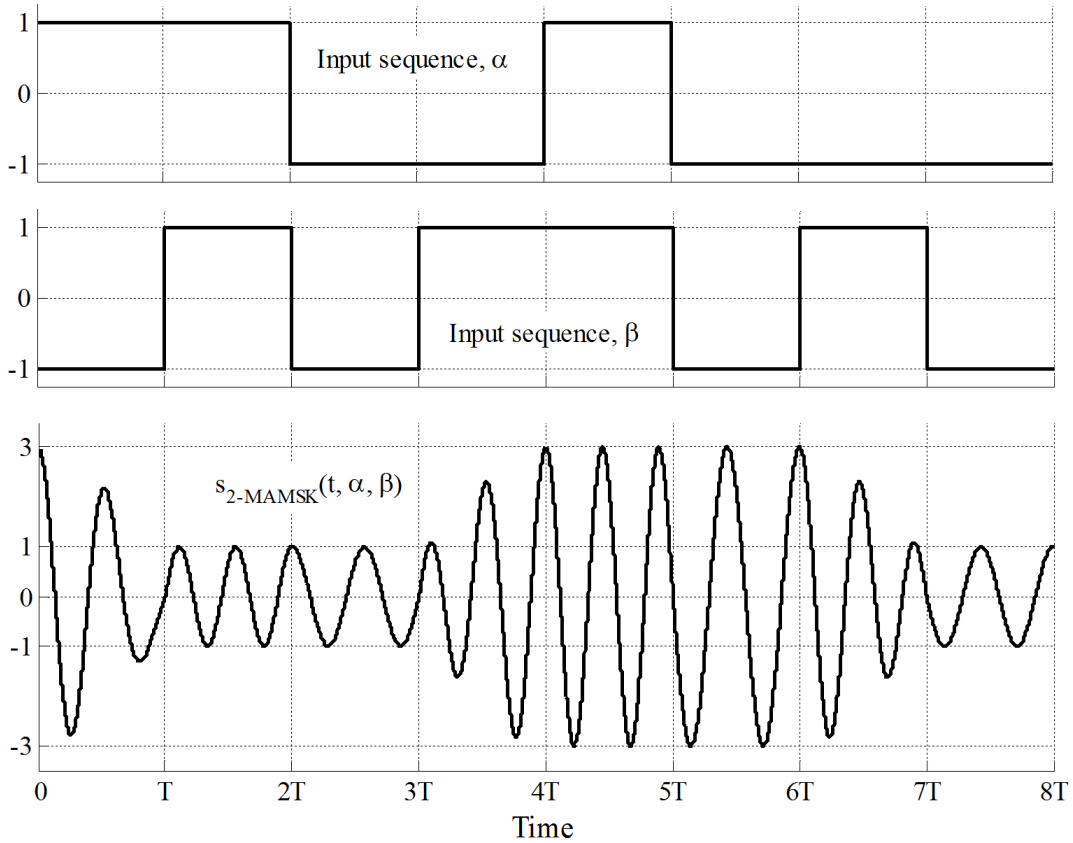
Figure 2-6 A 2-MAMSK signal at f_c=2 Hz

From Figure 2-6, we observe that $\beta_n = +1$ causes higher frequency transmission while $\beta_n = -1$ causes lower frequency transmission. For the time intervals where $\beta_n = \alpha_n$ the signal amplitude is constant, but there are amplitude changes in intervals when $\beta_n \neq \alpha_n$. As shown in the above figure, the signal amplitudes states are specified by an amplitude level from the set of amplitudes $\{\pm 1, \pm 3\}$. The amplitude level of ± 1 corresponds to the case when the two MSK signals are out of phase with each other by π

---

[3] The carrier frequency of 2 Hz is not realistic; it is used here only for demonstration purposes.

31

and an amplitude level of ± 3 occurs when both MSK signals are in phase with each other. Based on these results, the smaller MSK constituent is constrained such that at the start and end of each symbol interval, it is either in phase or out of phase by π radians with the larger MSK component.

2.6 The Maximum Likelihood Detector

The function of a demodulator is to estimate the transmitted information bits from the corrupted received signal. The process of demodulation can be accomplished in several ways. In this section, we discuss a maximum likelihood (ML) detector which is robust and makes an optimum decision assuming a signalling waveform transmitted through the AWGN channel. The ML detector is the receiver that selects the most likely signal sent, given the received signal $r(t)$ that it has observed. Consequently, the ML detector yields optimum BER performance [88, 89] among all detection methods, but its exponential complexity is the highest [90]. This is due to the fact that the ML algorithm is performed through an exhaustive search over all possible candidate vector symbols.

Assuming equally likely transmission of all symbols, that is if

$$P(\boldsymbol{s}_i) = \frac{1}{M}, \qquad \forall\, i = 1, 2, \dots, M. \tag{2.33}$$

Then assuming Gaussian noise, the optimum decision rule based on the ML criterion is obtained by calculating [7, 72], for each i

$$D(\boldsymbol{r},\, \boldsymbol{s}_i) = \int_0^T [r(t) - s_i(t)]^2 \; dt \tag{2.34}$$

where $D(\boldsymbol{r},\, \boldsymbol{s}_i)$, $i = 1, 2, \dots, M$ is the Euclidean distance metric. Now, expanding Equation (2.34), we get

$$D(\boldsymbol{r}, \boldsymbol{s}_i) = \int_0^T r^2(t)\ dt + \int_0^T s_i^2(t)\ dt - 2 \int_0^T r(t)\ s_i(t)\ dt \qquad (2.35)$$

We can see that the first term of the right hand side of Equation (2.35) is constant with respect to i, and, thus it may be omitted from the computation of the metrics. The receiver needs only to form the correlation metrics (last term of Equation (2.35)) and subtract it from the second term, which is the energy of $s_i(t)$. It is also to be noted that if all transmitted signals have equal energy, only the correlation between the received signal, $r(t)$ and each of the M possible signalling waveforms needs to be performed. A detector based on these calculations is called a correlation receiver [7, 72]. In chapter 3, the optimum bit error probability for M-MAMSK transmission through an AWGN channel is derived from these concepts.

2.7   2-MAMSK Phase and Complex Envelope

In this section, we provide analytical derivations of the phase and complex envelope of a 2-MAMSK signal. These two terms are essential for implementing and describing the 2-MAMSK differential detector proposed in [43]. From trigonometric identities, we have

$$\cos(A + B) = \cos A \cos B - \sin A \sin B \qquad (2.36)$$

Applying this identity to Equation (2.32), we obtain

$$s(t, \alpha, \beta) = A\big[\cos(2\pi f_c t) \cos\big(\phi(t, \alpha)\big) - \sin(2\pi f_c t) \sin\big(\phi(t, \alpha)\big) +$$

$$2 \cos(2\pi f_c t) \cos\big(\phi(t, \beta)\big) - 2\sin(2\pi f_c t) \sin\big(\phi(t, \beta)\big)\big] \qquad (2.37)$$

Factoring and simplifying the above expression yields,

$$s(t, \alpha, \beta) = A \cos(2\pi f_c t) \underbrace{\left[\cos(\phi(t, \alpha)) + 2 \cos(\phi(t, \beta))\right]}_{I - \text{Channel}}$$

(2.38)

$$- A \sin(2\pi f_c t) \underbrace{\left[\sin(\phi(t, \alpha)) + 2 \sin(\phi(t, \beta))\right]}_{Q - \text{Channel}}$$

We may then depict these I and Q components as in Figure 2-7.
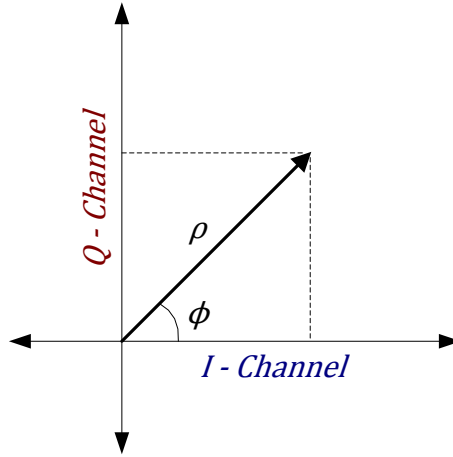
Figure 2-7 I and Q representation of 2-MAMSK signal

From the above figure, we can establish the following:

a) The phase of the signal is given by

$$\phi = \tan^{-1}\left(\frac{Q}{I}\right)$$

(2.39)

b) The magnitude (envelope) of the signal is given by

$$\rho = \sqrt{I^2 + Q^2}$$

(2.40)

Now, using the above relations with $I = \left[\cos(\phi(t, \alpha)) + 2 \cos(\phi(t, \beta))\right]$ and $Q = \left[\sin(\phi(t, \alpha)) + 2 \sin(\phi(t, \beta))\right]$, we can define the overall phase of a 2-MAMSK signal as

$$\phi(t, \alpha, \beta) = \tan^{-1}\left[\frac{\sin\phi(t,\alpha) + 2\sin\phi(t,\beta)}{\cos\phi(t,\alpha) + 2\cos\phi(t,\beta)}\right] \tag{2.41}$$

Note that the factor of "2", in the above equation, is dominant in determining the overall phase of a 2-MAMSK signal. In the next chapter, we will show this explicitly and extend it to M-MAMSK for $M > 2$.

Next, we substitute the previous values of I and Q into Equation (2.40) to obtain an expression for a 2-MAMSK signal envelope,

$$\rho(t, \alpha, \beta) = \sqrt{\begin{aligned}&\left\{\left[\cos\big(\phi(t,\alpha)\big) + 2\cos\big(\phi(t,\beta)\big)\right]^2 \\ &+ \left[\sin\big(\phi(t,\alpha)\big) + 2\sin\big(\phi(t,\beta)\big)\right]^2\right\}\end{aligned}} \tag{2.42}$$

Expanding Equation (2.42), we get

$$\rho(t, \alpha, \beta) = \sqrt{\begin{aligned}&\left\{\cos^2\big(\phi(t,\alpha)\big) + 4\cos\big(\phi(t,\alpha)\big)\cos\big(\phi(t,\beta)\big) \\ &+ 4\cos^2\big(\phi(t,\beta)\big) + \sin^2\big(\phi(t,\alpha)\big) \\ &+ 4\sin\big(\phi(t,\alpha)\big)\sin\big(\phi(t,\beta)\big) + 4\sin^2\big(\phi(t,\beta)\big)\right\}\end{aligned}}$$

$$\tag{2.43}$$

$$= \sqrt{\begin{aligned}&\left\{\sin^2\big(\phi(t,\alpha)\big) + \cos^2\big(\phi(t,\alpha)\big)\right\} + 4\left\{\sin^2\big(\phi(t,\beta)\big) \\ &+ \cos^2\big(\phi(t,\beta)\big)\right\} + 4\left\{\cos\big(\phi(t,\alpha)\big)\cos\big(\phi(t,\beta)\big) \\ &+ \sin\big(\phi(t,\alpha)\big)\sin\big(\phi(t,\beta)\big)\right\}\end{aligned}}$$

In order to simplify the above expression, we recall the trigonometric identities

$$\sin^2 A + \cos^2 A = 1 \tag{2.44}$$

$$\cos(A - B) = \cos A \cos B + \sin A \sin B \tag{2.45}$$

35

With these relationships, Equation (2.43) simplifies to

$$\rho(t, \alpha, \beta) = \sqrt{5 + 4\cos[\phi(t, \beta) - \phi(t, \alpha)]}, \qquad (2.46)$$

where, $\rho(t, \alpha, \beta)$ is the baseband representation of a 2-MAMSK signal envelope. The terms $\phi(t, \alpha)$ and $\phi(t, \beta)$ are defined as in section 2.4.1. For example, a 2-MAMSK signal phase and envelope generated by the information sequences $\alpha = \{-1, +1, +1, +1, +1, +1, +1, -1\}$ and $\beta = \{-1, -1, +1, +1, +1, -1, -1, +1\}$, are illustrated in Figure 2-8.
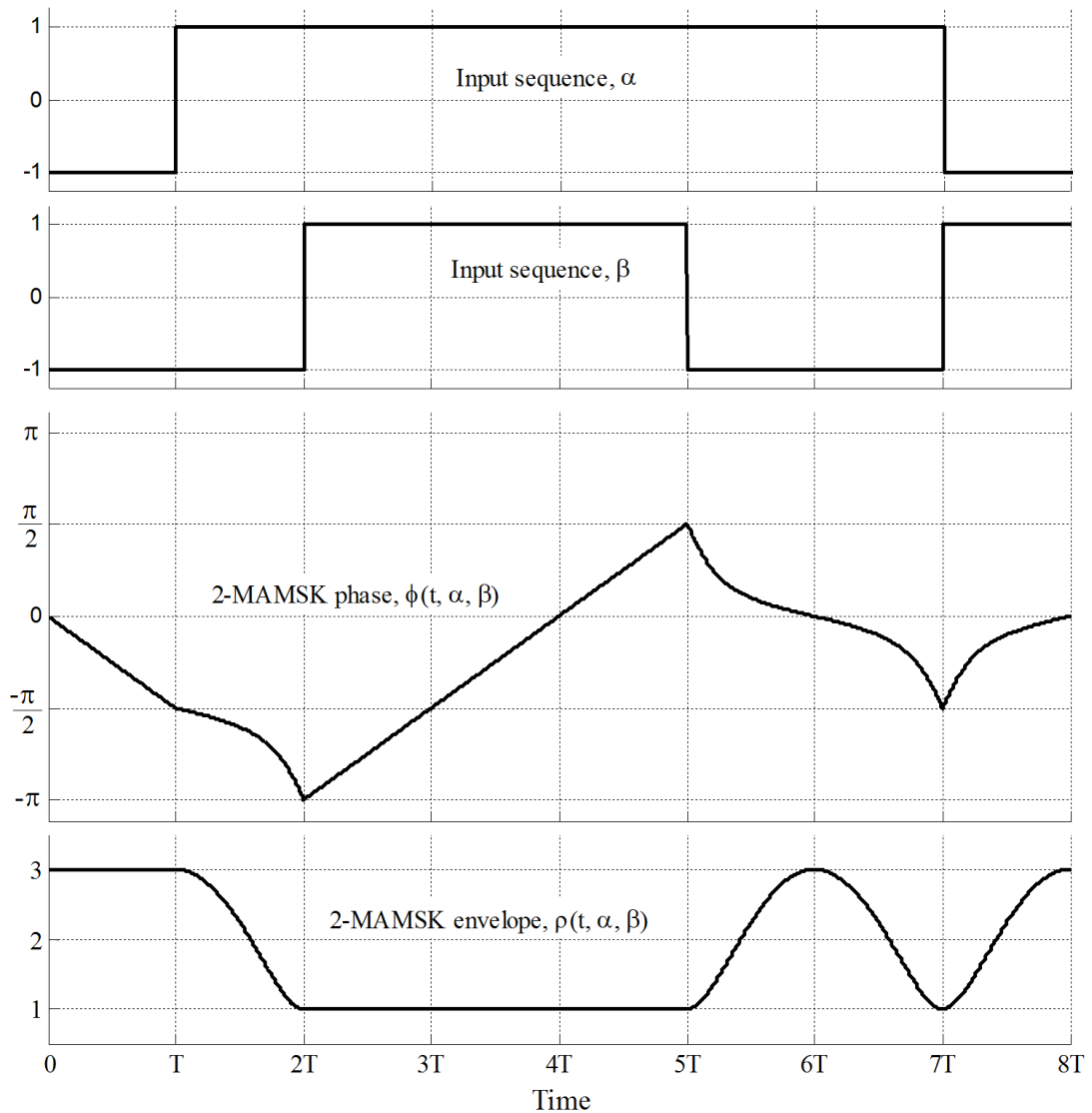
Figure 2-8 2-MAMSK signal phase and envelope for a given α and β

36

The overall 2-MAMSK signal phase shown in Figure 2-8 is a piecewise function of time and the input data sequences α and β. For the symbol intervals where $\alpha_n = \beta_n$, it can be seen that the 2-MAMSK signal phase is a piecewise linear function (see time intervals $2T - 5T$ in Figure 2-8). For the time intervals where $\alpha_n \neq \beta_n$ it is a curved function (see time intervals $5T - 7T$ in Figure 2-8). However, from Figure 2-8, we can see that the 2-MAMSK signal phase change within the symbol interval depends only on the input data sequence, β, which is carried by the larger MSK constituent. The phase of the smaller MSK component causes the "curvy" behaviour of the overall 2-MAMSK signal phase when α_n and β_n have opposite signs.

Based on this observation, the phase variation of a 2-MAMSK signal within one symbol interval depends primarily on the data transmitted by the MSK constituent with the larger amplitude. For example, $\beta_n = +1$, causes the overall phase to increase by $+^{\pi}/_2$, while $\beta_n = -1$, causes the overall phase to decrease by $-^{\pi}/_2$. Thus, the phase difference, $\Delta\phi(nT, \alpha, \beta)$ of the 2-MAMSK signal may be expressed as

$$\Delta\phi(nT, \alpha, \beta) = \frac{\pi}{2}\beta_n. \qquad (2.47)$$

The above equation is useful as it allows differential detection of the information sequence carried by the larger MSK component from the 2-MAMSK signal, as we shall see in the next section.

Furthermore, from Figure 2-8, we observe that the 2-MAMSK signal envelope is constant for the time intervals where $\alpha_n = \beta_n$; otherwise it changes from 1 to 3 as a sinusoidal function of time. From this observation, the data carried by the MSK component with the smaller amplitude can be recovered from the 2-MAMSK signal envelope. We will discuss this in more detail in the next section. Here, we have briefly summarised some aspects of a 2-MAMSK signal phase and envelope in order to present the 2-MAMSK differential detector. In chapter 3, we provide a more rigorous discussion and show a more in-depth analysis of these elements.

2.8   2-MAMSK Differential Detector

In this section a symbol by symbol differential detection for a 2-MAMSK signal is presented. The receiver structure [43] is illustrated in Figure 2-9.
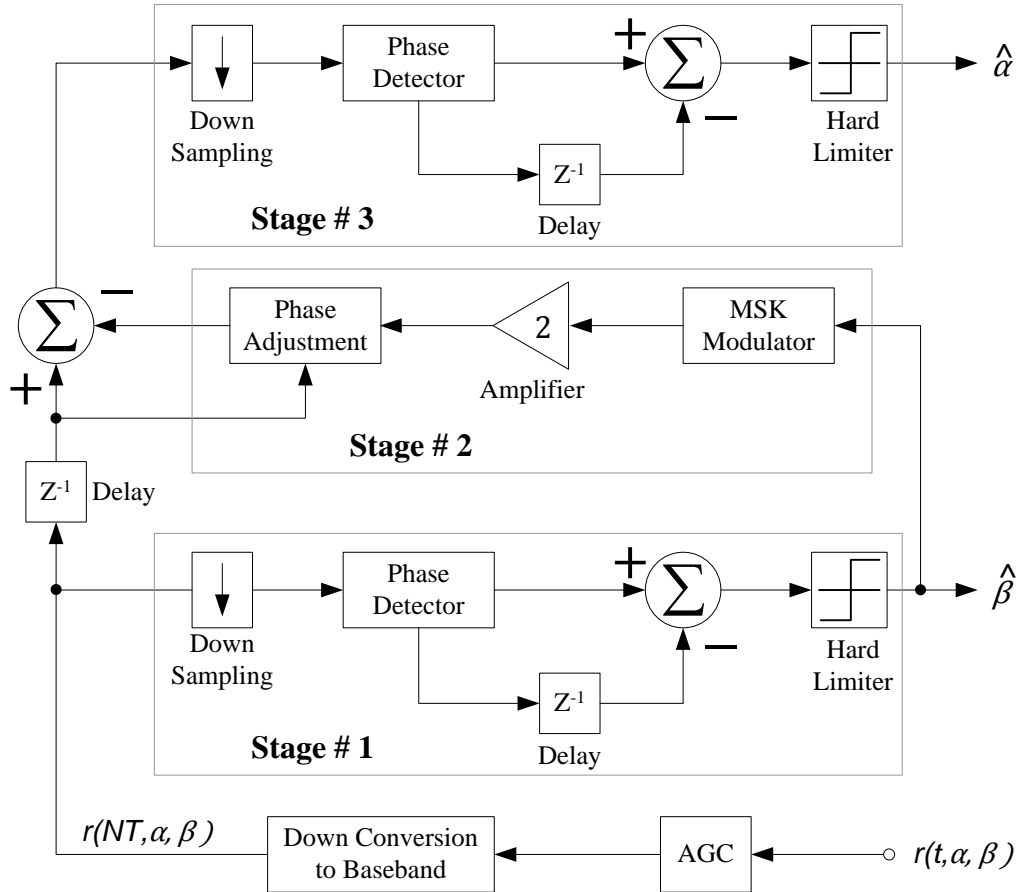
Figure 2-9   Block diagram of the differential detector

The first operation performed in the above receiver is to amplify the received 2-MAMSK signal by an automatic gain control (AGC) circuit in order to adjust the received signal power to an appropriate level.   After amplification, the signal is down-converted to an IF or baseband signal and sampled N times per interval. The sampled baseband 2-MAMSK signal at this point has N samples per symbol duration.

Before discussing the rest of the receiver, we need point out that the 2-MAMSK differential receiver is based on the following two properties:

a) The 2-MAMSK signal is generated by superimposing two MSK signals with unequal amplitudes. In particular the amplitude of the lager MSK signal is twice that of the smaller one.

b) The phase difference between symbol intervals of the received 2-MAMSK signal depends primarily on the input data sequence, β, which is carried by the MSK constituent with the larger amplitude. For now, we use it as a observation from simulation [7, 43], we will show the derivation of this observation in chapter 3.

If the above two properties hold, then the overall phase of the 2-MAMSK signal will always follow the phase of the MSK constituent with the larger amplitude. As a result, we can extract the information sequence, β from the phase of the received 2-MAMSK signal.

The baseband implementation of the differential receiver presented in Figure 2-9 is divided into three stages. The first stage begins with downsampling the received baseband signal to one sample per symbol. Specifically, samples are taken at the symbol rate (i.e. at the time instants $t = nT$). The function of the phase detector block is to extract the overall phase from the downsampled received signal; this process is based on Equation (2.41). Then, we calculate the phase difference, $\Delta\phi(nT, \alpha, \beta)$ between symbol intervals by subtracting the phase value delayed by one symbol from the current value. The difference in phase is given by

$$\Delta\phi(nT, \alpha, \beta) = \phi(nT, \alpha, \beta) - \phi\big((n-1)T, \alpha, \beta\big) \qquad (2.48)$$

It is seen from Figure 2-8 that the phase difference, $\Delta\phi(nT, \alpha, \beta)$ always takes its value from the set $\{-\pi\,/\,2,\ +\pi\,/\,2\,\}$. This corresponds to the values of β_n equal to -1 and $+1$, respectively. The outcome is then passed to the hard limiter and the following decisions are made:

$$\hat{\beta}_n = \begin{cases} +1 & if \quad \Delta\phi(nT, \alpha, \beta) \geq 0 \\ -1 & if \quad \Delta\phi(nT, \alpha, \beta) < 0 \end{cases} \qquad (2.49)$$

where $\hat{\beta}$ is an estimate of the input data sequence, β. Thus, we have now recovered the information sequence carried by the larger MSK constituent. In fact, the process carried out in stage 1 is identical to the differential detector [87] used for conventional MSK signals. Consequently, the existing MSK differential receivers can be used to recover the information carried by the larger MSK component from the received 2-MAMSK signal.

To recover the information sequence carried by the MSK constituent with the smaller amplitude, we perform the following procedures (stage 2 from Figure 2-9).

- First, we use the estimated data sequence, $\hat{\beta}$ as an input to the MSK modulator block to generate an MSK signal as described in section 2.3.3. The modulated MSK signal is amplified by a factor of 2 and sampled at the rate of N samples per symbol interval. This is with the intention of generating a locally MSK signal that would be approximately equivalent to the original transmitted MSK signal with the larger amplitude. Thus, we have

$$s_{MSK\,2}(t, \hat{\beta}) \approx s_{MSK\,2}(t, \beta), \qquad (2.50)$$

where $s_{MSK\,2}(t, \hat{\beta})$ is the locally generated MSK signal and $s_{MSK\,2}(t, \beta)$ is the original MSK signal with the larger amplitude.

- The responsibility of the Phase Adjustment block is to match the phase of the locally generated MSK signal to the received 2-MAMSK signal. To illustrate Phase Adjustment block operation, recall that the 2-MAMSK signal phase will always follow the phase of the larger MSK constituent. This result will allow us to make the following two statements:

  a) Provided that the locally generated MSK signal is exactly equal to the MSK constituent with larger amplitude, then under this condition, the phase difference between the symbol intervals of the received 2-MAMSK signal and the locally generated MSK signal is always zero. In other words, at the symbol transition times the phase value of the received 2-MAMSK signal should be equivalent to the phase value of the locally generated MSK signal.

b) On the rare occasions when an error has been made and the locally generated MSK signal is not equal to the larger MSK component. Then at the symbol transition times the phase value of the received 2-MAMSK signal differs from the phase value of the locally generated MSK signal by π radians.

Accordingly, the phase adjustment block calculates the difference between the phase of the received 2-MAMSK signal and the locally generated MSK signal at the symbol transition times $(t = nT)$. Subsequently, makes a decision based on the value of the calculated phase difference. If the outcome is not zero then it shifts the phase of the locally generated MSK signal by the calculated phase difference (π radians), otherwise do nothing. This is to ensure that the received 2-MAMSK signal and the locally generated MSK signal are always in phase with each other.

Now, the adjusted MSK signal is subtracted from the received signal in order to obtain the MSK component with the smaller amplitude as

$$
\begin{aligned}
s_{MSK\,1}(t, \alpha) &= r(t, \alpha, \beta) - s_{MSK\,2}(t, \hat{\beta}) \\
&= s_{MSK\,1}(t, \alpha) + s_{MSK\,2}(t, \beta) + n(t) - s_{MSK\,2}(t, \hat{\beta})
\end{aligned}
\tag{2.51}
$$

where $n(t)$ is the AWGN and all other terms are defined as before. From Equation (2.51), we observe that the received 2-MAMSK signal is reduced to the form of a conventional MSK signal. In fact it is a form of interference cancellation. Therefore, stage 3 is performed in a similar manner to stage 1 to recover the data sequence transmitted by the smaller MSK constituent. Thus, with this differential receiver we have successfully recovered the input data sequences, α and β from the received 2-MAMSK signal. Note that we have never explicitly used the envelope of the received 2-MAMSK signal to detect the information sequences α and/or β.

As described above, we have demonstrated that both information sequences α and β can be recovered from the received 2-MAMSK signal using two parallel differential MSK detectors. Consequently, construction of

41

the 2-MAMSK differential receiver can be implemented with existing MSK modems as shown in Figure 2-10.
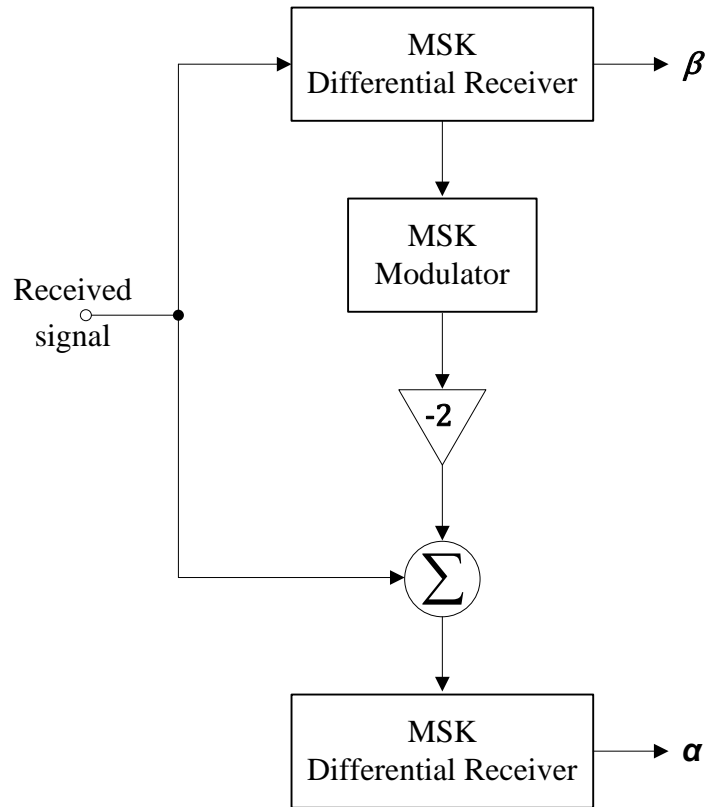
Figure 2-10 A simpler representation of the 2-MAMSK differential receiver

The envelope of the received signal can be explicitly used to provide an alternative approach to recover the information sequence, α from the received 2-MAMSK signal. In order to recover the information sequences α and β, it is necessary to obtain both the phase and envelope of the received 2-MAMSK signal. Figure 2-11 illustrates the block diagram of the differential phase and envelope detector. As shown in Figure 2-11, the non-coherent 2-MAMSK demodulator requires two stages to complete the process of detection. At the end of this section, we present the bit error probability performance of both the 2-MAMSK differential and non-coherent receivers.
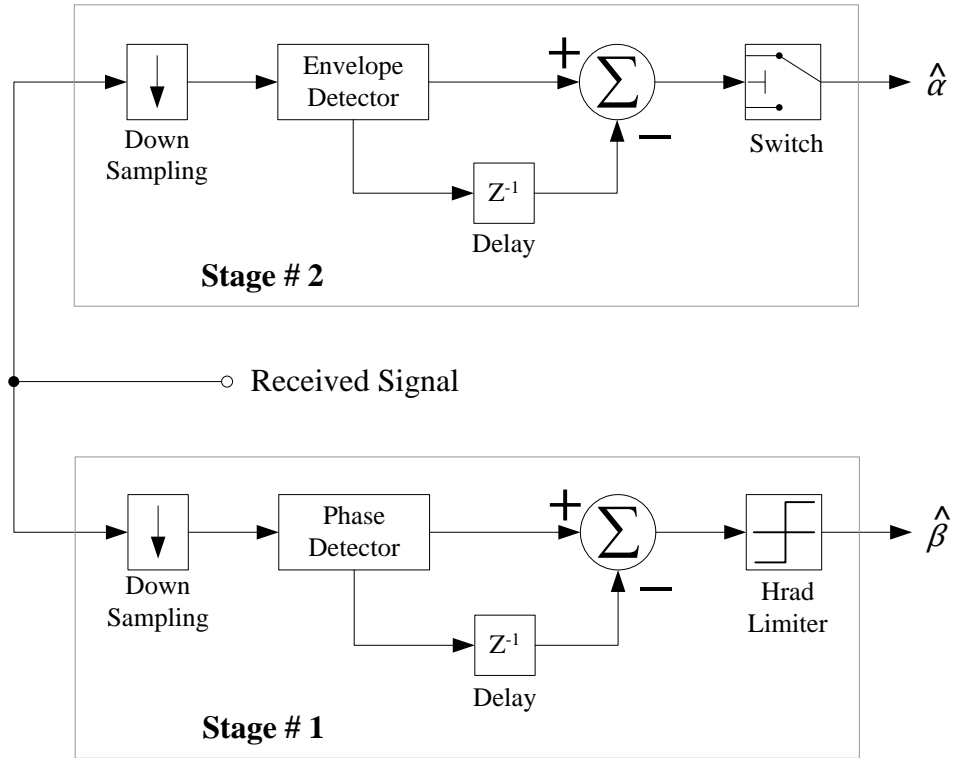
Figure 2-11 Block diagram of a non-coherent 2-MAMSK detector

From Figures 2-9 and 2-11, we observe that the first stage for both the differential and non-coherent receivers is identical. This means for the case of non-coherent detection, the process of recovering the information sequence, β transmitted by the larger MSK constituent is carried out in the same manner as in the case of the differential detector described earlier. However, the detection of the information sequence, α which is transmitted by the smaller MSK constituent, is based on the following observation:

a) The envelope of the received 2-MAMSK signal is constant between the symbol intervals if $\beta_n = \alpha_n$ (see time intervals $2T - 5T$ from Figure 2-8).

b) The envelope of the received 2-MAMSK signal varies between the symbol intervals if $\beta_n \neq \alpha_n$ (see time intervals $5T - 7T$ from Figure 2-8).

The Envelope Detector block extracts the envelope, $\rho(t, \alpha, \beta)$ from the received 2-MAMSK signal according to Equation (2.46). The difference in

envelope amplitudes, $\Delta\rho(nT, \alpha, \beta)$ between the symbol intervals is calculated by subtracting the envelope value delayed by one symbol from the current value. The difference in envelope values is the output of the summer given by,

$$\Delta\rho(nT, \alpha, \beta) = \rho(nT, \alpha, \beta) - \rho\big((n-1)T, \alpha, \beta\big). \tag{2.52}$$

From Figure 2-8, we observe that the difference in envelope values, $\Delta\rho$ is zero if $\beta_n = \alpha_n$ (i.e. the envelope does not change between these symbol intervals. For these symbol intervals we will simply end up with an MSK signal. This makes sense as MSK signals have constant envelope properties. For the cases where $\beta_n \neq \alpha_n$, the difference in envelope values at the time instants $t = NT$ is either -2 or 2. Accordingly, the calculated envelope difference, $\Delta\rho$ is then passed to the switch block and the switch selects its output based on the following conditions:

$$\hat{\alpha}_n = \begin{cases} \widehat{\beta}_n & if \quad \Delta\rho(nT, \alpha, \beta) \cong 0 \\ -\hat{\beta}_n & if \quad \Delta\rho(nT, \alpha, \beta) \neq 0 \end{cases} \tag{2.53}$$

where $\hat{\beta}$ is an estimate of the input data sequence, β and $\hat{\alpha}$ is an estimate of the input data sequence, α. In consequence, we have recovered the information sequences that are transmitted by the smaller and larger MSK constituents non-coherently.

As mentioned in chapter 1, 16-QAM offers the same data rate as a 2-MAMSK scheme. For this reason, the performance of the above two receivers are compared to that of 16-QAM in terms of error rate. The BER for Gray coded **16**-QAM on an AWGN channel given in [7, 8] as

$$P_b = \frac{3}{4} Q\left(\sqrt{\frac{4 E_b}{5 N_0}}\right), \tag{2.54}$$

where, E_b/N_0 is the average SNR per bit and $Q(x)$ is defined as

$$Q(x) = \frac{1}{\sqrt{2\pi}} \int_{x}^{\infty} e^{\frac{-t^2}{2}} \, dt \qquad (2.55)$$

The probability of a bit error, P_b for a 2-MAMSK signal and 16-QAM over an AWGN channel for multiple E_b/N_0 is plotted in Figure 2-12. The BER curve for 16-QAM is obtained from Equation (2.54), whereas the BER curves for 2-MAMSK are the results of simulations. The simulations were stopped after detecting 200 errors and at least 10×10^8 symbols were transmitted. From Figure 2-12, we can see that at high SNR ($i.e.\ E_b/N_0 \geq 10 \text{ dB}$), the differential receiver requires less than 1 dB of additional signal power per transmitted bit to achieve the same BER performance as theoretical 16-QAM. An additional 2 dB of average received signal power is required for the non-coherent 2-MAMSK receiver to achieve a comparable BER value.
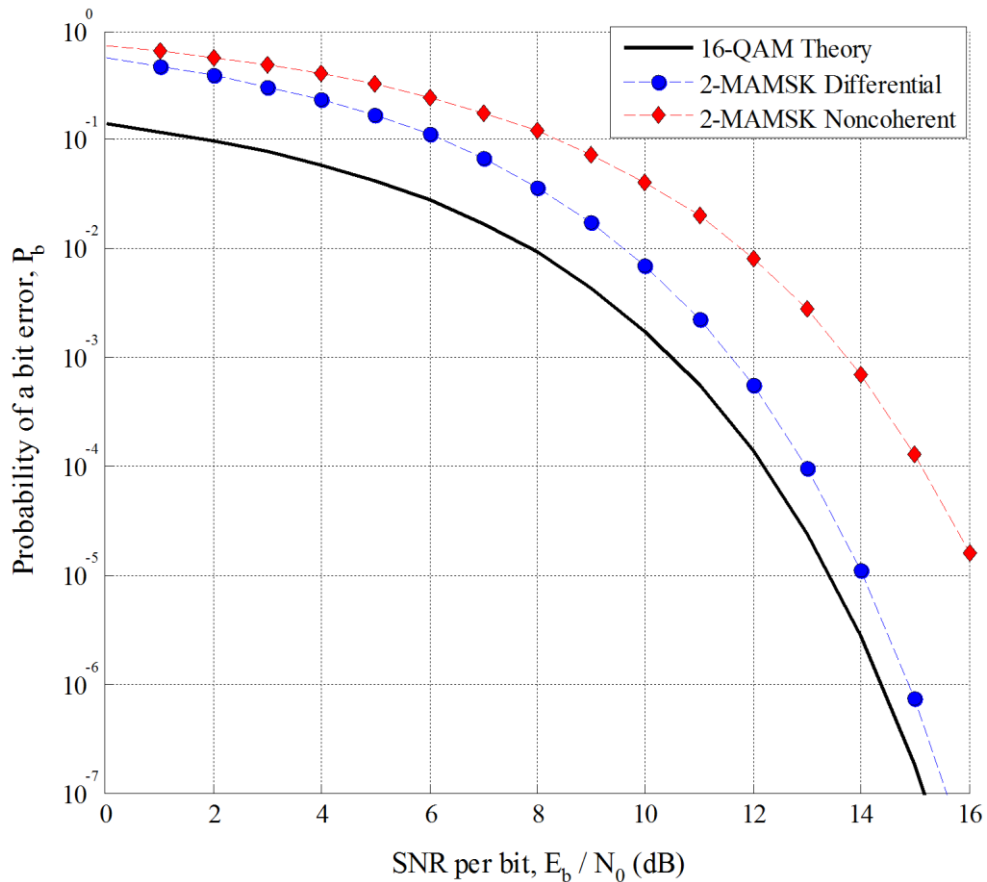
Figure 2-12 Probability of bit error for 2-MAMSK and 16-QAM in an AWGN

2.9 Space-Time Block Codes

Space-time block coding is a technique widely used in systems with multiple transmit and/or receive antennas. STBCs are used to provide diversity gain in wireless fading channels. A STBC scheme uses a sequence of ρ complex data symbols, $\{s_1,\ s_2,\ \dots,\ s_\rho\}$ to generate a code matrix, $\boldsymbol{S}$ of size $M \times \eta$, where M is the number of transmit antennas and η is the codeword block length. The matrix code, $\boldsymbol{S}$ is a linear function of these symbols and transmits the columns of $\boldsymbol{S}$ during η consecutive time intervals across the M antennas. The matrix code, $\boldsymbol{S}$ is defined in [91] as

$$S = \sum_{r=1}^{\rho} \left(s_r \boldsymbol{A}_r + s_r^* \boldsymbol{B}_r \right), \tag{2.56}$$

where s_r represents the complex data symbols for $r \in \{1, 2, \cdots, \rho\}$, $\boldsymbol{A}_r$ and $\boldsymbol{B}_r$ are fixed real-valued elementary code matrices of dimension $M \times \eta$.

A simple transmitter diversity scheme using two transmitter antennas was proposed by Alamouti in [6]. An extension to more than two transmitter antennas was presented in [5], where it was shown that the well-known Alamouti scheme is a special case of a STBC. The data rate, R of the STBCs is defined as

$$R = \frac{\rho}{\eta} \text{ symbols per time interval} \tag{2.57}$$

where ρ is the number of data symbols and η is the number of time slots in a STBC codeword.

2.9.1 The Alamouti Scheme

The case when the number of transmit antenna, $M = 2$ is a simple case of the above scheme and is known as the Alamouti code [6]. With $\rho = \eta = 2$ the scheme achieves full diversity and hence full data rate of $R = 1$. The

scheme works over two symbol periods where it is assumed that the channel gain is constant over this time. Over the first symbol period two different symbols s_1 and s_2 each with symbol energy $E_s/2$ are transmitted simultaneously from antennas 1 and 2, respectively. Over the next symbol period symbol $-s_2^*$ is transmitted from antenna 1 and symbol s_1^* is transmitted from antenna 2, each with symbol energy $E_s/2$. Accordingly, the space-time matrix code, $\boldsymbol{S}$ can be defined as

$$\boldsymbol{S} = \begin{bmatrix} s_1 & -s_2^* \\ s_2 & s_1^* \end{bmatrix}, \tag{2.58}$$

where each row denotes the separate transmitters and the columns represent transmission over the two symbol periods.

The Alamouti model for a 2×2 MIMO system is shown in Figure 2-13.
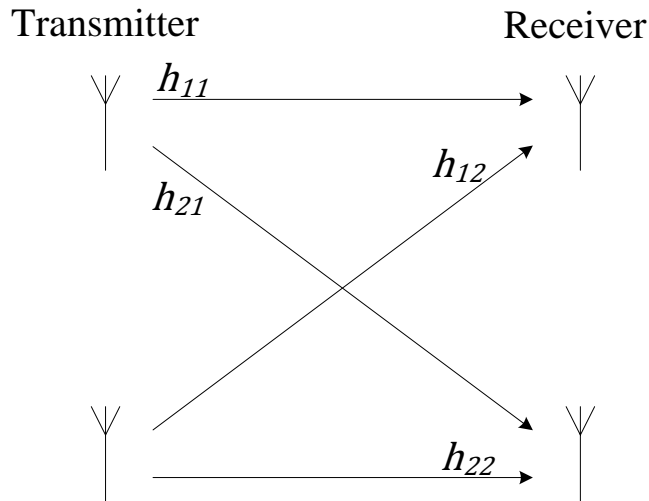
Figure 2-13 Alamouti scheme with two transmit and two receiver antennas

For a flat fading channel the channel gain matrix, $\boldsymbol{H}$ is given by

$$\boldsymbol{H} = \begin{bmatrix} h_{11} & h_{12} \\ h_{21} & h_{22} \end{bmatrix} \tag{2.59}$$

The received signal, R at the receiver then becomes,

$$R = H\,S + N, \tag{2.60}$$

where, N is a complex AWGN noise matrix at the receiver defined as

$$N = \begin{bmatrix} n_{11} & n_{12} \\ n_{21} & n_{22} \end{bmatrix}. \tag{2.61}$$

Then, the received signal, R can be written in the form,

$$R = \begin{bmatrix} r_{11} & r_{12} \\ r_{21} & r_{22} \end{bmatrix} = \begin{bmatrix} h_{11} & h_{12} \\ h_{21} & h_{22} \end{bmatrix} \begin{bmatrix} s_1 & -s_2^* \\ s_2 & s_1^* \end{bmatrix} + \begin{bmatrix} n_{11} & n_{12} \\ n_{21} & n_{22} \end{bmatrix}. \tag{2.62}$$

Equation (2.62) can be rearranged to obtain the following:

$$\begin{bmatrix} r_{11} \\ r_{21} \\ r_{12}^* \\ r_{22}^* \end{bmatrix} = \begin{bmatrix} h_{11} & h_{12} \\ h_{21} & h_{22} \\ h_{12}^* & h_{11}^* \\ h_{22}^* & h_{21}^* \end{bmatrix} \begin{bmatrix} s_1 \\ s_2 \end{bmatrix} + \begin{bmatrix} n_{11} \\ n_{21} \\ n_{12}^* \\ n_{22}^* \end{bmatrix} \tag{2.63}$$

The above equation implies that the signals s_1 and s_2 are transmitted via two orthogonal paths and hence linear maximum likelihood detection can be used to detect the signals independently. Consequently, using the Alamouti code provides higher diversity gain and does not require complicated receiver detection. Tarokh et al [5] discovered that the Alamouti scheme can be generalised to, $M > 2$ when the constellations are real, but if the constellations are complex the generalisation is only possible with a reduction in code rate.

Chapter 3

Characteristics of MAMSK Signals

3.1   Introduction

Minimum shift keying (MSK) is an attractive modulation scheme for wireless communications due to its useful characteristics of constant envelope and fast spectral roll-off [71, 74, 76, 92]. Multi level (M) multi-amplitude minimum shift keying (M-MAMSK) is a generalisation of MSK where the signal amplitude is allowed to vary over a set of well-defined values. Throughout earlier chapters, we have demonstrated the potentials and advantages of M-MAMSK signals. However, there are few papers [1, 2, 42-44, 83] discussing MAMSK signals and it has been characterised based on observations from simulation results.

In this chapter, we analytically characterise M-MAMSK signals, where performance can be defined by its phase and envelope variations, power and spectral efficiencies and decoding error probability. The overall phase values of M-MAMSK signal at the symbol transition times are identical to those of MSK. This characteristic is important as it allows low-complexity

differential detection of MAMSK signals. The M-MAMSK signal phase can evolve from on state to another via a linear or non-linear path; the specific path depends on the input data sequences and the phase differences between the MSK components. For M-MAMSK there are 2^{2M} distinct trajectories in the signal space diagram with each being specified by $2M$ input data bit. The power spectral density of M-MAMSK is identical to that of MSK but for a given data rate it is M times narrower. The theoretical bit error rate for M-MAMSK in AWGN is derived. The results show that M-MAMSK provides almost identical bit error performance to square M-QAM.

This chapter is organised as follows. After the definition of MAMSK, we analyse the overall phase of 2-MAMSK signal in great detail, then extend the idea to M-MAMSK for $M > 2$. The signal space diagram, power spectral density and probability of bit error for M-MAMSK are discussed in the following sections. The last section summarises the main points.

3.2   The Signal Description

In this section, we briefly review a 2-MAMSK modulated signal in order to explore its characteristics. A 2-MAMSK signal, as described in detail in sections 2.4 and 2.5, is obtained by superposition of two MSK signals with different amplitudes and may be expressed as

$$s(t, \alpha, \beta) = s_{MSK\,1}(t, \alpha) + s_{MSK\,2}(t, \beta)$$

$$= \sqrt{\frac{2E}{5T}} \left(\cos[2\pi f_c t + \phi(t, \alpha)] + 2\cos[2\pi f_c t + \phi(t, \beta)] \right)$$

(3.1)

where, $s_{MSK\,1}(t, \alpha)$ is the MSK component with the smaller amplitude, $s_{MSK\,2}(t, \beta)$ is that with the larger amplitude, f_c is the carrier frequency, E is the average signal energy per symbol interval and T is the duration of a symbol interval. The sequences α and β represent input data with values ± 1. $\phi(t, \alpha)$ and $\phi(t, \beta)$ are the information carrying parts of the MSK signal phases.

3.3 Analysis of Phase Tree and Trellis

The baseband representation of a 2-MAMSK signal can be expressed in polar form as a product of the signal envelope, $\rho(t, \alpha, \beta)$ and the real part of the overall signal phase, $\phi(t, \alpha, \beta)$ as

$$s(t, \alpha, \beta) = \rho(t, \alpha, \beta) \, \cos\big(\phi(t, \alpha, \beta)\big). \tag{3.2}$$

In chapter 2, we have shown that the signal envelope can be expressed as

$$\rho(t, \alpha, \beta) = \sqrt{5 + 4\cos[\phi(t, \beta) - \phi(t, \alpha)]}, \tag{3.3}$$

and the overall 2-MAMSK signal phase is given by,

$$\phi(t, \alpha, \beta) = \tan^{-1}\left[\frac{\sin \phi(t, \alpha) + 2\sin \phi(t, \beta)}{\cos \phi(t, \alpha) + 2\cos \phi(t, \beta)}\right], nT \le t \le (n+1)T \tag{3.4}$$

To demonstrate Equation (3.4), we sketch a set of phase trajectories, $\phi(t, \alpha, \beta)$ generated by all possible values of the information sequences, α and β. The set of phase trajectories beginning at time $t = 0$ is shown in Figure 3-1. This phase diagram is called the phase tree. It can be noted that the phase tree for all possible combinations is continuous and grows with time. The phase values at the transition points in Figure 3-1 are represented by small black circles.

From Figure 3-1, we observe that the phase trajectories for a 2-MAMSK signal can be piecewise linear or nonlinear functions. The phase behaviour depends on the value of α, β and the phase difference between the two MSK signals. For example, when $\alpha = \beta$ the phase follows the linear paths regardless of the phase difference between them. For $\alpha \ne \beta$, the phase follows the nonlinear paths. However, the specific nonlinear path is determined by the phase difference between the two MSK signals; we will come back to this point later. The phase trajectory generated by the information sequences, $\alpha = \{+1, +1, +1, -1\}$ and $\beta = \{+1, -1, -1, +1\}$ for a 2-MAMSK is illustrated in Figure 3-2.

51
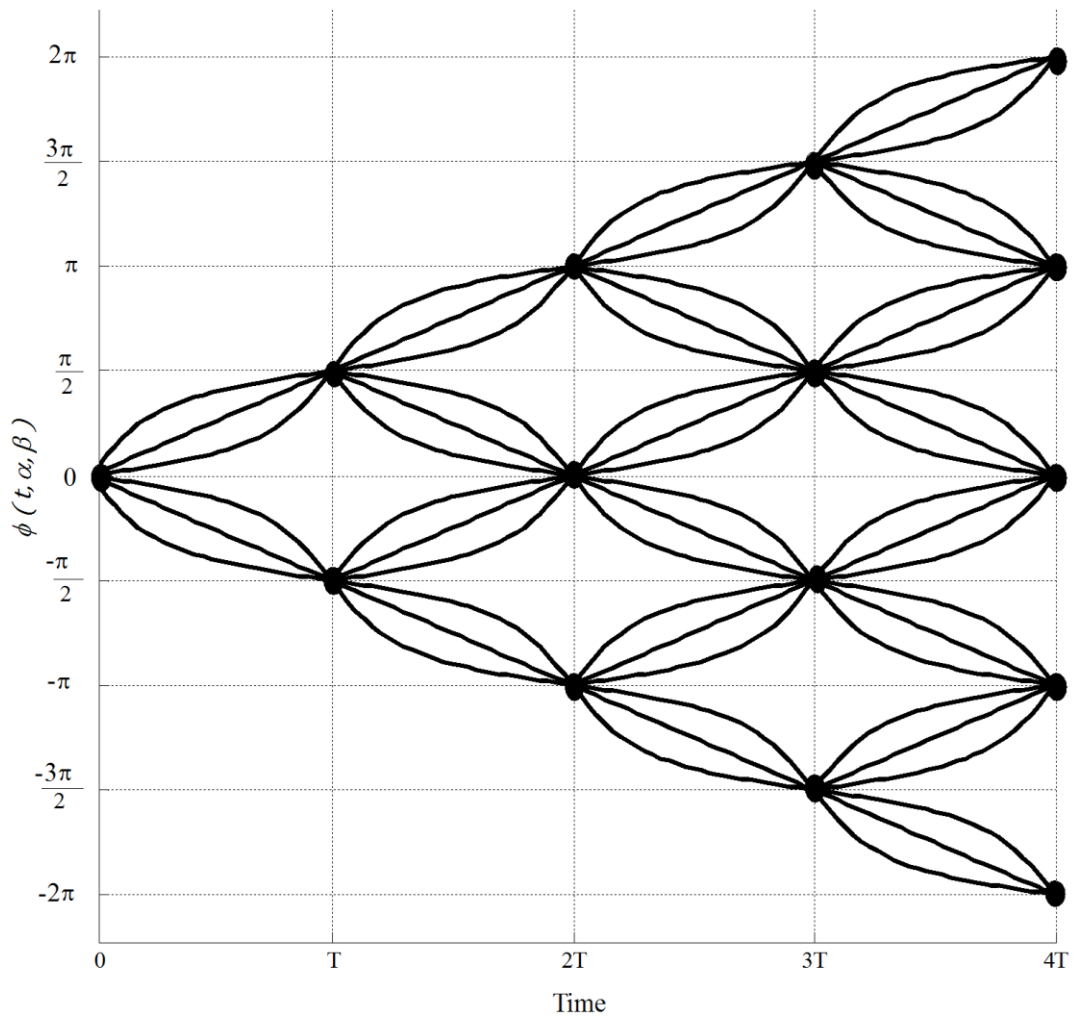
Figure 3-1 Phase tree for a 2-MAMSK signal

		π		π		0		π		0
α	+1		+1		+1		-1	
β	+1		-1		-1		+1	
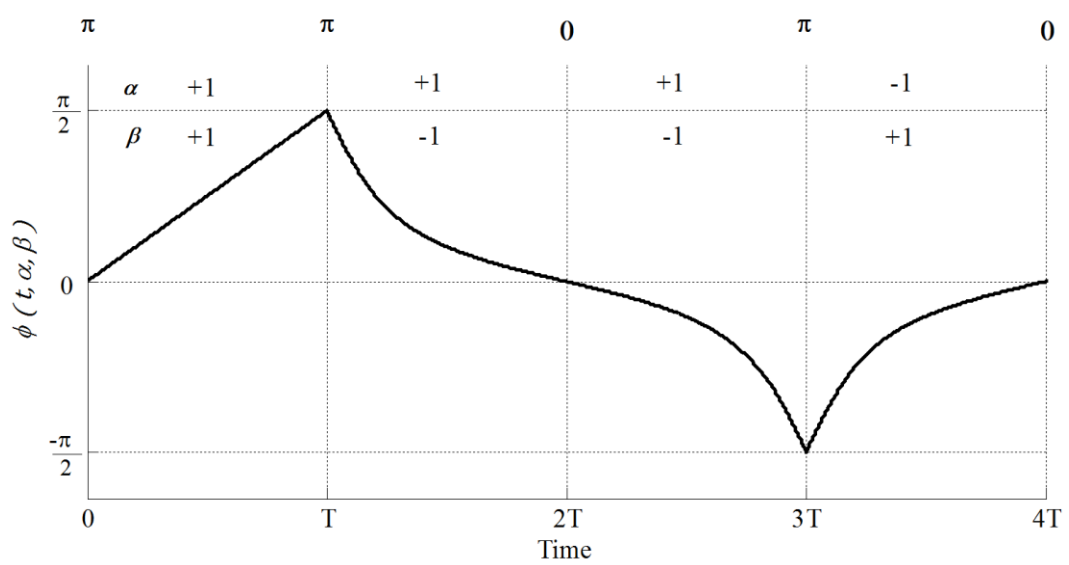
Figure 3-2 Phase trajectory of 2-MAMSK for a given α and β

The set of phase values $\{\pi, \pi, 0, \pi, 0\}$ shown at the top of Figure 3-2 represent the phase differences between the two MSK signals at the time instants $t = nT$. For demonstration purposes, we have set the initial phase difference at $t = 0$ between the two MSK signals to be π radians. This is to show that when $\alpha = \beta$ the overall phase selects the linear path regardless of the value of the phase difference. Since, the 2-MAMSK signal components are based on MSK modulation and during the first time interval $\alpha = \beta = +1$, then the phase of both MSK components ramp up linearly by $\pi/2$. Hence, the phase difference between them at the time instant $t = T$ remains at π radians. Then the overall phase of the 2-MAMSK signal selects the nonlinear path below the linear line.

In the next time interval, $\alpha = -\beta = +1$, these values cause the phase of the larger MSK component to decrease linearly by $\pi/2$ and the phase of the smaller MSK component increase linearly by $\pi/2$. This adds an additional π radians onto the current phase difference of π radians. Thus, the phase difference becomes zero at the time instant $t = 2T$, viewed modulo 2π. Then the overall phase of the 2-MAMSK signal selects the nonlinear path above the linear line. For the remaining time intervals the process repeats. In the remaining part of this section, we explicitly show this process in addition to proving that the overall 2-MAMSK signal phase at the symbol transitions (i.e. at the time instants $t = nT$) will always equal the phase of the larger MSK signal. In other words, we need to prove

$$\phi(nT, \alpha, \beta) = \phi(nT, \beta), \tag{3.5}$$

where, $\phi(nT, \alpha, \beta)$ and $\phi(nT, \beta)$ are the phases of the 2-MAMSK and larger MSK signals respectively, sampled at the time instants $t = nT$.

Proof: Let us start with the smaller MSK component. The phase of the smaller MSK signal defined in (2.16) may written as

$$\phi(t, \alpha) = \theta_n + \frac{\pi}{2T}\alpha_n(t - nT), \qquad nT \le t \le (n+1)T \tag{3.6}$$

where the term θ_n can be expressed as

$$\theta_n = \frac{\pi}{2} \sum_{k=-\infty}^{n-1} \alpha_k \tag{3.7}$$

It can be noted from Equations (3.6) and (3.7) that θ_n represents the build up of all symbols up to time $(n-1)T$. Now we can expand equation (3.6) further as follow, to note that the phase of the carrier in the interval, $nT \le t \le (n+1)T$, is

$$\begin{aligned}
\phi(t, \alpha) &= \frac{\pi}{2T} \alpha_n t - \frac{n\pi}{2} \alpha_n + \theta_n \\
&= \frac{\pi}{2T} \alpha_n t + \tilde{\theta}_n.
\end{aligned} \tag{3.8}$$

This shows that the phase, $\phi(t, \alpha)$ of the signal increases or decreases linearly with time during each bit interval of T seconds, where the term $\tilde{\theta}_n$ is phase of the carrier signal and defined as

$$\tilde{\theta}_n = \theta_n - \frac{n\pi}{2} \alpha_n \tag{3.9}$$

We now evaluate Equation (3.8) at the symbol transitions (terminals) to demonstrate the state transitions at the time instants $t = nT$. Now for, $nT \le t \le (n+1)T$, Equation (3.8) can be written as

$$\phi_n(t, \alpha) = \frac{\pi}{2T} \alpha_n t + \tilde{\theta}_n, \tag{3.10}$$

and for, $(n-1)T \le t \le nT$, Equation (3.8) can be expressed as

$$\phi_{(n-1)}(t, \alpha) = \frac{\pi}{2T} \alpha_{(n-1)} t + \tilde{\theta}_{(n-1)} \tag{3.11}$$

Since, the phase must be continuous at the symbol transitions, we can establish a boundary condition at $t = nT$ that

$$\phi_{(n-1)}(nT, \alpha) = \phi_n(nT, \alpha) \tag{3.12}$$

Thus, we have

$$\frac{\pi}{2}\alpha_{(n-1)}n + \tilde{\theta}_{(n-1)} = \frac{\pi}{2}\alpha_n n + \tilde{\theta}_n \tag{3.13}$$

Rearranging Equation (3.13) for $\tilde{\theta}_n$ we have

$$\tilde{\theta}_n = \tilde{\theta}_{(n-1)} + \frac{n\pi}{2}\left(\alpha_{(n-1)} - \alpha_n\right) \tag{3.14}$$

Since, α is a sequence of information binary symbols taking values from the set $\{+1, -1\}$, then from Equation (3.14), we can observe two possible cases

Case I: when $\alpha_{(n-1)} = \alpha_n$, then

$$\tilde{\theta}_n = \tilde{\theta}_{(n-1)} \tag{3.15}$$

Case II: when $\alpha_{(n-1)} \neq \alpha_n$, then

$$\tilde{\theta}_n = \tilde{\theta}_{(n-1)} \pm n\pi \tag{3.16}$$

Without the loss of generality, we set the initial phase of the carrier as $\tilde{\theta}_0 = 0$ and then we get

$$\tilde{\theta}_n\big|_{\mod 2\pi} = 0 \text{ or } \pi \tag{3.17}$$

Now imposing these results on Equation (3.8), then we have

$$\phi(t) = \pm \frac{\pi}{2T}t + 0 \text{ or } \pi \tag{3.18}$$

The $+$ sign corresponds to $\alpha_n = +1$ and the $-$ sign corresponds to $\alpha_n = -1$. Thus, we have a phase difference over one bit interval with respect to the phase of the carrier signal of $+\pi/2$ or $-\pi/2$ corresponding to $\alpha_n = +1$ and $\alpha_n = -1$ respectively. In other words, the phase of an MSK signal increases by $+\pi/2$ when we send $+1$ and decreases by $-\pi/2$ when we

send -1. When we view the phase given in Equation (3.18), modulo 2π, say in the range $-\pi$ and π, then we can show that the phase can take only the two values of $\pm\pi/2$ at odd multiples of T (i.e. $t = (2k + 1)T$) and only the two values 0 and π at even multiples of T (i.e. $t = 2kT$). The result is summarised in Table 3-1.

$\tilde{\theta}_n$	$\phi(T)$	α_n
0	$+\pi/2$	$+1$
0	$-\pi/2$	-1
π	$+\pi/2$	-1
π	$-\pi/2$	$+1$

Table 3-1 Possible phase states of MSK signal in the range $(-\pi, \pi)$

Table 3-1 shows that the MSK signal phase may take one of four possible values depending on the values of $\tilde{\theta}_n$ and $\phi(T)$. For all possible cases shown in Table 3-1, we can see that the variation of the phase over the duration of an interval is $\pm\pi/2$. A similar approach can be applied to describe the phase of the larger MSK signal, $\phi(t,\beta)$. Then the phase of the larger MSK signal is also $\pm\pi/2$ at odd multiples of T and 0 and π at even multiples of T.

Now summarising and assuming that both α and β are related to two independent binary information sequences each taking values from the set $\{+1, -1\}$, we can conclude the following:

Case I: When t is an odd multiple of T

At odd multiples of T, both $\phi(t,\alpha)$ and $\phi(t,\beta)$ can have independently one of two possible values $\pm\pi/2$, or equivalently

$$\phi(t,\alpha) = \pm\frac{\pi}{2} \qquad (3.19)$$

$$\phi(t,\beta) = \pm\frac{\pi}{2} \tag{3.20}$$

Case II: When t is an even multiple of T

At even multiples of T, both $\phi(t,\alpha)$ and $\phi(t,\beta)$ can have independently one of two possible values 0 or π, or equivalently

$$\phi(t,\alpha) = 0 \text{ or } \pi \tag{3.21}$$

$$\phi(t,\beta) = 0 \text{ or } \pi \tag{3.22}$$

To evaluate all possible combination of $\phi(t,\alpha)$ and $\phi(t,\beta)$ at the time instants $t = nT$, we need to split n into even and odd portions. From the definition of odd and even numbers we have

$$n = \begin{cases} 2k, & \text{for even } n \\ 2k+1, & \text{for odd } n \end{cases} \tag{3.23}$$

where k is an integer. All possible groupings of $\phi(nT,\alpha)$ and $\phi(nT,\beta)$ are shown in Table 3-2.

Time instants $t = nT$	$\phi(t,\alpha)$	$\phi(t,\beta)$
$t = 2kT$	0	0
$t = 2kT$	0	π
$t = 2kT$	π	0
$t = 2kT$	π	π
$t = (2k+1)T$	$-\dfrac{\pi}{2}$	$-\dfrac{\pi}{2}$
$t = (2k+1)T$	$-\dfrac{\pi}{2}$	$+\dfrac{\pi}{2}$
$t = (2k+1)T$	$+\dfrac{\pi}{2}$	$-\dfrac{\pi}{2}$
$t = (2k+1)T$	$+\dfrac{\pi}{2}$	$+\dfrac{\pi}{2}$

Table 3-2   All possible combination of $\phi(t,\alpha)$ and $\phi(t,\beta)$ at $t = nT$

To show that the overall phase of 2-MAMSK is equal to the phase of the larger MSK signal at the symbol transition points, we have to prove that equality holds in (3.5) for all possible combinations of $\phi(nT, \alpha)$ and $\phi(nT, \beta)$ shown in Table 3-2. Recall that the overall 2-MAMSK signal phase at the time instants $t = nT$ is given by

$$\phi(nT, \alpha, \beta) = \tan^{-1} \left[\frac{\sin \phi(nT, \alpha) + 2 \sin \phi(nT, \beta)}{\cos \phi(nT, \alpha) + 2 \cos \phi(nT, \beta)} \right] \tag{3.24}$$

Let $y = \sin \phi(nT, \alpha) + 2 \sin \phi(nT, \beta)$ and $x = \cos \phi(nT, \alpha) + 2 \cos \phi(nT, \beta)$. Then (3.24) gives

$$\phi(nT, \alpha, \beta) = \tan^{-1} \frac{y}{x}. \tag{3.25}$$

When n is even (i.e. $n = 2k$), we have

$$y = \sin(0 \text{ or } \pi) + 2 \sin(0 \text{ or } \pi) \quad \text{and} \quad x = \cos(0 \text{ or } \pi) + 2 \cos(0 \text{ or } \pi).$$

Since, $\sin 0 = \sin \pi = 0$, then $y = 0$ for all possible combinations of even multiples of n, and also $\cos 0 = -\cos \pi = 1$, then $x = \pm 1 + 2(\pm 1)$, where the term $+1$ corresponds to $\cos 0$ and the -1 term corresponds to $\cos \pi$. Now from the definition of arctangent in the range of $-\pi$ and π we have

$$\phi(2kT, \alpha, \beta) = \tan^{-1} \left(\frac{y}{x} \right) = \begin{cases} 0, & y = 0, \ x > 0 \\ \pi, & y = 0, \ x < 0 \end{cases} \tag{3.26}$$

Equation (3.26) shows that the phase of the 2-MAMSK signal at even multiples of n is either 0 or π, depending on the sign of x. Consequently, the overall 2-MAMSK phase, $\phi(2kT, \alpha, \beta)$ at even multiples of nT is 0 when x is positive and π when x is negative. It is clear that the second term of x is dominant in determining the sign, due to the fact that there is a factor of "2" associated with it. We know that the multiplier "2" corresponds to the amplitude of the larger MSK signal being twice the amplitude of the smaller MSK component. Thus, we have established that the 2-MAMSK phase at symbol transition times is equal to the phase of the larger MSK component

for even multiples of n. The remaining task is to show that Equation (3.5) is also true at odd multiples of n.

When n is odd (i.e. $n = 2k + 1$), we have

$$y = \sin\left(\pm\frac{\pi}{2}\right) + 2\sin\left(\pm\frac{\pi}{2}\right) \quad \text{and} \quad x = \cos\left(\pm\frac{\pi}{2}\right) + 2\cos\left(\pm\frac{\pi}{2}\right).$$

Since, $\cos\frac{\pi}{2} = \cos-\frac{\pi}{2} = 0$, then $x = 0$ for all possible combinations of odd multiples of n. Also $\sin\frac{\pi}{2} = -\sin-\frac{\pi}{2} = 1$, then we have $y = \pm 1 + 2(\pm 1)$. Where, the term $+1$ corresponds to $\sin\frac{\pi}{2}$ and the -1 term corresponds to $\sin-\frac{\pi}{2}$. Now from the definition of arctangent in the range of $-\pi$ and π we have

$$\phi((2k+1)T, \alpha, \beta) = \tan^{-1}\left(\frac{y}{x}\right) = \begin{cases} +\dfrac{\pi}{2}, & x = 0, \ y > 0 \\[2mm] -\dfrac{\pi}{2}, & x = 0, \ y < 0 \end{cases} \tag{3.27}$$

Similar to the situation for even multiples of nT, the overall 2-MAMSK phase value at odd multiples of nT is determined by the sign of the term y. Since, there is a multiplier of "2" coupled with the second term of y, then the sign of y is always determined from the sign of the second term. This factor of "2" is associated with the larger MSK signal. From Equation (3.27), we can clearly see that the overall 2-MAMSK phase at odd multiples of nT always equals the phase of the larger MSK signal.

Instead of the above explanation, we could simply evaluate the 2-MAMSK signal phase for all possible combinations of $\phi(nT, \alpha)$ and $\phi(nT, \beta)$ as shown in Table 3-3. Note, the values of 2-MAMSK signal phase, $\phi(nT, \alpha, \beta)$ shown in Table 3-3, were calculated based on Equation (3.24). From Table 3-3, we can see that the overall 2-MAMSK phase values at the time instants $t = nT$ are the same as the phase values of the larger MSK signal, for all combinations of $\phi(t, \alpha)$ and $\phi(t, \beta)$.

Time instants $t = nT$	$\phi(t, \alpha)$	$\phi(t, \beta)$	$\phi(t, \alpha, \beta)$
$t = 2kT$	0	0	0
$t = 2kT$	0	π	π
$t = 2kT$	π	0	0
$t = 2kT$	π	π	π
$t = (2k+1)T$	$-\dfrac{\pi}{2}$	$-\dfrac{\pi}{2}$	$-\dfrac{\pi}{2}$
$t = (2k+1)T$	$-\dfrac{\pi}{2}$	$+\dfrac{\pi}{2}$	$+\dfrac{\pi}{2}$
$t = (2k+1)T$	$+\dfrac{\pi}{2}$	$-\dfrac{\pi}{2}$	$-\dfrac{\pi}{2}$
$t = (2k+1)T$	$+\dfrac{\pi}{2}$	$+\dfrac{\pi}{2}$	$+\dfrac{\pi}{2}$

Table 3-3 Overall 2-MAMSK phase $\boldsymbol{\phi(t, \alpha, \beta)}$ at the time instants $\boldsymbol{t = nT}$

We have evaluated 2-MAMSK phase values at the ends of each bit period (at the time instants $t = nT$). The next step is to consider how the 2-MAMSK phase changes over the time intervals $(nT \leq t \leq (n+1)T)$. Based on Equation (3.8), the phase of the larger and smaller MSK signals over the duration of an interval with respect to the phase of the carrier signal is given in Table 3-4, for all possible value of α and β.

$\phi(t, \alpha)$	α
$-\dfrac{\pi}{2T}t + 0$	-1
$+\dfrac{\pi}{2T}t + 0$	$+1$
$-\dfrac{\pi}{2T}t + \pi$	-1
$+\dfrac{\pi}{2T}t + \pi$	$+1$

$\phi(t, \beta)$	β
$-\dfrac{\pi}{2T}t + 0$	-1
$+\dfrac{\pi}{2T}t + 0$	$+1$
$-\dfrac{\pi}{2T}t + \pi$	-1
$+\dfrac{\pi}{2T}t + \pi$	$+1$

a) Smaller MSK phase relative to α b) Larger MSK phase relative to β

Table 3-4 Possible MSK signal phase variation with in a symbol interval

To establish how the 2-MAMSK phase evolves with time, we need to consider all possible combinations of $\phi(t, \alpha)$ and $\phi(t, \beta)$ shown in Table 3-4. For the case where $\alpha = \beta$, the initial carrier phase of the larger MSK signal is 0 and the initial carrier phase of the smaller MSK signal can be 0 or π, we have

$$
\begin{aligned}
\phi(nt, \alpha, \beta) &= \tan^{-1} \left[\frac{\sin\left(\frac{\pi}{2}\alpha t + 0 \text{ or } \pi\right) + 2\sin\left(\frac{\pi}{2}\beta t\right)}{\cos\left(\frac{\pi}{2}\alpha t + 0 \text{ or } \pi\right) + 2\cos\left(\frac{\pi}{2}\beta t\right)} \right] \\
&= \tan^{-1} \left[\frac{\pm \sin\left(\frac{\pi}{2}\alpha t\right) + 2\sin\left(\frac{\pi}{2}\beta t\right)}{\pm \cos\left(\frac{\pi}{2}\alpha t\right) + 2\cos\left(\frac{\pi}{2}\beta t\right)} \right] \\
&= \tan^{-1} \left[\frac{\sin\left(\frac{\pi}{2}\beta t\right)}{\cos\left(\frac{\pi}{2}\beta t\right)} \right] \\
&= \frac{\pi}{2}\beta t.
\end{aligned}
\tag{3.28}
$$

For the case when $\alpha = \beta$, the initial carrier phase of the larger MSK signal is π and the initial carrier phase of the smaller MSK signal can be 0 or π. We have

$$
\begin{aligned}
\phi(nt, \alpha, \beta) &= \tan^{-1} \left[\frac{\sin\left(\frac{\pi}{2}\alpha t + 0 \text{ or } \pi\right) + 2\sin\left(\frac{\pi}{2}\beta t + \pi\right)}{\cos\left(\frac{\pi}{2}\alpha t + 0 \text{ or } \pi\right) + 2\cos\left(\frac{\pi}{2}\beta t + \pi\right)} \right] \\
&= \tan^{-1} \left[\frac{\pm \sin\left(\frac{\pi}{2}\alpha t\right) - 2\sin\left(\frac{\pi}{2}\beta t\right)}{\pm \cos\left(\frac{\pi}{2}\alpha t\right) - 2\cos\left(\frac{\pi}{2}\beta t\right)} \right] \\
&= \tan^{-1} \left[\frac{-\sin\left(\frac{\pi}{2}\beta t\right)}{-\cos\left(\frac{\pi}{2}\beta t\right)} \right] \\
&= \tan^{-1} \left[\frac{\sin\left(\frac{\pi}{2}\beta t + \pi\right)}{\cos\left(\frac{\pi}{2}\beta t + \pi\right)} \right] \\
&= \frac{\pi}{2}\beta t + \pi
\end{aligned}
\tag{3.29}
$$

From Equations (3.28) and (3.29), we can see that when $\alpha = \beta$ the 2-MAMSK phase variation over one bit interval is exactly same as the phase variation of the larger MSK signal, regardless of the initial carrier phase of the smaller MSK signal. Thus, 2-MAMSK phase for the time intervals $\alpha = \beta$ linearly increases by $+\pi/2$ for $\alpha = \beta = +1$ and linearly decreases by $-\pi/2$ for $\alpha = \beta = -1$. This result is as expected because when $\alpha = \beta$ we get two MSK signal exactly on top of each other, hence the superimposed signal is also an MSK signal.

For the case when $\alpha \neq \beta$ and the initial carrier phase of both the larger and smaller MSK signals are 0. We have

$$\phi(nt, \alpha, \beta) = \tan^{-1}\left[\frac{\sin\left(\frac{\pi}{2}\alpha t\right) + 2\sin\left(\frac{\pi}{2}\beta t\right)}{\cos\left(\frac{\pi}{2}\alpha t\right) + 2\cos\left(\frac{\pi}{2}\beta t\right)}\right] \tag{3.30}$$

Since, $\alpha \neq \beta$, $\cos -x = \cos x$ and both α and β taking values from the set $\{-1, +1\}$, then Equation (3.30) becomes

$$\phi(nt, \alpha, \beta) = \tan^{-1}\left[\frac{\pm \sin\left(\frac{\pi}{2}t\right)}{3\cos\left(\frac{\pi}{2}t\right)}\right] \tag{3.31}$$

Thus, we have

$$\phi(nt, \alpha, \beta) = \tan^{-1}\left[\pm\frac{1}{3}\tan\left(\frac{\pi t}{2}\right)\right], \tag{3.32}$$

where the $+$ corresponds to the case when $-\alpha = +\beta = +1$ and the $-$ corresponds to the case when $-\alpha = +\beta = -1$. Hence, Equation (3.32) reduces to

$$\phi(nt, \alpha, \beta) = \tan^{-1}\left[\frac{1}{3}\beta\tan\left(\frac{\pi}{2}t\right)\right] \tag{3.33}$$

For the case when $\alpha \neq \beta$ and the initial carrier phase of the larger and smaller MSK signals are 0 and π respectively. We have

$$\phi(nt, \alpha, \beta) = \tan^{-1} \left[\frac{\sin\left(\frac{\pi}{2}\alpha t + \pi\right) + 2\sin\left(\frac{\pi}{2}\beta t\right)}{\cos\left(\frac{\pi}{2}\alpha t + \pi\right) + 2\cos\left(\frac{\pi}{2}\beta t\right)} \right]$$

$$= \tan^{-1} \left[\frac{-\sin\left(\frac{\pi}{2}\alpha t\right) + 2\sin\left(\frac{\pi}{2}\beta t\right)}{-\cos\left(\frac{\pi}{2}\alpha t\right) + 2\cos\left(\frac{\pi}{2}\beta t\right)} \right]$$

$$= \tan^{-1} \left[\frac{\pm 3\sin\left(\frac{\pi}{2}t\right)}{\cos\left(\frac{\pi}{2}t\right)} \right] \tag{3.34}$$

$$= \tan^{-1} \left[\pm 3 \tan\left(\frac{\pi}{2}t\right) \right]$$

$$= \tan^{-1} \left[3\beta \tan\left(\frac{\pi}{2}t\right) \right]$$

For the case when $\alpha \neq \beta$ and initial carrier phase of the larger and smaller MSK signals are π and 0 respectively. We have

$$\phi(nt, \alpha, \beta) = \tan^{-1} \left[\frac{\sin\left(\frac{\pi}{2}\alpha t\right) + 2\sin\left(\frac{\pi}{2}\beta t + \pi\right)}{\cos\left(\frac{\pi}{2}\alpha t\right) + 2\cos\left(\frac{\pi}{2}\beta t + \pi\right)} \right]$$

$$= \tan^{-1} \left[\frac{\sin\left(\frac{\pi}{2}\alpha t\right) - 2\sin\left(\frac{\pi}{2}\beta t\right)}{\cos\left(\frac{\pi}{2}\alpha t\right) - 2\cos\left(\frac{\pi}{2}\beta t\right)} \right]$$

$$= \tan^{-1} \left[\frac{\mp 3\sin\left(\frac{\pi}{2}t\right)}{-\cos\left(\frac{\pi}{2}t\right)} \right]$$

$$= \tan^{-1} \left[\frac{-3\beta \sin\left(\frac{\pi}{2}t\right)}{-\cos\left(\frac{\pi}{2}t\right)} \right] \tag{3.35}$$

$$= \tan^{-1} \left[\frac{3\beta \sin\left(\frac{\pi}{2}t + \pi\right)}{\cos\left(\frac{\pi}{2}t + \pi\right)} \right]$$

$$= \tan^{-1} \left[3\beta \tan\left(\frac{\pi}{2}t + \pi\right) \right]$$

For the case when $\alpha \neq \beta$ and the initial carrier phase of both the larger and smaller MSK signals are π. We have

$$\phi(nt, \alpha, \beta) = \tan^{-1}\left[\frac{\sin\left(\frac{\pi}{2}\alpha t + \pi\right) + 2\sin\left(\frac{\pi}{2}\beta t + \pi\right)}{\cos\left(\frac{\pi}{2}\alpha t + \pi\right) + 2\cos\left(\frac{\pi}{2}\beta t + \pi\right)}\right]$$

$$= \tan^{-1}\left[\frac{-\sin\left(\frac{\pi}{2}\alpha t\right) - 2\sin\left(\frac{\pi}{2}\beta t\right)}{-\cos\left(\frac{\pi}{2}\alpha t\right) - 2\cos\left(\frac{\pi}{2}\beta t\right)}\right]$$

$$= \tan^{-1}\left[\frac{\mp\sin\left(\frac{\pi}{2}t\right)}{-3\cos\left(\frac{\pi}{2}t\right)}\right] \tag{3.36}$$

$$= \tan^{-1}\left[\frac{-\beta\sin\left(\frac{\pi}{2}t\right)}{-3\cos\left(\frac{\pi}{2}t\right)}\right]$$

$$= \tan^{-1}\left[\frac{\beta\sin\left(\frac{\pi}{2}t + \pi\right)}{3\cos\left(\frac{\pi}{2}t + \pi\right)}\right]$$

$$= \tan^{-1}\left[\frac{1}{3}\beta\tan\left(\frac{\pi}{2}t + \pi\right)\right]$$

From Equations (3.33), (3.34), (3.35) and (3.36), we can see that the 2-MAMSK signal phase increases nonlinearly by $+\pi/2$ for $\beta = +1$, and decreases nonlinearly by $-\pi/2$ for $\beta = -1$. When these possible phase trajectories are plotted modulo 2π, in the range $(-\pi, \pi)$, they collapse into a structure called a phase trellis as shown in Figure 3-3. From Figure 3-3, we observe that for every multiple of the bit time the phase can only take one of the two possible values, the values being 0 and π for even multiples of $t = 2kT$ and $\pm \pi/2$ for odd multiples of $t = (2k + 1)T$.

However, the time varying phase between time intervals can take one of three possible paths labelled as A, B, and C in Figure 3-3. The path it takes depends on the input binary data sequences α and β and the initial phase. For example, when $\alpha = \beta = +1$ and the initial phases of both the larger and the smaller MSK signals are 0, then the phase variation goes through the straight path, B. When $-\alpha = \beta = +1$ and the initial carrier phase of the larger and smaller MSK signals are 0 and π respectively, then it takes the

curvy path A. When $-\alpha = \beta = +1$ and the initial carrier phase of both the larger and smaller MSK signals are 0, then it takes the curvy path C.
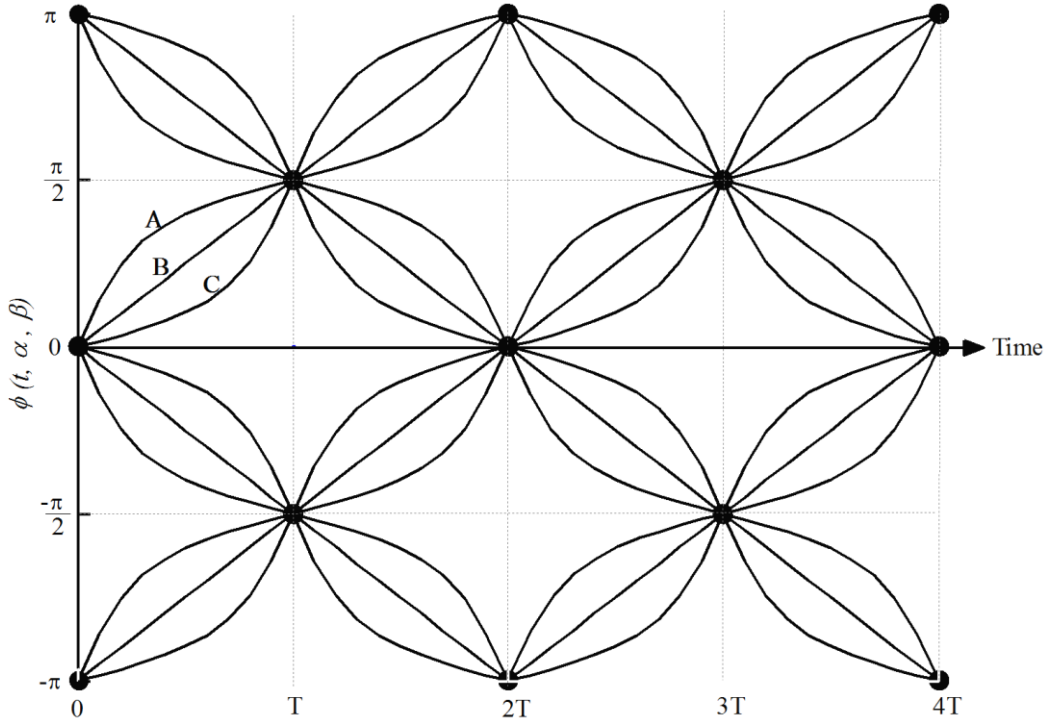
Figure 3-3   Phase trellis of a 2-MAMSK signal in the range $(-\pi, \pi)$

Thus, we can conclude that the data sequence, β is responsible to evolve the overall 2-MAMSK phase from one state to another, and the contribution of the data sequence α is to add the "curvature" to the path it takes when it has opposite sign to β. As illustrated earlier, the linear path is due to that fact that both the larger and smaller MSK signals employ rectangular pulse shaping. The "curvy" path of the 2-MAMSK phase is because of its nonlinear behaviour as was shown in Equations (3.33), (3.34), (3.35) and (3.36).

To clarify all these points, we plot the overall 2-MAMSK phase generated by all possible values of α, β and the phase difference between the two MSK signals, denoted ξ, on the y axis and time on the x axis as shown in Figure 3-4. It can be noted that the 2-MAMSK phase is only plotted for the duration of one bit interval. From Figure 3-4, we observe that

the two nonlinear paths closer to the x axis correspond to the case when $\alpha \neq \beta$ and the phase difference between the two MSK signals is zero. The other two nonlinear paths also correspond to the case when $\alpha \neq \beta$ but when there is a phase difference of π radians between the two MSK signals. The two linear paths always correspond to the case when $\alpha = \beta$ regardless of the phase difference between the two MSK signals.
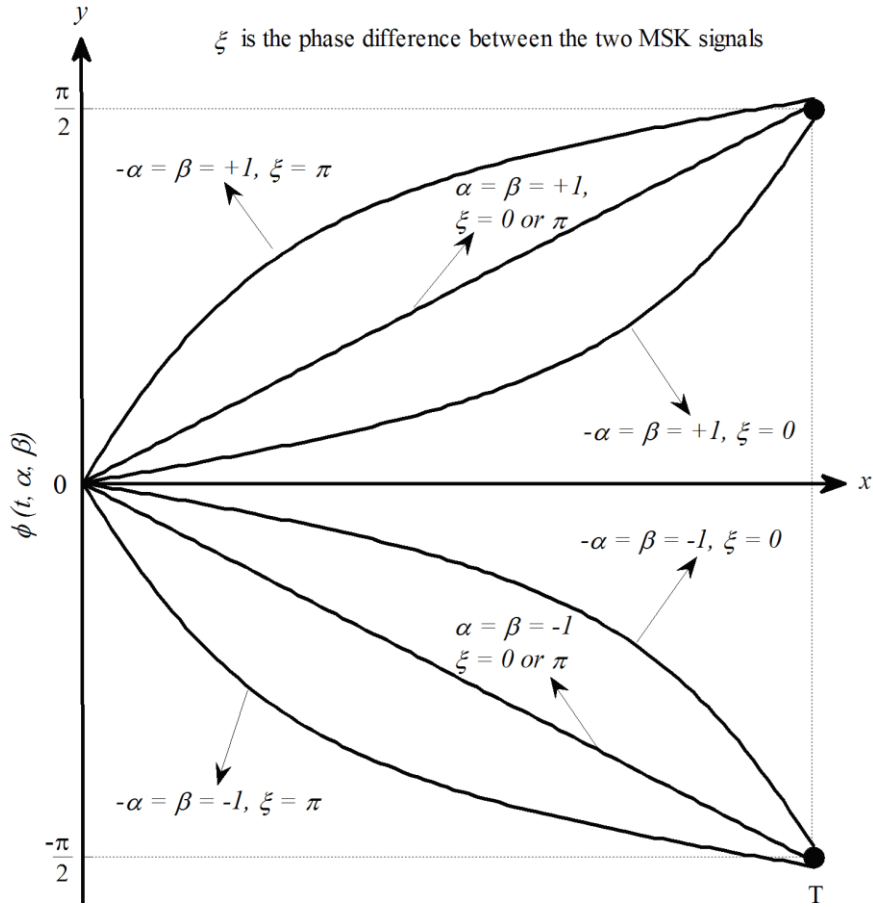
Figure 3-4 2-MAMSK phase trajectory for $0 \leq t < T$

Hence, we have an overall phase difference of a 2-MAMSK signal over one bit interval with respect to the initial phase of the carrier as

$$\Delta\phi = \phi\big((n+1)T, \alpha, \beta\big) - \phi(nT, \alpha, \beta) = \begin{cases} +\dfrac{\pi}{2}, & \beta = +1 \\[2mm] -\dfrac{\pi}{2}, & \beta = -1 \end{cases} \qquad (3.37)$$

66

Based on Equation (3.37), we can sketch an alternative diagram to the state trellis, which also demonstrates the state transitions at the time instants $t = nT$ and the phase variation between the terminals without explicitly showing the phase as function of time. Figure 3-5 shows the phase variation between terminals as a function of the data sequence β.
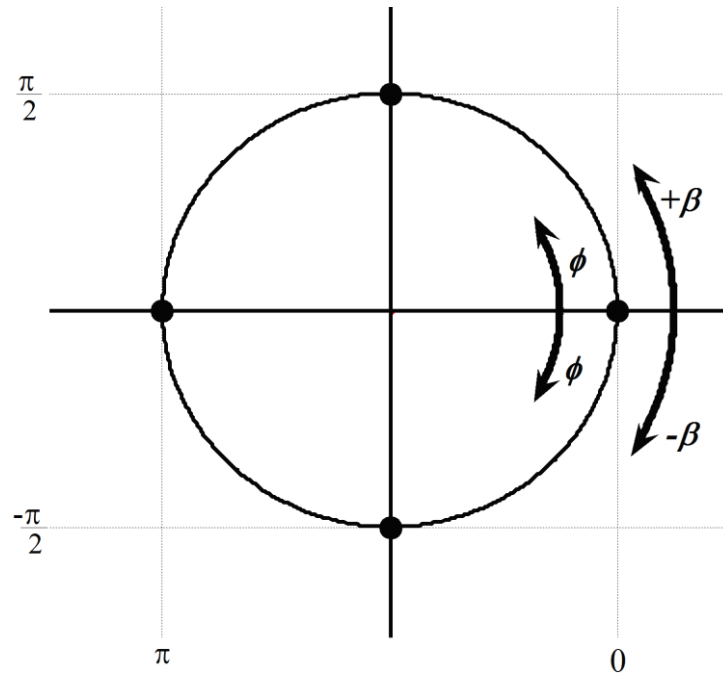
Figure 3-5 Phase variation with respect to β

The small black circles shown Figure 3-5 represent the terminal values of the 2-MAMSK phase at the time instants $t = nT$. This is a more compact version of 2-MAMSK phase as only possible phase values and their transitions are displayed in the diagram. In Figure 3-5, we can see that MAMSK signal have four possible states, namely $\{-\pi/2, 0, \pi/2, \pi\}$. The phase can progress from one state to another depending on the sign of the data sequence β.

To demonstrate all the above, we plot the 2-MAMSK signal phase, $\phi(t, \alpha, \beta)$ alongside the two MSK signal phases, $\phi(t, \alpha)$ and $\phi(t, \beta)$ as shown in Figure 3-6. The phase trajectories shown in Figure 3-6 are generated by the data sequences $\alpha = \{-1, +1, +1, +1, +1, +1, +1, -1\}$ and $\beta = \{-1, -1, +1, +1, +1, -1, -1, +1\}$.
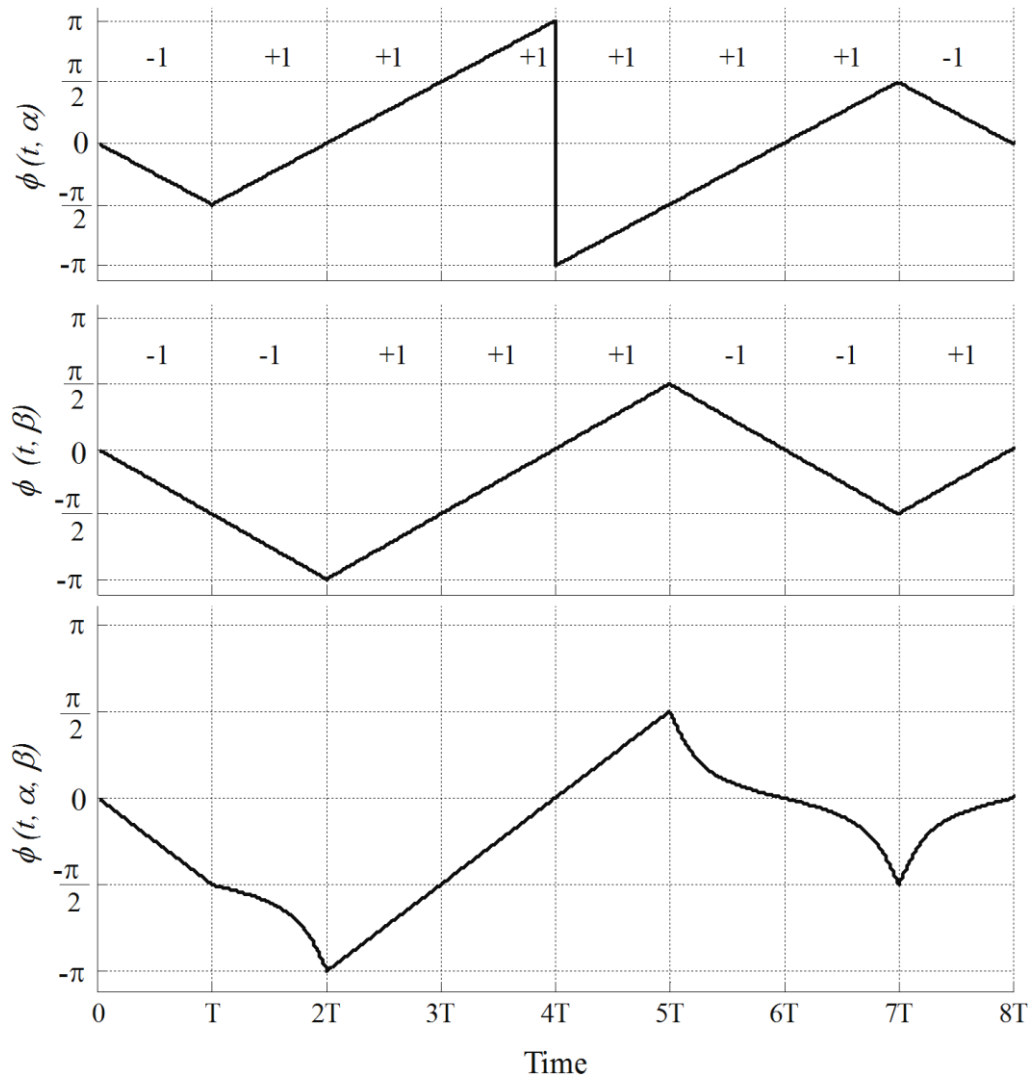
Figure 3-6   2-MAMSK phase with the two MSK phases

From the above figure, we can see that the phase trajectories of a 2-MAMSK signal follow the phase of the MSK component with larger amplitude. In fact at the time instants $t = nT$, the larger MSK signal and the 2-MAMSK signal have the same phase values at integer multiples of $\pi/2$. However, the 2-MAMSK signal phase has a "curvy" characteristics for the time intervals when $\beta_n \neq \alpha_n$, while the phase of the larger MSK constituent is always linear. The only difference between the 2-MAMSK phase $\phi(t, \alpha, \beta)$ and the larger MSK signal phase $\phi(t, \beta)$ is the nonlinear behaviour for the time intervals when $\alpha \neq \beta$. Hence, the results shown in Figure 3-6 clearly agree with our analysis as discussed earlier.

3.4 M-MAMSK Signal Phase

It is straightforward to extend the results from the previous section to M-MAMSK for $M > 2$. To demonstrate, we modify our previously defined x and y as follows

$$x = \sum_{i=1}^{M} 2^{i-1} \cos \phi(t, \alpha_i) \qquad (3.38)$$

$$y = \sum_{i=1}^{M} 2^{i-1} \sin \phi(t, \alpha_i) \qquad (3.39)$$

where $\phi(t, \alpha_i)$ is the phase of the ith MSK component. x and y are the I and Q channels of the M-MAMSK signal, respectively. For more details regarding M-MAMSK see section 2.4.1.

Provided that all components of M-MAMSK are based on conventional MSK, then for $i = 1, 2, \dots, M$ we have

$$\phi(t, \alpha_i) = 0 \text{ or } \pi, \quad \text{for} \quad t = 2kT \qquad (3.40)$$

$$\phi(t, \alpha_i) = \pm \frac{\pi}{2}, \quad \text{for} \quad t = (2k+1)T \qquad (3.41)$$

Substituting Equations (3.40) and (3.41) into (3.38) and (3.39), gives

$$x = \pm\, 2^{M-1} + \sum_{i=1}^{M-1} \pm\left(2^{i-1}\right), \quad \text{and} \quad y = 0 \quad \text{for} \quad t = 2kT \qquad (3.42)$$

$$y = \pm\, 2^{M-1} + \sum_{i=1}^{M-1} \pm\left(2^{i-1}\right), \quad \text{and} \quad x = 0 \quad \text{for} \quad t = (2k+1)T \quad (3.43)$$

Next, it is easy to show that

$$(2^{M-1}) > \sum_{i=1}^{M-1} (2^{i-1}) \qquad (3.44)$$

Equation (3.44) suggests that the amplitude level of "2^{M-1}" associated with the largest MSK component is greater than the sum of the amplitudes of the other $(M-1)$ MSK components. Accordingly, the multiplier of "2^{M-1}" is responsible for determining the signs of x and y at even and odd multiples of T, respectively.

From the definition of arctangent described by Equations (3.26) and (3.27), we can establish the following:

- For $t = 2kT$, the M-MAMSK phase values are determined from the sign of x.

- For $t = (2kT + 1)$, the M-MAMSK phase values are determined from the sign of y.

We can summarise the above discussion with the following relationships:

The factor of "2^{M-1}"controls the signs of x and y and the signs of both x and y are used to determine the values of overall M-MAMSK phase.

Therefore, based on the above relationships, we conclude that the overall phase of M-MAMSK for $M \geq 2$ will always follows the phase of the MSK component with the largest amplitude value. The remaining $(M-1)$ MSK components cause the "curvy" behaviour. For convenience, the phase tree for a 3-MAMSK signal is illustrated in Figure 3-7.

The phase tree for a 3-MAMSK signal is similar to that of 2-MAMSK but with more nonlinear paths. The increase in the number of nonlinear paths is because more combinations exist among $\alpha_1, \alpha_2, \alpha_3$ and the phase differences among the MSK components. Again, the linear paths correspond to the case when the information sequences carried by all MSK components have the same sign. The nonlinear paths occur when the information sequence carried by any of the MSK components has a different sign.
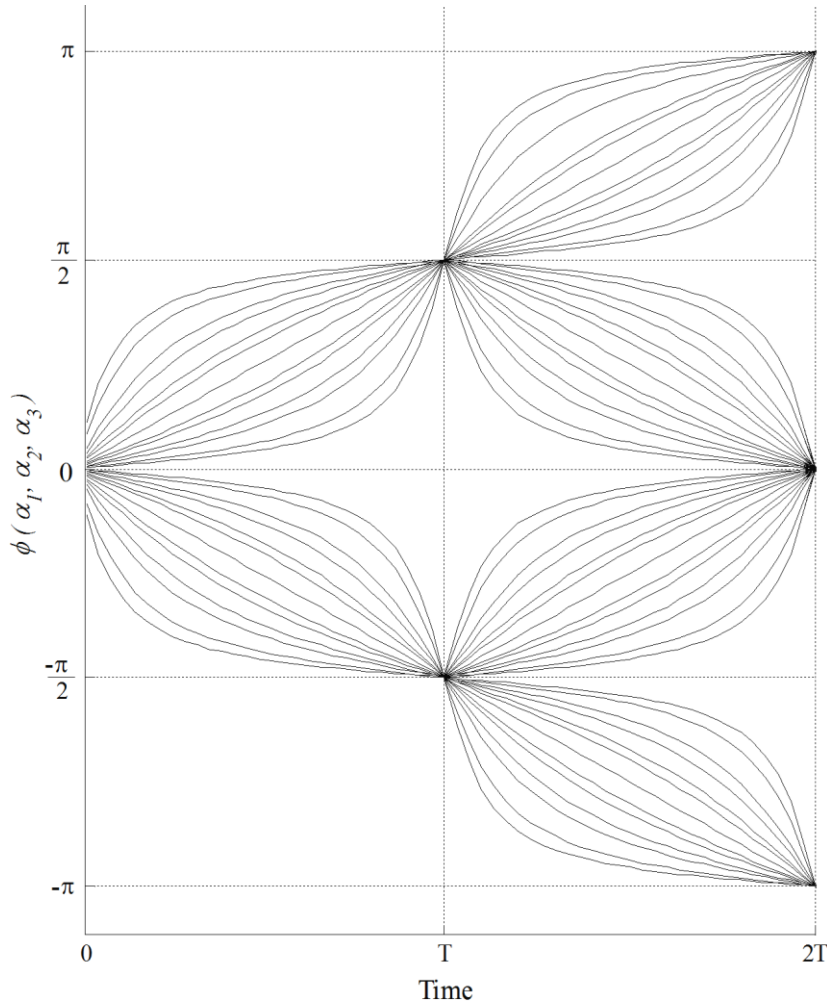
Figure 3-7 Phase tree for a 3-MAMSK signal

By now, one can imagine the phase tree pattern for an arbitrary value of M. In general, there exist $\left(2^{2(M-1)} - 2^{M-1} + 1\right)$ paths, only one of them is linear, the others are not. However, the important outcome is that for $M \geq 1$, the overall M-MAMSK phase can take only the two values of $\pm \pi/2$ at odd multiples of T and only the two values 0 and π at even multiples of T, viewed modulo 2π in the range $-\pi$ and π. Another point to consider, is that the M-MAMSK phase for $M \geq 2$ can evolve from one state to another via a linear or nonlinear path. As in the case of conventional MSK, over one bit interval the phase of an M-MAMSK increases by $+\pi/2$ when $\alpha_M = +1$ and decreases by $-\pi/2$ when $\alpha_M = -1$. α_M is the information sequence carried by the MSK component with highest amplitude value.

71

3.5 MAMSK Signal Space Diagram

In the case of continuous phase signals, the phase of the carrier is time variant. Hence, modulation schemes with memory cannot be represented by discrete points in a signal space diagram as in the case of QAM. Instead, continuous phase signals are described by the various paths or trajectories from one phase state to another. Figure 3-8 illustrates the signal space diagram for a 2-MAMSK signal where the component signals have unequal amplitudes.

The beginning and ending points of these phase trajectories are marked in the figure by symbol points (bold dots). It is noticed from Figure 3-8, that the 2-MAMSK signal never reaches zero signal energy. This is due to the amplitude of the larger MSK constituent being twice the amplitude of the smaller MSK constituent. Note that for 2-MAMSK, there are 4 arcs or trajectories in each quadrant of the signal space with each being specified by 4 input data bits, as there are $2^4 = 16$ distinct trajectories.
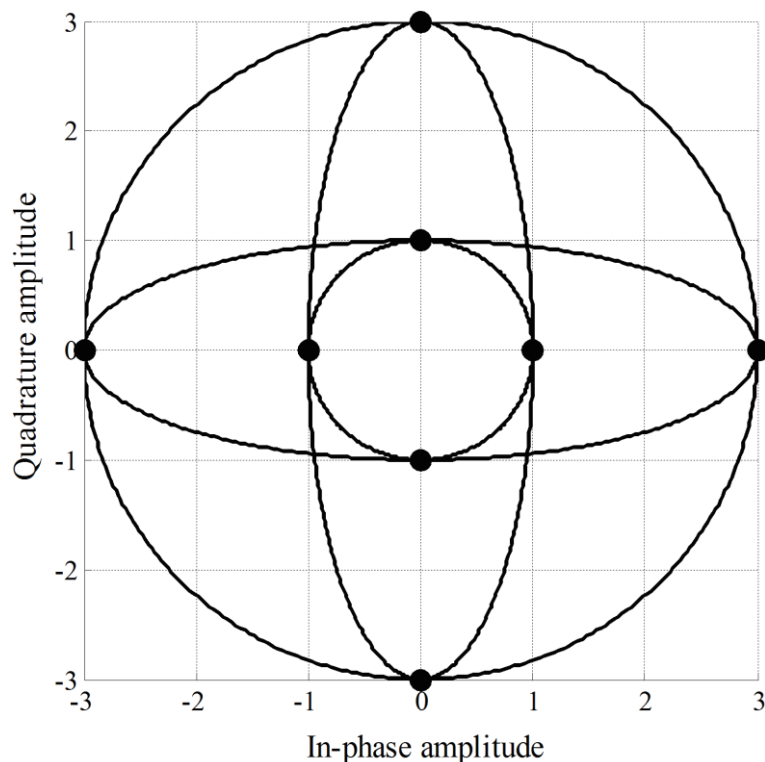
Figure 3-8   Signal trajectory for a 2-MAMSK signal

To demonstrate the diagram, first we consider the time instants $t = nT$. In section 3.3, we have established that the two MSK components at $t = nT$ are either in-phase or out of phase by π radians. Or equally the phase difference, $\phi(nT, \beta) - \phi(nT, \alpha)$ is equal to 0 or π. Taking this into account and using Equation (3.3), we obtain the following values for a 2-MAMSK signal envelope.

$$\rho(nT, \alpha, \beta) = \sqrt{5 + 4\cos 0} = 3 \tag{3.45}$$

$$\rho(nT, \alpha, \beta) = \sqrt{5 + 4\cos \pi} = 1 \tag{3.46}$$

The above envelope values suggest that the 2-MAMSK symbol points must land on a circle of radius 3 or 1, corresponding to the phase difference of 0 and π, respectively. Consequently, when the two MSK signals are in-phase the start or end of each signalling interval is represented by one of the four symbol points shown on the outer circle. The remaining symbol points represent the case when there is a phase difference of π between the two MSK components.

It can be noted that at $t = nT$ the data sequence α and/or β was not taken into consideration. However, to be able to identify a specific arc in between the signalling intervals (i.e. $nT < t < (n+1)T$). We need to consider these information sequences alongside the phase differences. Using Equation (3.18) and considering all possible combinations of α and β and the phase differences between the two MSK signals, denoted ξ. We can establish the following relationships between $\phi(t, \alpha)$ and $\phi(t, \beta)$ as shown in Table 3-5.

$\alpha = \beta$	$\xi = 0$	$\phi(t, \beta) = \phi(t, \alpha)$
$\alpha = \beta$	$\xi = \pi$	$\phi(t, \beta) = \phi(t, \alpha) + \pi$
$\alpha \neq \beta$	$\xi = 0$	$\phi(t, \beta) = -\phi(t, \alpha)$
$\alpha \neq \beta$	$\xi = \pi$	$\phi(t, \beta) = -\phi(t, \alpha) + \pi$

Table 3-5   Relationships between $\boldsymbol{\phi(t, \alpha)}$ and $\boldsymbol{\phi(t, \beta)}$

Now substituting each row of Table 3-5 into Equation (3.1), yields the results as shown in Table 3-6.

$\alpha = \beta$	$\xi = 0$	$s(t) = A\{3\,I(t)\cos 2\pi f_c t - 3\,Q(t)\sin 2\pi f_c t\}$
$\alpha = \beta$	$\xi = \pi$	$s(t) = A\{\ I(t)\cos 2\pi f_c t - \ Q(t)\sin 2\pi f_c t\}$
$\alpha \neq \beta$	$\xi = 0$	$s(t) = A\{3\,I(t)\cos 2\pi f_c t - \ Q(t)\sin 2\pi f_c t\}$
$\alpha \neq \beta$	$\xi = \pi$	$s(t) = A\{\ I(t)\cos 2\pi f_c t - 3\,Q(t)\sin 2\pi f_c t\}$

Table 3-6   Four possible signalling based on α, β and ξ

Where $I(t) = \cos\phi(t,\beta)$ and $Q(t) = \sin\phi(t,\beta)$ and A is defined by Equation (2.20). Each row shown in Table 3-6 corresponds to one of the four arcs in the order:

- Row 1 $\rightarrow$ Outer circle
- Row 2 $\rightarrow$ Inner circle
- Row 3 $\rightarrow$ Horizontal ellipse
- Row 4 $\rightarrow$ Vertical ellipse

To clarify these relationships, consider the following two examples.

Example 1- Assume that at the start of a signalling interval, $\alpha_n = \beta_n$ and the phase difference between the two MSK signals is π radians, ($\xi = \pi$). Then, the symbol point will evolve from one state to another via a circle of radius 1 (the inner circle shown in Figure 3-8).

Example 2- This time assume that for any singling intervals where $\alpha_n \neq \beta_n$ and $\xi = 0$. Then the symbol points for these combinations evolve via an ellipse with the major axis of 3 along the x axis and the minor axis of 1 along the y axis (Horizontal ellipse shown in Figure 3-8).

In the remaining part of the section, we extend these results to M-MAMSK for $M > 2$. As discussed in the previous section, the M MSK

components at the beginning and end of each symbol interval are either in-phase or out of phase with each other by π radians. Thus, there exist 2^{M-1} possible combinations of phase differences among the M MSK components. This would result in 2^{M-1} different amplitude levels.

To specify these amplitude levels, we consider the possible combinations of phase differences at the time instants $t = nT$. The highest amplitude level occurs when all M MSK components are in-phase with each other. Under this condition, the highest amplitude value, denoted A_h, can be calculated by

$$A_h = \pm \sum_{i=1}^{M} 2^{i-1} = \pm(2^M - 1) \tag{3.47}$$

The lowest amplitude occurs when the $(M-1)$ MSK component are out of phase with the largest MSK component. The lowest amplitude value, denoted A_l, can be calculated as

$$A_l = \pm \left(2^{M-1} - \sum_{i=1}^{M-1} 2^{i-1} \right) = \pm 1 \tag{3.48}$$

Other amplitude levels occur in between these two levels, depending on the phase differences. For example, if the $(M-2)$ MSK components are out of phase with the largest and smallest MSK components, then this would result in a amplitude level of ± 3 or equally,

$$A = \pm \left(1 + 2^{M-1} - \sum_{i=2}^{M-1} 2^{i-1} \right) = \pm 3 \tag{3.49}$$

In a similar manner, if we consider all the possibilities then we would obtain different amplitude levels taking values from the set $\{\pm 1, \pm 3, \pm 5, \cdots, \pm 2^M - 1\}$. These amplitude levels can be expressed as,

$$A = \pm \left(2^{M-1} + \sum_{i=1}^{M-1} 2^{i-1} \cos \xi_i \right), \tag{3.50}$$

where, A represents different amplitude levels which can be obtained from different phase combinations. ξ_i is the phase difference between the ith and the largest MSK components. $\xi_i = 0$, if the ith and largest MSK components are in phase and $\xi_i = \pi$ if they are out of phase.

The above results imply that the symbol points for M-MAMSK must land on circles of radius 1, 3, 5, $\cdots$, $2^M - 1$, with the centre of the circles at the origin. For the time intervals, where the information sequences transmitted by all MSK components are the same then the symbol points evolve via an arc of a circle its radius specified from the set $\{1, 3, 5, \cdots, 2^M - 1\}$. For the time intervals, where at least one of the information sequences differ from the remaining $(M - 1)$ data sequences then the symbol points evolve via an arc of an ellipse. The values for the major and minor axis of the ellipse also specified from the set $\{1, 3, 5, \cdots, 2^M - 1\}$. To clarify, we plot a signal trajectory for a 3-MAMSK as shown in Figure 3-9.
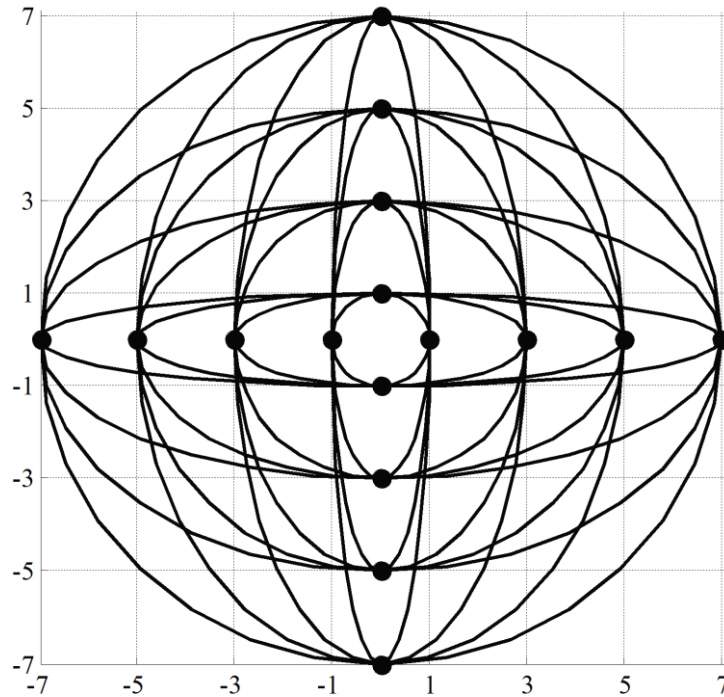
Figure 3-9 Signal trajectory for a 3-MAMSK signal

For the case of 2-MAMSK, we had only two circles, because only two possible combinations of phase differences exist, since we only had 2 MSK

components. For a 3-MAMSK there are four circles because $2^{(3-1)} = 4$, possible combinations of phase differences exist among the three MSK components. In the case of a 2-MAMSK, each symbol point can only evolve via one ellipse which is due to there being only one possible situation where $\alpha \neq \beta$. For a 3-MAMSK each symbol can evolve via 3 ellipses, because there are $2^{(3-1)} - 1 = 3$ combinations exist among α_i for $i = 1,2,3$. However, the specific elliptical path is controlled by the phase difference among the MSK components.

In summary, for $M \geq 2$ there exist $2^{(M-1)}$ different amplitude levels. Consequently, each symbol point can progress from one amplitude level to another via $2^{(M-1)}$ paths. From these paths, one is a circular path corresponding to the case where $\alpha_i = \alpha_M$ for $i = 1, 2, 3, \cdots, M - 1$. The remaining $2^{(M-1)} - 1$ paths are elliptical paths and they occur where $\alpha_i \neq \alpha_M$ for any $i \in \{1, 2, 3, \cdots, M - 1\}$. These paths are controlled by the information sequences, α_i and the phase differences between the M MSK components. The highest amplitude level of $\pm(2^M - 1)$ occurs when the M MSK components are in-phase with each other. The lowest amplitude value of ± 1 corresponds to the case where the there is a phase difference of π radians between the largest and remaining $(M - 1)$ MSK components.

3.6   Power Spectral Density of MAMSK

We now compare the power spectral density (PSD) of the 2-MAMSK and 16-QAM modulation schemes. We begin with the analysis of the autocorrelation function and its Fourier transform followed by the results obtained from simulations. Finally, we develop the idea for M-MAMSK when $M > 2$. It has been established in [7, 8], that it is sufficient to determine the PSD of a bandpass signal from its complex baseband equivalent. Furthermore, they show that the PSD of the complex envelope

depends on the symbol pulse shaping. More specific, the PSD is equal to the energy spectral density of the pulse shape divided by the symbol duration.

We use the results of Table 3-6 together with Equation (2.6) in order to obtain the symbol pulse shaping used for a 2-MAMSK signal. Based on these results, the complex baseband representation of a 2-MAMSK signal can be expressed as

$$s(t) = A\left[a_I(t)\cos\left(\frac{\pi t}{2T}\right) + j\,a_Q(t)\sin\left(\frac{\pi t}{2T}\right)\right], \quad nT \le t \le (n+1)T \quad (3.51)$$

where A is the amplitude defined in Equation (2.15), T is the bit period. $a_I(t)$ and $a_Q(t)$ map the information bits into the 2-MAMSK symbols, each taking values from the set $\{\pm 1, \pm 3\}$. From Equation (3.51), it can be seen that 2-MAMSK signal can also be viewed as offset 16-QAM with half cycle sinusoidal pulse shaping. Equation (3.51) is valid, since 2-MAMSK phase can only increase or decrease by $\pm\pi/2$ over one bit interval. For more details, see Sections 3.3 and 3.5.

From Equation (3.51), we observe that the pulse shaping of a 2-MAMSK signal is exactly the same as that of MSK. This was expected, because superimposing two pulses of the same shape with different amplitudes also results in a pulse of the same shape but at a different amplitude level. Consequently, the spectral shape of 2-MAMSK is identical to that of conventional MSK. A common method of evaluating PSD is first to obtain an expression for the autocorrelation function, $R(\tau)$ of the transmitted signal and then take the Fourier transform of $R(\tau)$.

The autocorrelation function of MSK (2-MAMSK) with half cycle sinusoidal pulse shaping is given in [7, 16] as

$$R(\tau) = \frac{A^2\,T}{\pi}\left[\pi\left(1 - \frac{|\tau|}{2T}\right)\cdot\cos\left(\pi\frac{|\tau|}{2T}\right) + \sin\left(\pi\frac{|\tau|}{2T}\right)\right] \quad (3.52)$$

With the bit time duration and A normalised to 1 (i.e. $T = 1$ sec and $A = 1$) the above equation is plotted in Figure 3-10.
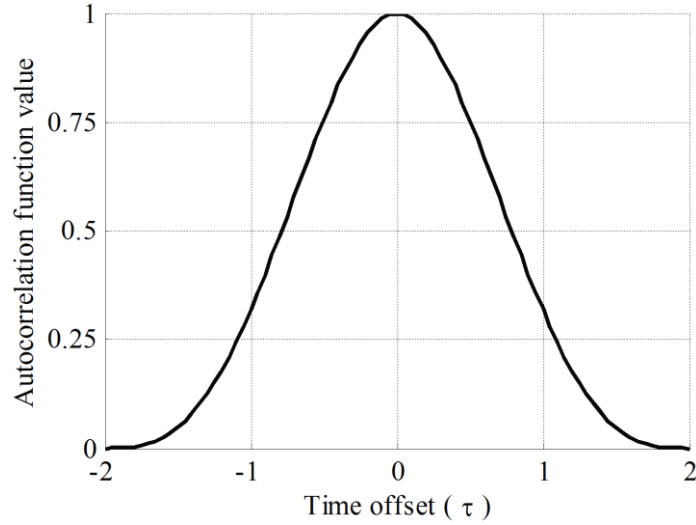
Figure 3-10 MSK (2-MAMSK) autocorrelation function

The power density spectrum of 2-MAMSK or MSK [8, 76] is obtained by taking the Fourier transform of Equation (3.52) resulting in

$$S_{2-MAMSK}(f) = \frac{16\,A^2\,T}{\pi^2}\left[\frac{\cos(2\pi Tf)}{1-(4Tf)^2}\right]^2 \tag{3.53}$$

The power spectral density of unfiltered 16-QAM [7, 8] is given by

$$S_{16-QAM}(f) = A^2\,T\left[\frac{\sin(2\,\pi\,T\,f)}{2\,\pi\,Tf}\right]^2. \tag{3.54}$$

Note, for the case of 2-MAMSK and 16-QAM, A is the average amplitude of the signal, but for MSK A is the amplitude since it is a constant envelope modulation.

Figure 3-11 shows the power spectral densities (PSDs) of 2-MAMSK and 16-QAM which are obtained from Equations (3.53) and (3.54), respectively. Figure 3-12 shows the PSDs obtained from simulation results. Both graphs are plotted as a function of f normalised to the data rate $R = 1/T$.
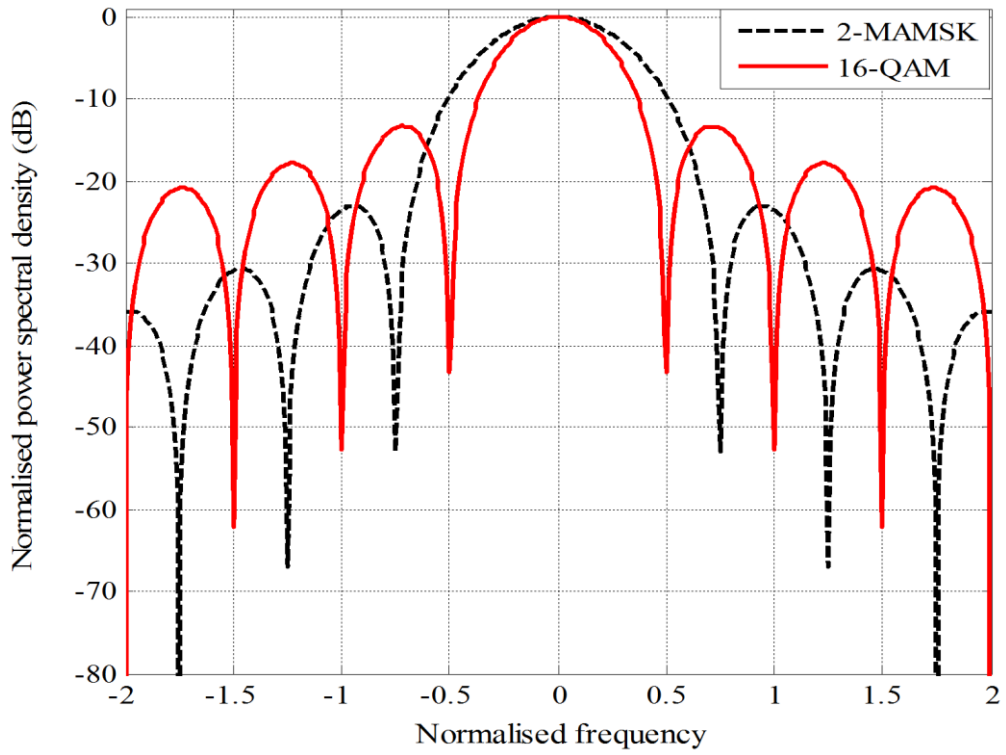
Figure 3-11 Power spectral density of 2-MAMSK Vs 16-QAM— Analytical
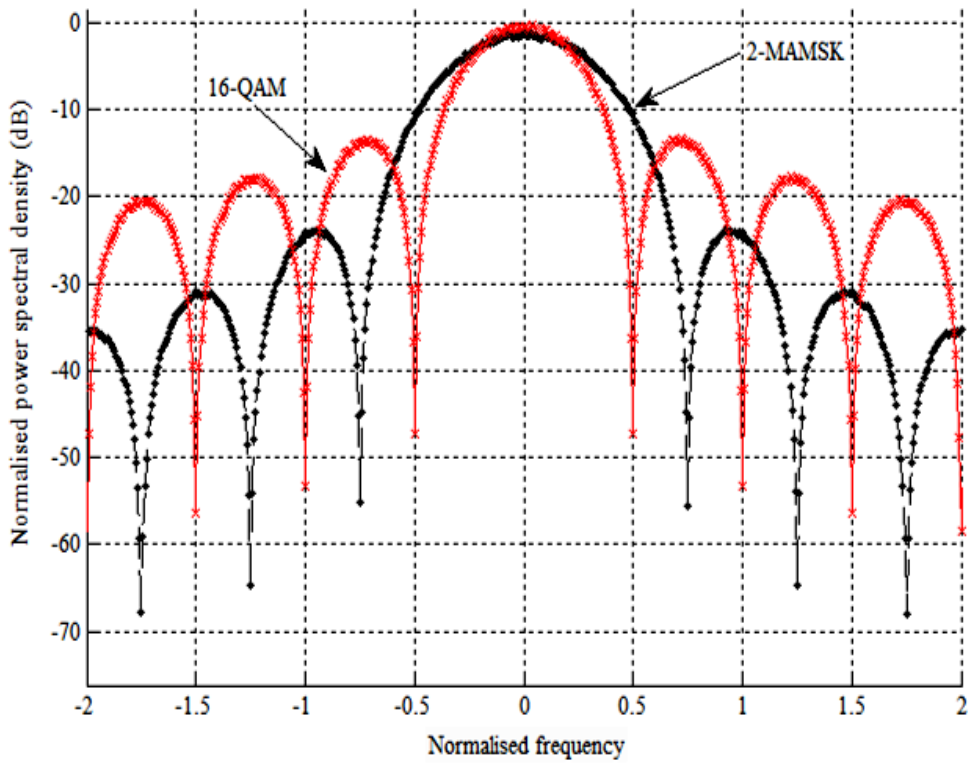
Figure 3-12 PSDs of 2-MAMSK Vs 16-QAM obtained from simulations

From the above figures, it can be seen that the simulation results are consistent with the analytical results. Here, we briefly discuss the main differences between the two PSDs (for a comprehensive study, see [8]). We observe that for large f, the rate of roll-off of the 2-MAMSK spectrum is proportional to f^{-4}, whereas the 16-QAM PSD falls off at a rate of f^{-2}. The main lobe of the 2-MAMSK spectrum is 50% wider than that of 16-QAM. The first nulls of 16-QAM and 2-MAMSK occur at $f = 0.5$ and $.75$, respectively. More precisely, if we consider a frequency scale factor which depends on the number of bits per symbol, then the first nulls appear at $f = 0.25$ and $.375$ for 16-QAM and 2-MAMSK, respectively.

The extension of 2-MAMSK to M-MAMSK for $M > 2$, is now obvious. As discussed earlier, for any modulation scheme the evaluation of the PSD is dependent on the type of the pulse shaping used. Equation (3.51) still holds for M-MAMSK, where $a_I(t) = \pm 1, \pm 3, \cdots, 2^M - 1$ and $a_Q(t) = \pm 1, \pm 3, \cdots, 2^M - 1$. This suggests that the pulse shape did not change but there are more amplitude levels. Thus, for M-MAMSK we maintain the same pulse shaping as for MSK. Accordingly, the spectral shape of M-MAMSK is identical to that of MSK but the magnitude of the PSD is determined from the average power of the M-MAMSK signal set. The PSD of M-MAMSK for $M \geq 2$ can be expressed as

$$S_{M-MAMSK}(f) = \frac{16\, A_{av}^2\, T}{\pi^2} \left[\frac{\cos(2\pi Tf)}{1 - (4Tf)^2} \right]^2, \qquad (3.55)$$

where A_{av} is the average amplitude of the M-MAMSK signal set. From Equation (3.55), we observe that the PSD magnitude for M-MASK is the same as that shown in Figure 3-11, if its average amplitude is equal to the amplitude of MSK signal. However, for a fixed data rate its spectral shape is M times narrower than that of MSK, because an M-MAMSK signal can encode $2M$ bits per symbol. Hence, when compared with MSK, M-MAMSK is exactly M times as bandwidth efficient.

3.7   The Eye Diagram of MAMSK

The eye diagram is another useful tool used for qualitative analysis of digitally modulated signals. Independent eye diagrams can be generated, one for the in-phase channel and another for the quadrature channel. Figure 3-13 illustrates undistorted eye diagram of a 2-MAMSK signal.
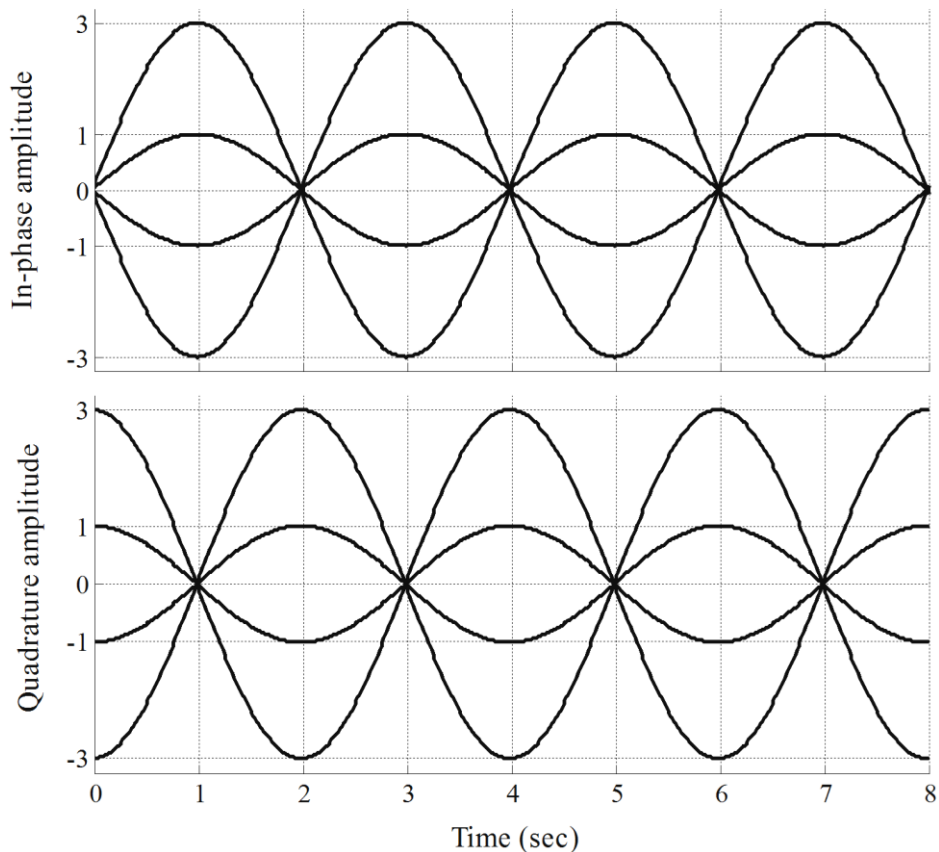
Figure 3-13 Eye diagram of a 2-MAMSK signal

The open part of the eye represents the time that we can safely sample the signal without error. Obviously, from the above eye diagram we can see that the ideal sampling period for a 2-MAMSK is 1, 3, 5, 7, $\cdots$ for the in-phase channel and 0, 2, 4, 6, 8, $\cdots$ for the quadrature channel. From Figure 3-13, we observe that each of the I and Q channels have two amplitude levels with sinusoidal pulse shaping, which is consistent with the previous discussions. The eye diagram of M-MAMSK for $M > 2$ has the same pattern of a 2-MAMSK signal but with more amplitude levels (see section 3.5 for details).

3.8 Theoretical BER for M-MAMSK

In this section, we evaluate the decoded error performance of a 2-MAMSK signal achieved with maximum likelihood sequence estimation (MLSE). Finally, we generalise the results to M-MAMSK for $M \geq 2$. The optimum bit error probability derived here is only valid for the white Gaussian noise channel. Throughout this section for simplicity of notation, we write $s(t)$ in place of $s_{M-MAMSK}(t, \alpha_1, \alpha_2, \cdots, \alpha_M)$.

In section 2.6, we have described the basics of maximum likelihood detection. Based on the results, we must determine the minimum Euclidean distance between paths through a trellis that separates at a node at $t = 0$ and re-emerges at a later time. For phase varying signals the distance between them depends on the phase difference between the two signals. To illustrate this, assume that we have two signals $s_i(t)$ and $s_j(t)$ differing over N intervals. Thus, the Euclidean distance between them over an interval of length NT, where $1/T$ is the symbol rate is can be defined as

$$d_{ij}^2 = \int_0^{NT} \left[s_i(t) - s_j(t) \right]^2 dt$$

$$= \int_0^{NT} s_i^2(t)\, dt + \int_0^{NT} s_j^2(t)\, dt - 2 \int_0^{NT} s_i(t)\, s_j(t)\, dt$$

(3.56)

Using Equation (3.1), we can define $s_i(t)$ and $s_j(t)$ as follows:

$$s_i(t) = \sqrt{\frac{2E}{5T}} \left(\cos[2\pi f_c t + \phi(t, \alpha_i)] + 2 \cos[2\pi f_c t + \phi(t, \beta_i)] \right)$$

(3.57)

$$s_j(t) = \sqrt{\frac{2E}{5T}} \left(\cos[2\pi f_c t + \phi(t, \alpha_j)] + 2 \cos[2\pi f_c t + \phi(t, \beta_j)] \right)$$

(3.58)

where, E is the average signal energy per symbol interval.

To avoid long and messy equations, we will work with each term of Equation (3.56) separately and then combine the outcomes for each term to obtain the final result. Let us start off by integrating the first term of the right hand side of (3.56), we have

$$\int_0^{NT} s_i^2(t)\,dt = \frac{2E}{5T}\int_0^{NT} (\cos[2\pi f_c t + \phi(t, \alpha_i)]$$
$$+ 2\cos[2\pi f_c t + \phi(t, \beta_i)])^2\,dt \tag{3.59}$$

Now using the fact that

$$\int_0^T \cos^2(2\pi x)\,dx = \frac{T}{2}$$

Equation (3.59) can be simplified to

$$\int_0^{NT} s_i^2(t)\,dt = \frac{2E}{5T}\left(\frac{NT}{2} + \frac{4NT}{2}\right) + \frac{8E}{5T}$$
$$\cdot\left(\int_0^{NT} \cos[2\pi f_c t + \phi(t, \alpha_i)]\cos[2\pi f_c t + \phi(t, \beta_i)]\,dt\right) \tag{3.60}$$

From trig relations we have that

$$2\cos[A + B]\cos[A + C] = \cos[B - C] + \cos[2A + B + C] \tag{3.61}$$

Using the above identity Equation (3.60) becomes

$$\int_0^{NT} s_i^2(t)\,dt = NE + \frac{4E}{5T}\int_0^{NT} \cos[\phi(t, \alpha_i) - \phi(t, \beta_i)]\,dt$$
$$+ \frac{4E}{5T}\int_0^{NT} \cos[4\pi f_c t + \phi(t, \alpha_i) + \phi(t, \beta_i)]\,dt \tag{3.62}$$

Assuming that $f_c \gg \frac{1}{T}$, Equation (3.62) can be simplified to

$$\int_0^{NT} s_i^2(t)\, dt = NE + \frac{4E}{5T}\int_0^{NT} \cos[\phi(t,\alpha_i) - \phi(t,\beta_i)]\ dt + O\left(\frac{1}{f_c}\right) \quad (3.63)$$

where the term $O\left(\frac{1}{f_c}\right)$ denotes a term of order $\frac{1}{f_c}$, $\phi(t,\alpha_i)$ and $\phi(t,\beta_i)$ are the phases corresponding to the carrier of $s_i(t)$. As the carrier frequency becomes large to a very good approximation the term $O\left(\frac{1}{f_c}\right)$ approaches zero and we have

$$\int_0^{NT} s_i^2(t)\, dt = NE + \frac{4E}{5T}\int_0^{NT} \cos[\phi(t,\alpha_i) - \phi(t,\beta_i)]\ dt \quad (3.64)$$

Now, we need to find an expression for the phase difference, $\phi(t,\alpha_i) - \phi(t,\beta_i)$, based on Equation (3.10), we have

$$\begin{aligned}
\phi(t,\ \alpha_i) - \phi(t,\ \beta_i) &= \frac{\pi}{2T}\alpha_i t - \frac{\pi}{2T}\beta_i t \\
&= \frac{\pi}{2T} t\ (\alpha_i - \beta_i) \qquad (3.65) \\
&= \phi(t,\ \alpha_i - \beta_i)
\end{aligned}$$

If we let $\boldsymbol{\zeta_1} = \alpha_i - \beta_i$, Equation (3.64) become

$$\int_0^{NT} s_i^2(t)\, dt = NE + \frac{4E}{5T}\int_0^{NT} \cos[\phi(t,\ \boldsymbol{\zeta_1})]\ dt \quad (3.66)$$

Since the sequences α and β represent two independent binary data symbols that take the values from the set $\{-1,\ +1\}$. Consequently, any element of $\boldsymbol{\zeta_1}$ can take values from the set $\{-2,\ 0,\ +2\}$. A similar approach as used to integrate $s_i^2(t)$ over an integral of length NT can be applied to integrate the second term of (3.56), and thus we have

$$\int_0^{NT} s_j^2(t)\, dt = NE + \frac{4E}{5T} \int_0^{NT} \cos[\,\phi(t,\, \zeta_2)]\, dt \tag{3.67}$$

where $\zeta_2 = \alpha_j - \beta_j$. Note that ζ_2 also takes values from the set $\{-2,\ 0,\ +2\}$.

Finally, we need integrate the last term of Equation (3.56). Substituting Equations (3.57) and (3.58) into the last term of Equation (3.56) and after expanding and factoring we obtain,

$$-2\int_0^{NT} s_i(t)\, s_j(t)\, dt = -\frac{2E}{5T}\, dt \cdot \Bigg($$

$$+ 2 \int_0^{NT} \cos[2\pi f_c t + \phi(t, \alpha_i)] \cos[2\pi f_c t + \phi(t, \alpha_j)]$$

$$+ 4 \int_0^{NT} \cos[2\pi f_c t + \phi(t, \alpha_i)] \cos[2\pi f_c t + \phi(t, \beta_j)] \tag{3.68}$$

$$+ 4 \int_0^{NT} \cos[2\pi f_c t + \phi(t, \beta_i)] \cos[2\pi f_c t + \phi(t, \alpha_j)]$$

$$+ 8 \int_0^{NT} \cos[2\pi f_c t + \phi(t, \beta_i)] \cos[2\pi f_c t + \phi(t, \beta_j)]\Bigg)$$

Using the identity defined by Equation (3.61) and ignoring all the $O\left(1/f_c\right)$ terms we have

$$-2\int_0^{NT} s_i(t)\, s_j(t)\, dt = -\frac{2E}{5T} \cdot \Bigg(\int_0^{NT} \cos[\phi(t, \alpha_i) - \phi(t, \alpha_j)]\, dt \tag{3.69}$$

$$+ \int_0^{NT} 2 \cos[\phi(t, \alpha_i) - \phi(t, \beta_j)] \, dt$$

$$+ \int_0^{NT} 2 \cos[\phi(t, \beta_i) - \phi(t, \alpha_j)] \, dt$$

$$\left. + \int_0^{NT} 4 \cos[\phi(t, \beta_i) - \phi(t, \beta_j)] \, dt \right)$$

By noting that $\phi(t, x) - \phi(t, y) = \phi(t, x - y)$ Equation (3.69) becomes

$$-2 \int_0^{NT} s_i(t) \, s_j(t) \, dt = -\frac{2E}{5T} \cdot \left(\int_0^{NT} \cos[\phi(t, \alpha_i - \alpha_j)] \, dt \right.$$

$$+ \int_0^{NT} 2 \cos[\phi(t, \alpha_i - \beta_j)] \, dt \qquad (3.70)$$

$$+ \int_0^{NT} 2 \cos[\phi(t, \beta_i - \alpha_j)] \, dt$$

$$\left. + \int_0^{NT} 4 \cos[\phi(t, \beta_i - \beta_j)] \, dt \right)$$

Now define $\zeta_3 = \alpha_i - \alpha_j$, $\zeta_4 = \alpha_i - \beta_j$, $\zeta_5 = \beta_i - \alpha_j$ and $\zeta_6 = \beta_i - \beta_j$. Then the right hand side of (3.70) becomes

$$= -\frac{2E}{5T} \cdot \left(\int_0^{NT} \cos[\phi(t, \zeta_3)] \, dt + \int_0^{NT} 2 \cos[\phi(t, \zeta_4)] \, dt \right.$$

$$\left. + \int_0^{NT} 2 \cos[\phi(t, \zeta_5)] \, dt + \int_0^{NT} 4 \cos[\phi(t, \zeta_6)] \, dt \right) \qquad (3.71)$$

where any element ζ_x (for $x = 3, 4, 5, 6$) can take values from the set $\{-2, \ 0, \ +2\}$, except that $\zeta_6 \neq 0$.

Now collecting all the terms and considering that d_{ij}^2 on the interval $[0, \ NT]$ is N times the value of d_{ij}^2 on the interval $[0, \ T]$. Then we have

the final expression for the average squared Euclidean distance between the two signals, $s_i(t)$ and $s_j(t)$ as

$$
\begin{aligned}
d_{ij}^2 = \frac{2NE}{5T} \cdot \Bigg(&\int_0^T 5\, dt + 2\int_0^T \cos[\phi(t, \zeta_1)]\, dt \\
&+ 2\int_0^T \cos[\phi(t, \zeta_2)]\, dt - \int_0^T \cos[\phi(t, \zeta_3)]\, dt \\
&- 2\int_0^T \cos[\phi(t, \zeta_4)]\, dt - 2\int_0^T \cos[\phi(t, \zeta_5)]\, dt \\
&- 4\int_0^T \cos[\phi(t, \zeta_6)]\, dt \Bigg)
\end{aligned}
\tag{3.72}
$$

Hence, the Euclidean distance is related to the phase difference between the paths in the phase trellis. The pairwise error probability in the case that we detect signal $s_j(t)$ when signal $s_i(t)$ has been sent is given by

$$
P_b = Q\left(\sqrt{\frac{d_{ij}^2}{2\, N_0}} \right),
\tag{3.73}
$$

where N_0 is the noise power spectral density and d_{ij}^2 is the average squared Euclidean distance over N symbols intervals. In general, it is desirable to normalise the distance d_{ij}^2 and express it in terms of the bit energy, E_b. The normalised Euclidean distance is given by

$$
\delta_{ij}^2 = \frac{d_{ij}^2}{2\, E_b},
\tag{3.74}
$$

where E_b is the average energy ber bit.

Provided that $E = k\, E_b$, where, k is the number of bits in the symbol interval. For a 2-MAMSK signal k can be expressed as

$$k = (\log_2 M + \log_2 M) = 2 \log_2 M \tag{3.75}$$

Using these results, we can define the squared and normalised average Euclidean distance, δ_{ij}^2 as

$$
\begin{aligned}
\delta_{ij}^2 = \frac{2N \log_2 M}{5T} \cdot \Bigg(& \int_0^T 5 \, dt + 2 \int_0^T \cos[\phi(t, \boldsymbol{\zeta_1})] \, dt \\
& + 2 \int_0^T \cos[\phi(t, \boldsymbol{\zeta_2})] \, dt - \int_0^T \cos[\phi(t, \boldsymbol{\zeta_3})] \, dt \\
& - 2 \int_0^T \cos[\phi(t, \boldsymbol{\zeta_4})] \, dt - 2 \int_0^T \cos[\phi(t, \boldsymbol{\zeta_5})] \, dt \\
& - 4 \int_0^T \cos[\phi(t, \boldsymbol{\zeta_6})] \, dt \Bigg),
\end{aligned}
\tag{3.76}
$$

where $\boldsymbol{\zeta_x}$ for $x = 1, 2, \dots 6$ can take values from the set $\{-2, \ 0, \ +2\}$.

For high signal-to-noise ratio, the bit error rate performance for a coherent receiver may be approximated by [7, 72, 92]

$$P_b \approx Q\left(\sqrt{\frac{E_b}{N_0} \, \delta_{\min}^2} \ \right), \tag{3.77}$$

where, $\delta_{\min}$ is the lowest of δ_{ij} between any two different set of data sequences, $(\alpha_i, \ \beta_i)$ and $(\alpha_j, \ \beta_j)$ and defined as

$$\delta_{\min}^2 = \min_{\substack{i,j \\ i \neq j}} \{\delta_{ij}^2\} \tag{3.78}$$

The phase tree is an important diagram and is used to calculate and find the properties of $\delta_{\min}^2$ for CPM signals. Figure 3-1 shows a phase tree for a 2-MAMSK signal over the interval $[0, \ 4T]$. To calculate $\delta_{\min}^2$ for an observation of length N symbol intervals, all pairs of phase trajectories in the phase tree over N symbol intervals must be inserted into Equation (3.76).

The pair of phase trajectories having the root node at time $t = 0$ must not coincide, which means that $\beta_i \neq \beta_j$. On the other hand, there is no restriction on the binary data sequences α_i and α_j. This is because the overall 2-MAMSK phase, $\phi(t, \alpha, \beta)$ is controlled by the information sequence carried by the larger MSK component. It is worth noting that the sequences α_i and α_j control the "curvy" behaviour of the phase trajectories shown in Figure 3-1. For more details on 2-MAMSK phase see section 3.3.

A pair of phase trajectories merge at a certain time if they coincide for all time after that. Employing this approach to the trajectories of Figure 3-1 it is seen that if a pair of sequences

$$\beta_i = \cdots, +1, -1, \beta_1, \beta_2, \ldots \quad , \quad \beta_j = \cdots, -1, +1, \beta_1, \beta_2, \ldots$$

$$\alpha_i \text{ and } \alpha_j \text{ can take any value from the set } \{-1, +1\}$$

is chosen, the two phase trajectories coincide for all $t \geq 2T$. The sequences β_i and β_j can be exchanged with each other, and the resulting δ_{ij}^2 will be the same. Furthermore, since the cosine function is symmetric ($\cos -x = \cos x$) then the difference sequences, ζ_x can always be chosen to be positive. Taking into account the above considerations, the corresponding value of the difference sequences ζ_x for all possible values of α_i, α_j, β_i and β_j are summarised as

β_i	β_j	α_j	α_i	ζ_1	ζ_2	ζ_3	ζ_4	ζ_5	ζ_6
1	-1	-1	-1	2	0	0	0	2	2
1	-1	1	1	0	2	0	2	0	2
1	-1	-1	1	0	0	2	2	2	2
1	-1	1	-1	2	2	2	0	0	2

Table 3-7 The corresponding difference sequences

Since, $\beta_i \neq \beta_j$ for all possible cases then $\zeta_6 \neq 0$, but ζ_x for $x = 1, 2, 3, 4, 5$ can take any value from the set $\{0, +2\}$. It can be noted that

when the value is -2 it is converted to 2 and the resulting ζ_x will be the same because the cosine is an even function. Row 4 shown in Table 3-7, gives the minimum normalised squared Euclidean distance. This corresponds to the case when $\alpha_i = \beta_j$ and $\alpha_j = \beta_i$. This result is logical, because that is the case where the larger and smaller MSK components for both signals $s_i(t)$ and $s_j(t)$ are out of phase with each other. Thus the superimposed signals are destructive and the resulting signal is in its lowest energy state for both paths i and j. This represents the inner circle shown in Figure 3-8.

As mentioned earlier, the two phase trajectories merge after the second symbol (i.e. $N = 2$). Now the normalised squared Euclidean distance for this event is easily calculated from Equation (3.76) and provides an upper bound on $\delta^2_{\min}$, this upper bound for $M = 2$ and $N = 2$ is given by

$$
\begin{aligned}
d_B^2 &= \frac{4}{5} \cdot \left(5 + \frac{2\sin\pi}{\pi} + \frac{2\sin\pi}{\pi} - \frac{\sin\pi}{\pi} - 2 - 2 - \frac{4\sin\pi}{\pi} \right) \\
&= \frac{4}{5}
\end{aligned}
\tag{3.79}
$$

For comparison, the upper bound d_B^2 for an MSK signal is 2. The above expression for the upper bound d_B^2 was obtained from Equation (3.76) in this way. If the difference sequence $\zeta_x = 2$ then the phase separation is π and if $\zeta_x = 0$ then the phase separation is 0 or equally

$$
\Delta\phi = \begin{cases} \pi & if \quad \zeta_x = 2 \\ 0 & if \quad \zeta_x = 0 \end{cases}
\tag{3.80}
$$

where $\Delta\phi$ is the phase separation over a symbol interval. Thus, all the terms in Equation (3.76) correspond to two possible phase separations based on the value of ζ_x. We could have two possible cases as given below

Case I: when $\zeta_x = 0$

$$\int \cos[0 \cdot t] \, dt = 1 \tag{3.81}$$

Case II: when $\zeta_x = 2$

$$\int \cos[\pi \cdot t] \, dt = \frac{\sin\pi}{\pi} \tag{3.82}$$

Thus, at large SNR the probability of bit error rate performance of 2-MAMSK signal with a coherent receiver may be approximated by

$$P_b \approx Q\left(\sqrt{\frac{4\,E_b}{5\,N_0}}\right) \tag{3.83}$$

The bit error rate evaluated from the above expression and one obtained by simulation is shown in Figure 3-14.
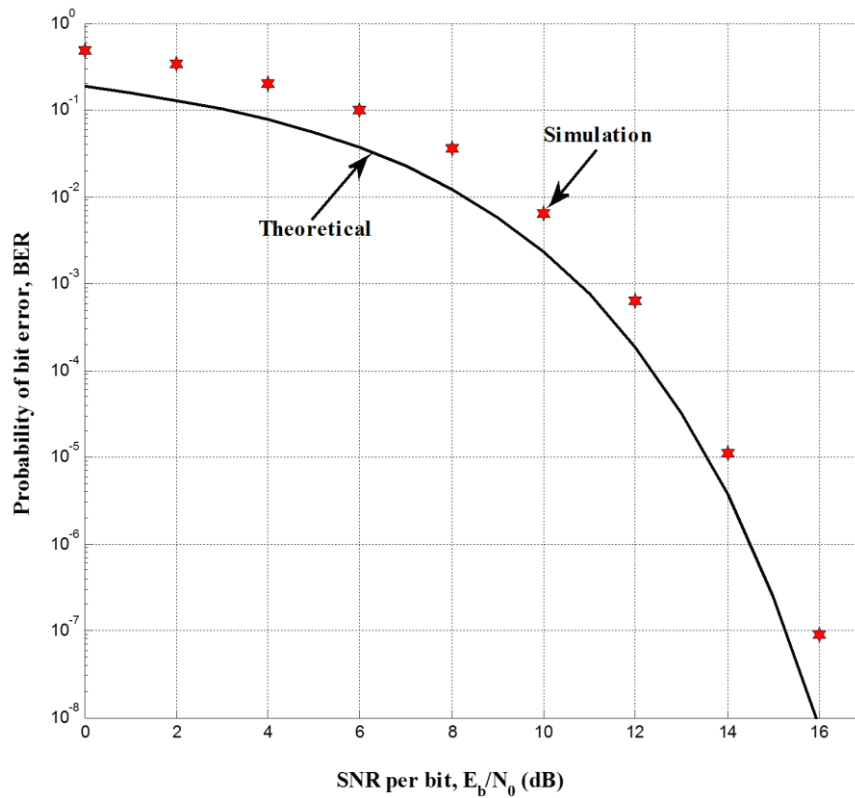
Figure 3-14 Probability of bit error for MAMSK signals

In the remaining part of this section, we will extend the result to M-MAMSK for $M > 2$. For the case of 2-MAMSK, we have established that the minimum normalised squared Euclidean distance occur when the two MSK components are out of with each other by π radians. For M-MAMSK this corresponds to the case when there is a phase difference of π radians between the largest MSK and the remaining $(M-1)$ MSK components. Using Equation (2.21), the minimum amplitude can be expressed as

$$A_{min} = \frac{\sqrt{(2E/T)}}{\sqrt{\sum_{i=1}^{M} 2^{2(i-1)}}} \left(2^{M-1} + \sum_{i=1}^{M-1} 2^{i-1} \cos \xi_i \right). \tag{3.84}$$

Given that $\xi_i = \pi$ for $i = 1, 2, \cdots, M-1$, then Equation (3.84) becomes

$$\begin{aligned} A_{\min} &= \frac{\sqrt{(2E/T)}}{\sqrt{\sum_{i=1}^{M} 2^{2(i-1)}}} \left(2^{M-1} - \sum_{i=1}^{M-1} 2^{i-1} \right) \\ &= \frac{\sqrt{(2E/T)}}{\sqrt{\sum_{i=1}^{M} 2^{2(i-1)}}} \left(2^{M-1} - [2^{M-1} - 1] \right) \end{aligned} \tag{3.85}$$

From the geometric series formula we have

$$\sum_{i=1}^{M} 2^{2(i-1)} = \frac{1}{3}(4^M - 1) \tag{3.86}$$

Substituting (3.86) into (3.85) and simplifying, we obtain an expression for the minimum amplitude as

$$A_{\min} = \sqrt{\frac{6 \cdot E}{T \cdot (4^M - 1)}}, \tag{3.87}$$

where E is the average signal energy and T is the duration of one symbol.

As mentioned earlier, the minimum squared Euclidean distance is determined from the energy of the signal with the lowest amplitude. The minimum energy of an M-MAMSK signal defined in terms of its average energy can be calculated as

$$E_{\min} = \frac{T}{2} A_{\min}^2$$

$$= \left(\frac{T}{2}\right) \cdot \frac{6 \cdot E}{T \cdot (4^M - 1)} = \frac{3 \cdot E}{(4^M - 1)} \tag{3.88}$$

To find the minimum squared Euclidean distance between the two signals $s_i(t)$ and $s_j(t)$, consider the geometric representation of the signal as shown in Figure 3-15.
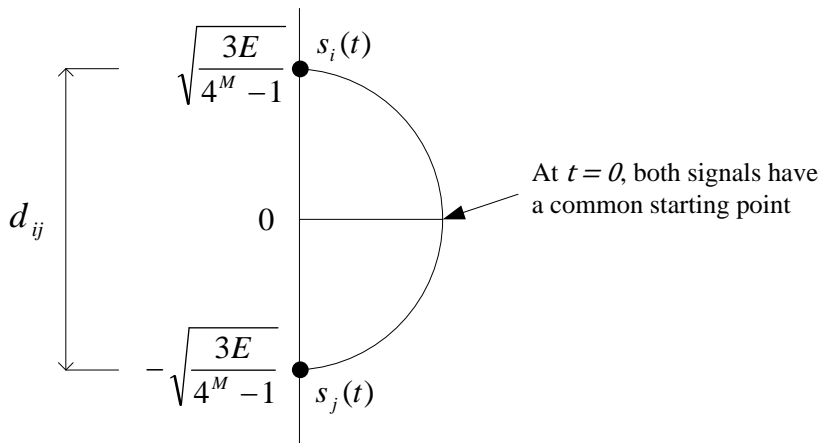
Figure 3-15 Geometric representation of signals

It is clear from Figure 3-15 that the minimum squared Euclidean distance between the two signals $s_i(t)$ and $s_j(t)$ can be defined as

$$d_{\min}^2 = 4\,E_{\min} = \frac{12 \cdot E}{(4^M - 1)} \tag{3.89}$$

where E is the average energy per symbol and with $E = ME_b$, Equation (3.89) becomes

94

$$d^2_{\min} = \frac{12\,M\,E_b}{(4^M - 1)} \tag{3.90}$$

The normalised minimum squared Euclidean distance for M-MAMSK can be expressed as

$$\delta^2_{\min} = \frac{d^2_{\min}}{2E_b} = \frac{6M}{(4^M - 1)} \tag{3.91}$$

Accordingly, at large SNR the probability of bit error rate of M-MAMSK for $M \geq 1$ with a coherent receiver may be approximated by

$$P_b \approx Q\left(\sqrt{\delta^2_{\min}\frac{E_b}{N_0}}\right) \approx Q\left(\sqrt{\frac{6M}{(4^M - 1)} \cdot \frac{E_b}{N_0}}\right) \tag{3.92}$$

where M is number of MSK components to be summed. In contrast, an expression for the bit error rate of Gray coded square QAM is given in [93] as

$$P_b \approx \frac{4}{\log_2 M} \cdot \left(1 - \frac{1}{\sqrt{M}}\right) \sum_{i=1}^{\frac{\sqrt{M}}{2}} Q\left((2i - 1)\sqrt{\frac{3\log_2 M}{(M - 1)} \cdot \frac{E_b}{N_0}}\right) \tag{3.93}$$

where M is the modulation order and defined as $M = 2^k$ where k is the number of bits per symbol.

The 2, 3 and 4-MAMSK signals are spectrally equivalent to 16, 64 and 256-QAM signals, respectively. In general, the transmission rate of square QAM system is comparable to that of M-MAMSK scheme or equally

$$\text{M} - \text{MAMSK} = 4^M - \text{QAM} \tag{3.94}$$

where M is the number of MSK components.

For the above reasons, the error performance of M-MAMSK modulation scheme is compared to 4^M-QAM. For $M = 2$, 3 and 4, the probability of bit error evaluated from Equations (3.92) and (3.93) are shown in Figure 3-16. From Figure 3-16, we observe that at high SNR there is a difference of around $0.1\,\text{dB}$ between the BER curves of M-MAMSK and 4^M-QAM, for $M = 2$, 3 and 4. This result also holds for any $M \geq 4$, for the sake of clarity, the BER curves for higher M values are not shown in Figure 3-16. Based on our analysis, we can conclude that ideally for $M \geq 1$ M-MAMSK and 4^M-QAM (square QAM) have identical BER performance for the same average energy. It can be noted that Equation (3.92) can be used as an alternative to estimate the theoretical BER of M-QAM, where M can be written as 4^n, for $n = 1, 2, 3, \cdots$.
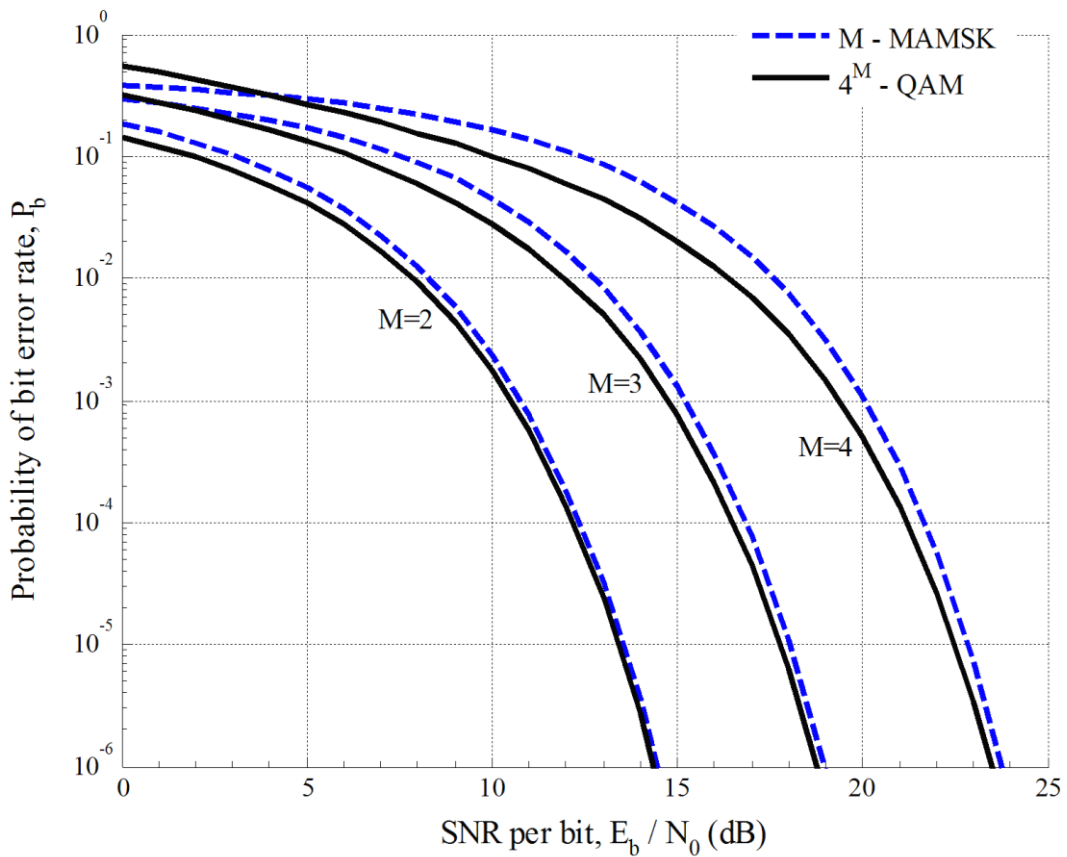

Figure 3-16 Theoretical BER of M-MAMSK Vs 4^M-QAM

3.9   Summary

In this chapter, we have characterised M-MAMSK signals for $M \geq 2$. The phase trellis of M-MAMSK is identical to that of MSK. However, the time varying phase between time intervals evolves via either straight or curved paths according to the input binary data sequences and the phase differences between the M MSK components. The information sequence carried by the largest MSK component controls the overall phase of M-MAMSK, whereas any of the other information sequences causes the curvature when it has opposite sign to the binary data sequence carried by the MSK component with highest amplitude.

The signal space diagram of M-MAMSK is represented by various circles and ellipses. Each circle represents an amplitude level defined from the set $\{\pm 1, \pm 3, \cdots, \pm 2^M - 1\}$. Hence, each symbol point can evolve from one level to another though 2^{M-1} trajectories. Only one of these trajectories is circular, the others are elliptical arcs. The highest amplitude level occurs when there is a phase difference of 0 among the M MSK components. A phase difference of π radians between the largest MSK component and the remaining $(M-1)$ MSK components causes the lowest amplitude level.

The power spectral density of M-MAMSK was derived and compared to that of M-QAM. The comparison was in favour of M-MAMSK in terms of spectral sidelobe roll-off rate, whereas the main lobe of the M-MAMSK spectrum is 1.5 times that of M-QAM. This is not a serious drawback for M-MAMSK as 99% of the signal power falls within the main lobe and it has the same throughput as square QAM. Finally, the error probability expression of M-MAMSK in AWGN was derived and compared to that of QAM system having a square constellation of size $M = 4^n$ for $n = 1, 2, 3, \cdots$. The results show that both schemes achieve almost identical BER performance for the same average-transmit power. The theoretical BER expression for an M-MAMSK can be used as an alternative to approximate the error performance of Gray coded square QAM over an AWGN channel.

Chapter 4

Space-Time Block Codes With Differentially Detected Multi-Amplitude Minimum Shift Keying

4.1 Introduction

Continuous phase signals are useful modulation schemes for wireless transmission because of their characteristics of constant envelope and fast spectral roll-off [63]. Minimum shift keying (MSK) is a continuous phase modulation (CPM) scheme, which has a modulation index of 1/2. A 2-level multi-amplitude minimum shift keying (2-MAMSK) signal retains many of the characteristics of CPM signals and has the potential to increase the data rate of an existing MSK system by a factor of two. Furthermore, we have established that the phase values of a 2-MAMSK signal at the symbol transition times are identical to that of MSK. This allows differential

detection of the 2-MAMSK signal. Differential detectors are attractive in wireless communications due to their low complexity and robustness to carrier phase variations [86, 87].

Multipath fading causes the received signal power to fluctuate [11] and hence degrades system reliability and performance [12, 14]. Diversity techniques [25, 26, 47, 56] have been deployed to combat the effect of multipath fading and improve performance. Space-time block codes (STBCs) are techniques widely used in systems with multiple transmit and/or receive antennas to achieve diversity gain in wireless fading channels. In space-time block coded systems digital symbols from different antennas are encoded into redundant copies and usually are sent over different time slots. One form of STBC is the so-called orthogonal STBC (OSTBC). These achieve full diversity gain and allow simple linear decoding at the receiver. Orthogonal STBCs suffer from loss of throughput as the number of transmit antennas is increased. The Alamouti code [6] is a special case of orthogonal STBCs with two transmit antennas that achieves full data rate.

In this chapter, we propose the design and implementation of orthogonal space-time block coded systems utilising 2-MAMSK signals (OSTBC 2-MAMSK). The 2-MAMSK signal used in this chapter is modelled as a superposition of two constant envelop MSK signals with different amplitudes. This allows us to amplify each of the two constant-envelope MSK signals individually with a nonlinear amplifier prior to addition. A second and most important reason is that a simple and inexpensive differentially 2-MAMSK demodulator proposed by Javornik and Kandus [43] can be used to detect the transmitted binary data sequence.

The nonlinearity and inherent memory of CPM makes the design of space-time coded CPM (STC-CPM) complicated. To overcome the complexity of the nonlinearity introduced in the phase of the CPM signal a sampling approach as in [54] is used. Hence, the 2-MAMSK signal becomes an offset 16-QAM and thus the implementation of orthogonal STBCs

becomes possible. Despite the fact that 2-MAMSK is a non-constant envelope scheme, the proposed system provides a high-capacity data network and retains most of the benefits of CPM signals. It provides the same throughput as STBC 16-QAM. Compared with STC MSK [49, 54], our scheme has twice the bandwidth efficiency by carrying information not only on the phases but also on the amplitudes. Simulation results show that the OSTBC 2-MAMSK can provide the same probability of bit error rate (BER) as 16-QAM with maximal ratio combining (16-QAM MRC). The proposed system has advantage of using a differential receiver rather than the complex maximum likelihood detection (MLD) used for 16-QAM MRC [14, 94].

The rest of the chapter is organised as follows. In the next section, we present the structure of the OSTBC 2-MAMSK transmitter. Primarily, we focus on the Alamouti STBC [6] with two transmit antennas as well as the orthogonal STBC [5, 95] for three transmit antennas with a rate of 3/4. The channel model assumed and the components of the 2-MAMSK receiver are described in the following sections, respectively. The chapter concludes with simulation results and a short summary.

4.2   OSTBC 2-MAMSK Transmitter

The design of the OSTBC 2-MAMSK transmitter is performed in several stages. A simplified block diagram of the proposed transmitter is illustrated in Figure 4-1. The first stage of operation (2-MAMSK modulator) is described in details in section 2.5. Here, we review the key elements that need to be covered in order to describe the proposed transmitter. The input data sequence, d_k with values ± 1 is converted into two parallel streams. This is achieved using a serial to parallel converter. Each of the two parallel streams is destined to an MSK modulator. For our referencing, the upper parallel stream is labelled as α and the lower stream is labelled as β. Accordingly, the data sequence, α is the input to the MSK modulator with the smaller amplitude and the data sequence, β is the input to the MSK

modulator with the larger amplitude. Both α and β represent two independent binary information sequences that take values from the set $\{-1, +1\}$. Under this condition, we can assume that the outputs of the two MSK modulators are identical but independent of each other.
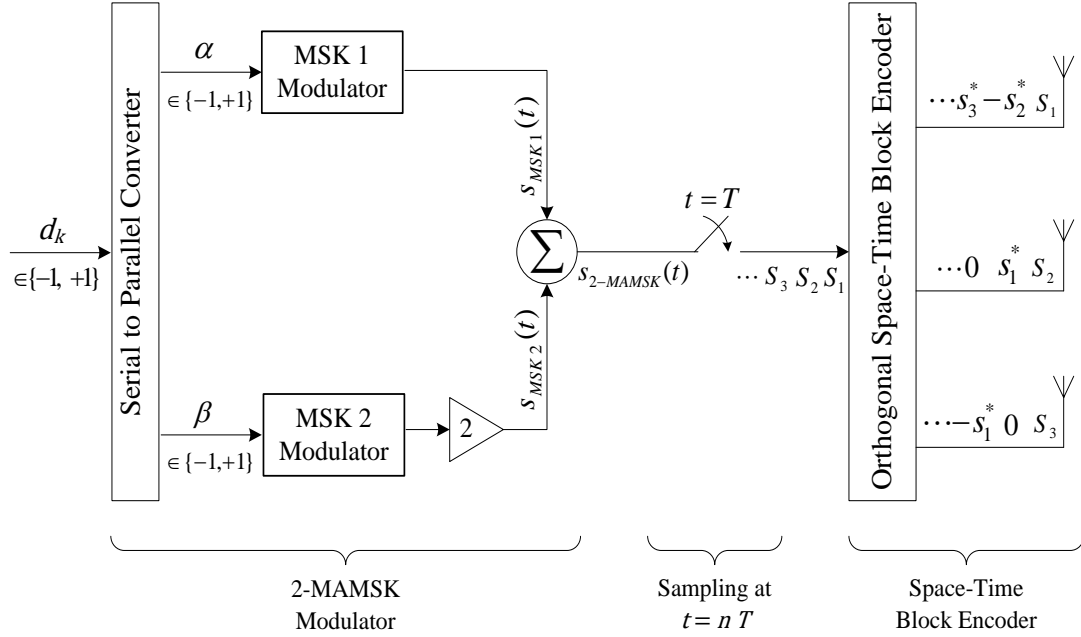
Figure 4-1 Block diagram of the OSTBC 2-MAMSK transmitter

The two MSK Modulator blocks take the two independent binary information sequences α and β as their input. The output of each modulator block is an MSK signal with continuous phase, constant envelope and a modulation index of $h = 1/2$. For detailed discussions, see sections 2.2, 2.3.1 and 2.3.3. We denote the output of MSK 1 Modulator as $s_{MSK\,1}(t)$ and the output of the MSK 2 Modulator after the amplification as $s_{MSK\,2}(t)$.

Using Equation (2.6), the complex baseband MSK signals, $s_{MSK\,1}(t)$ and $s_{MSK\,2}(t)$ as function of time can be expressed as

$$s_{MSK\,1}(t) = \pm \cos\left(\frac{\pi t}{2T}\right) \pm j \, \sin\left(\frac{\pi t}{2T}\right), \qquad nT \leq t \leq (n+1)T \qquad (4.1)$$

$$s_{MSK\,2}(t) = \pm\,2\,\cos\left(\frac{\pi t}{2T}\right) \pm j\,2\,\sin\left(\frac{\pi t}{2T}\right), \qquad nT \leq t \leq (n+1)T \quad (4.2)$$

where T is the bit period of the data streams, $s_{MSK\,1}(t)$ is the MSK component with the smaller amplitude and $s_{MSK\,2}(t)$ is that with the larger amplitude. It can be noted that the amplitude of the larger MSK signal is twice that of the smaller MSK.

From Figure 4-1, we observe that the outputs of the two MSK modulators are summed to give the complex 2-MAMSK signal, denoted $s_{2-MAMSK}$. Subsequently, we may describe a 2-MAMSK signal as a superposition of two MSK signals with unequal amplitudes and defined over the interval $nT \leq t \leq (n+1)T$ as

$$s_{2-MAMSK}(t) \triangleq s_{MSK\,1}(t) + s_{MSK\,2}(t) \qquad\qquad (4.3)$$

By substituting Equations (4.1) and (4.2) into (4.3), we obtain an expression for the complex baseband representation of a 2-MAMAK signal as

$$
\begin{aligned}
s_{2-MAMSK}(t) &= \left[\pm\cos\left(\frac{\pi t}{2T}\right) \pm j\,\sin\left(\frac{\pi t}{2T}\right)\right] \\
&\quad + \left[\pm 2\cos\left(\frac{\pi t}{2T}\right) \pm j\,2\sin\left(\frac{\pi t}{2T}\right)\right] \\
&= (\pm 1 \pm 2)\cos\left(\frac{\pi t}{2T}\right) + j\,(\pm 1 \pm 2)\sin\left(\frac{\pi t}{2T}\right) \\
&= a_I(t)\cos\left(\frac{\pi t}{2T}\right) + j\,a_Q(t)\sin\left(\frac{\pi t}{2T}\right)
\end{aligned}
\qquad (4.4)
$$

where $a_I(t)$ and $a_Q(t)$ encode the information bits into the 2-MAMSK symbols, each taking values independently from the set $\{\pm 1, \pm 3\}$. In section 3.5, we have shown that the values of $a_I(t)$ and $a_Q(t)$ depend on the phase difference between the two MSK signals and the information sequences α and β. Using the results of Table 3-6, we can define $a_I(t)$ and $a_Q(t)$ in terms of α, β and the phase difference as

$$a_I(t) = 2\beta + \beta \cos(\xi) \tag{4.5}$$

$$a_Q(t) = 2\beta + \alpha \cos(\xi) \tag{4.6}$$

where ξ is the phase difference between the two MSK signals, which takes on values of 0 or π at the symbol transition times.

The in-phase and quadrature pulse shaping, denoted as $p(t)$ and $q(t)$, can be written as

$$p(t) = \cos\left(\frac{\pi t}{2T}\right), \qquad nT \le t \le (n+1)T \tag{4.7}$$

$$q(t) = p(t - T) = \sin\left(\frac{\pi t}{2T}\right), \qquad nT \le t \le (n+1)T \tag{4.8}$$

Now, the complex baseband 2-MAMSK signal, denoted $s(t)$ can be written in the form

$$s(t) = a_I(t) \cdot p(t) + j\, a_Q(t) \cdot q(t) \tag{4.9}$$

where $a_I(t)$ and $a_Q(t)$ are the equivalent in-phase and quadrature data terms, which are defined by Equations (4.5) and (4.6), respectively. The terms $p(t)$ and $q(t)$ represent the in-phase and quadrature symbol weightings, respectively.

From Equations (4.7) and (4.8) and (4.9), we observe that the equivalent in-phase data term, $a_I(t)$, which takes on values from the set $\{\pm 1, \pm 3\}$, can only change value at the zero crossing of $p(t)$. Similarly, the quadrature data term, $a_Q(t)$, can only change value at the zero crossing of $q(t)$. Since the quadrature symbol weighting $q(t)$ is delayed by T second (half a symbol period) with respect to $p(t)$, the 2-MAMSK signal of (4.9) can be viewed as an offset 16-QAM signal with a half-cycle sinusoidal symbol pulse shape.

Also note that the input binary information sequences α and β are of rate $1/T$, whereas the equivalent data pulses in both the in-phase and the quadrature channels are of duration $2T$. Clearly, the 2-MAMSK modulator

presented here could easily be generalised to M-MAMSK for $M \geq 2$. In particular, the ith component for $i = 2, 3, \cdots, M$ would have an amplitude which is 2^{i-1} times that of the first component. For more details on 2-MAMSK and M-MAMSK, see sections 2.4 and 2.5 along with chapter 3.

The next operation performed in the OSTBC 2-MAMSK transmitter shown in Figure 4-1 is sampling the 2-MAMSK signal at the symbol transition points (i.e. at the time instants $t = nT$). In other words, the 2-MAMSK signal of (4.9) sampled at the rate of $1/T$ samples per second. Thus, the 2-MAMSK signal becomes a $\pi/2$ shifted (offset) 16-QAM and as a result, we would obtain 16 unique symbols as shown in Figure 4-2. It can be noted that each symbol contains 4 bits and these points can be Gray coded.
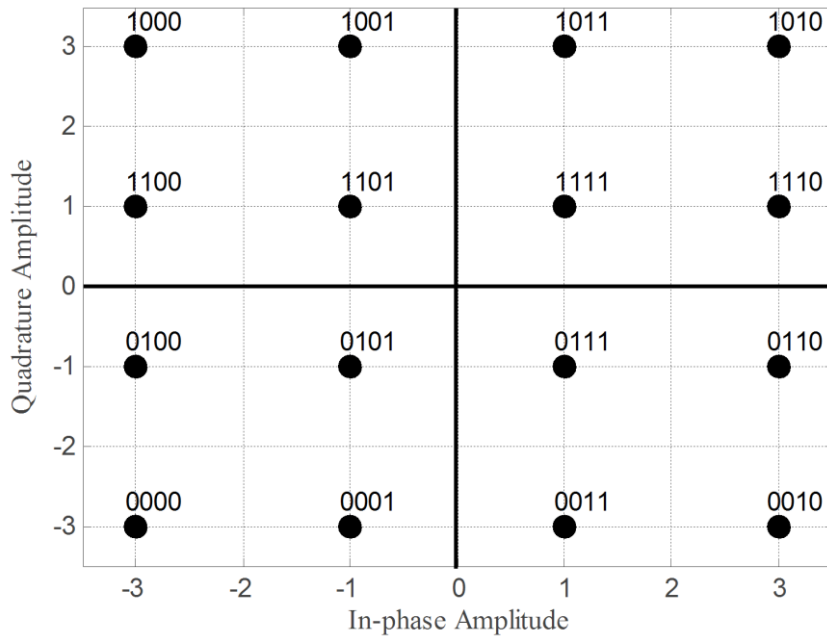

Figure 4-2 Signal constellation for 2-MAMSK sampled at a rate $^1/_T$

The constellation points can be conveniently expressed in terms of $a_I(t)$ and $a_Q(t)$. The resulting symbol set s_i can be written in the form,

$$s_i = a_I(t) + j\, a_Q(t) \tag{4.10}$$

The data terms $a_I(t)$ and $a_Q(t)$ are constant over a duration of T seconds, since the phase difference, ξ and the sequences α and β are constant over T seconds. Hence, we can define the sampled complex 2-MAMSK symbols as

$$s_i = \{\pm 1, \pm 3\} + j\,\{\pm 1, \pm 3\}, \qquad \text{for } i = 1, 2, 3, \cdots, 2^4 \tag{4.11}$$

The complex 2-MAMSK symbols from the output of the sampler are then space-time block encoded. At first, we consider the Alamouti STBC [6] with two transmit antennas. The Orthogonal Space-Time Block Encoder for the case of the Alamouti scheme has the transmission code matrix, $\boldsymbol{S}$

$$\boldsymbol{S} = \begin{bmatrix} s_1 & -s_2^* \\ s_2 & s_1^* \end{bmatrix} \tag{4.12}$$

where the rows represents the two transmit antennas and the columns represent the two time slots. In the first time interval s_1 is transmitted from one transmit antenna and simultaneously, s_2 from the other. During the second time instant the conjugate values of $-s_2$ and s_1 are transmitted from antenna one and two, respectively. The symbols s_1 and s_2 are selected from the constellation alphabet given by (4.11). Note also that each symbol has only half the total transmitted power. Hence, the columns of $\boldsymbol{S}$ have unit length and are orthogonal to each other.

As a generalisation to more than two transmit antennas, we consider the matrix code proposed in [95] for three transmit antennas

$$\boldsymbol{S} = \begin{bmatrix} s_1 & -s_2^* & s_3^* & 0 \\ s_2 & s_1^* & 0 & s_3^* \\ s_3 & 0 & -s_1^* & -s_2^* \end{bmatrix} \tag{4.13}$$

This transmission code matrix has a rate of 3/4 because it requires 4 time slots to transmit 3 symbols. The output of the sampler s_1, s_2 and s_3 are the input symbols to the OSTBC encoder block and its output is given by (4.13). The matrix index (i, l) indicates the symbol transmitted from the ith antenna in the lth time slot. The value of i can range from 1 to N_t, the

number of transmit antennas. The value of l can range from 1 to the codeword block length. As before, the columns of S have unit length and are orthogonal to each other. The technique can be easily modified to accommodate any orthogonal STBC design. The matrix code for higher numbers of transmit antennas are given in [23].

4.3　Channel Model

The channel model considered is a quasi-static Rayleigh fading with perfect channel state information (CSI) at the receiver. We assume the channel gains remain constant over the transmission of a codeword block and vary independently from one codeword block to another. The multiple input multiple output (MIMO) channel is denoted by the matrix, H with coefficients h_{ji} that represent the channel fading coefficient from the ith transmit antenna to the jth receive antenna. The parameters h_{ji} are zero mean Gaussian random variables of unit variance. For a multipath environment, the MIMO channel can be described by a complex matrix, H

$$
H = \begin{bmatrix} h_{11} & \cdots & h_{1N_t} \\ \vdots & \ddots & \vdots \\ h_{N_r 1} & \cdots & h_{N_r N_t} \end{bmatrix} \tag{4.14}
$$

of dimension $N_r \times N_t$, where N_t and N_r are the numbers of transmit and receive antennas, respectively.

There will be an additional noise due to the receiver's front end. The noise is assumed to be additive white Gaussian noise (AWGN) with mean zero and variance σ_n^2. For detailed discussions on the channel characteristics, refer to section 1.2.

4.4   OSTBC 2-MAMSK Differential Receiver

Figure 4-3 illustrates a simplified block diagram of the proposed OSTBC 2-MAMSK differential receiver. As shown, the proposed receiver consists of two subsystems: the OSTBC combiner and the 2-MAMSK differential detection. Consequently, the recovery of the transmitted data sequence, d_k is a two step process. The first step involves the decoding of the OSTBC signals. This is followed by the differential detection of the 2-MAMSK signals.
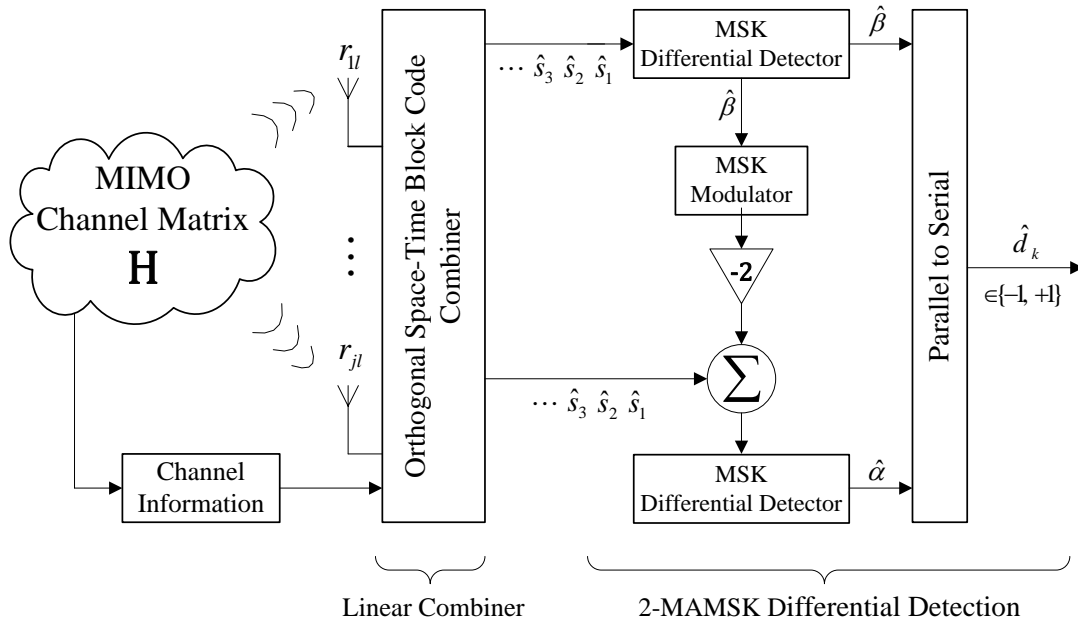
Figure 4-3   Block diagram of the OSTBC 2-MAMSK differential receiver

The OSTBC 2-MAMSK signals of (4.12) and (4.13) are transmitted over a MIMO channel of size $N_r \times N_t$. As discussed in the previous section, the received signal is a combination of transmitted signals multiplied by the channel gains, h_{ji} and degraded by noise at the receiver. At first, we consider, a multiple input single output (MISO) system with two transmit antennas and one receive antenna (2×1 MISO system). Then we provide a

more general solution that can be applied to accommodate any number of receive antennas for $j = 1, \cdots, N_r$.

For a 2×1 MISO system, the received signal during the first time slot, denoted r_{11}, can be written as

$$r_{11} = h_{11}\, s_1 + h_{12}\, s_2 + n_{11} \tag{4.15}$$

Similarly, the received signal during the second time slot, denoted r_{12}, can be expressed as

$$r_{12} = -h_{11}s_2^* + h_{12}\, s_1^* + n_{12} \tag{4.16}$$

where n_{11} and n_{12} are complex Gaussian noise and $(\cdot)^*$ denotes complex conjugate. The coefficients h_{11} and h_{12} are the channel gains, which are assumed to remain constant over two time slots.

The OSTBC combiner block combines the received signals of (4.15) and (4.16) with the CSI to estimate the soft information of the encoded symbols. To obtain an estimate of s_1, the combiner multiplies the conjugates of h_{11} and h_{12} by r_{11} and r_{12}, respectively. Then neglecting the noise terms, we have

$$h_{11}^* r_{11} = |h_{11}|\, s_1^{\,2} + h_{11}^* h_{12}\, s_2 \tag{4.17}$$

$$h_{12}^* r_{12} = -h_{12}^* h_{11} s_2^* + |h_{12}|^2\, s_1^* \tag{4.18}$$

By taking the conjugate of Equation (4.18) and adding the outcome to Equation (4.17), we obtain an estimate for s_1 as

$$\hat{s}_1 = \frac{h_{11}^* r_{11} + h_{12}\, r_{12}^*}{|h_{11}|^2 + |h_{12}|^2} \tag{4.19}$$

where $\hat{s}_1$ is a soft estimate of s_1. Similarly, we multiply r_{11} and r_{12} by conjugates of h_{12} and h_{11}, respectively and we obtain an estimate for s_2 as

$$\hat{s}_2 = \frac{h_{12}^* r_{11} - h_{12} r_{12}^*}{|h_{11}|^2 + |h_{12}|^2} \tag{4.20}$$

where $\hat{s}_2$ is a soft estimate of s_2. Note that the receiver is assumed to have knowledge of the channel experienced by the signal.

Now, we provide a more general solution for the proposed system. The received signal, $\boldsymbol{R}$ can be written in matrix form as

$$\boldsymbol{R} = \boldsymbol{HS} + \boldsymbol{N}, \tag{4.21}$$

where $\boldsymbol{R}$ is of dimension $N_r \times \eta$ with r_{jl} denoting the received signal on the jth receive antenna during the lth time slot, $\boldsymbol{H}$ is the MIMO channel matrix defined by Equation (4.14) and $\boldsymbol{N}$ is a complex AWGN matrix at the receiver of size $N_r \times \eta$, with n_{jl} denoting a random noise variable generated by the jth receive antenna during the lth time slot.

The OSTBC combiner shown in Figure 4-3 takes the received signal of (4.21) as its input and outputs an estimate of the transmitted symbols

$$\begin{bmatrix} \hat{s}_1 \\ \vdots \\ \hat{s}_k \end{bmatrix} = \frac{1}{|H|^2} \sum_{j=1}^{N_r} \begin{bmatrix} h_{j1}^* r_{j1} + h_{j2} r_{j2}^* - h_{j3} r_{j3}^* \\ h_{j2}^* r_{j1} - h_{j1} r_{j2}^* - h_{j3} r_{j4}^* \\ h_{j3}^* r_{j1} + h_{j1} r_{j3}^* + h_{j2} r_{j4}^* \end{bmatrix} \tag{4.22}$$

where $\hat{s}_k$ is the estimated k^{th} symbol in the code matrix, $\boldsymbol{S}$ and h_{ji} represents the channel gain from the ith transmit antenna and the jth receive antenna. The value of i can range from 1 to the number of transmit antennas, N_t, and the value of j can range from 1 to the number of receive antennas, N_r. r_{jl} represents the lth symbol at the jth receive antenna per codeword block. The value of l can range from 1 to the codeword block length, η. $|H|^2$ is the sum of the channel gains defined as

$$|H|^2 = \sum_{i=1}^{N_t} \sum_{j=1}^{N_r} |h_{ji}|^2. \tag{4.23}$$

The soft estimates of the data symbols are fed to the 2-MAMSK differential detector, which is the second stage of the detection process. The operation of the 2-MAMSK differential detector is discussed in detail in section 2.8 and reference [43]. Hence, we only briefly describe the key elements that are essential to retrieve the original binary data stream. In chapter 3, we have shown $\beta = +1$ causes the 2-MAMSK signal phase to increase by $\pi/2$ and $\beta = -1$ causes the phase to decrease by $-\pi/2$, over a T-sec interval. Using this result, a symbol-by-symbol differential MSK detector [86, 87] is used to estimate the information sequence carried by the larger MSK signal, denoted $\hat{\beta}$.

The estimated data sequence, $\hat{\beta}$ is used to regenerate the original transmitted MSK signal with the larger amplitude. The regenerated MSK signal is subtracted from the soft estimates in order to obtain the smaller MSK signal. At the point, the 2-MAMSK signal is reduced to conventional MSK and hence differential MSK detection [86, 87] is used to retrieve the information sequence carried by the smaller MSK signal, denoted $\hat{\alpha}$. Finally, a parallel to serial convertor is used to form an estimate of the transmitted data sequence, denoted $\hat{d}_k$.

4.5   Simulation Results

The proposed system provides the same throughput as systems utilising 16-QAM signals. To evaluate the decoding BER performance, we have compared the proposed OSTBC 2-MAMSK system with the well-known MRC 16-QAM system for various diversity orders. More specific, for our system we consider the following transmit and receive antenna configurations: two transmit antennas, one receive antenna (2×1 MISO), two transmit antennas, two receive antennas (2×2 MIMO) and three transmit antennas, two receive antennas (3×2 MIMO).

The average probability of bit error rate for square M-QAM with MRC over Rayleigh fading channels is given in [14, 94] as

$$P_b$$

$$= \frac{2}{\pi\sqrt{M}\,\log_2\sqrt{M}}$$

$$\times \sum_{k=1}^{\log_2\sqrt{M}} \sum_{i=0}^{(1-2^{-k})\sqrt{M}-1} \left\{ (-1)^{\left(\frac{i2^{k-1}}{\sqrt{M}}\right)} \left(2^{k-1} - \left[\frac{i2^{k-1}}{\sqrt{M}} + \frac{1}{2} \right] \right) \right. \qquad (4.24)$$

$$\left. \times \int_0^{\pi/2} \prod_{l=1}^{L} \left(\frac{1}{1-s\gamma_l} \right) \left(-\frac{(2i+1)^2\, 3/[2(M-1)]}{\sin^2\theta} \right) d\theta \right\}$$

where M is the modulation order and defined as $M = 2^k$, where k is the number of bits per symbol. L represents number of diversity branches, $\gamma_l = E_b/N_0$ is the average SNR per bit per branch and s is a complex dummy variable. Note that the term $(1-s\gamma_l)^{-1}$ is the moment generating function (MGF) of Rayleigh fading and the expression only involves the integration with respect to θ over the integral of $[0, \ \pi/2]$.

The BER curves for OSTBC 2-MAMSK versus MRC 16-QAM in Rayleigh fading channel with diversity orders of $L = 2, 4$ and 6 are shown in Figure 4-4. For the case of MRC 16-QAM, Equation (4.24) is used to evaluate the average bit error probability, P_b whereas the BER curves obtained for OSTBC 2-MAMSK are the results of simulations. At each SNR, the simulations were stopped after detecting 500 errors and at least 10×10^8 symbols were transmitted. For reference, the error rates of 2-MAMSK and 16-QAM in a Rayleigh fading channel without diversity ($L = 1$) is also plotted on the same figure. For both the transmit and receive diversity, the total power is normalised across all the diversity branches, i.e. the E_b/N_0 parameter is scaled by a factor of $L = 2, 4$ and 6. Otherwise, the 2-MAMSK transmit diversity would have a 3 dB disadvantage when compared to MRC receive diversity.

From Figure 4-4, we observe that the 2×1, 2×2 and 3×2 systems provide the same diversity orders as the MRC systems with one transmit

antenna and two, four and six receive antennas, respectively. The resulting simulation results show that at high SNR, the proposed receiver requires only around 1 dB of additional signal power per transmitted bit to achieve the same BER performance as theoretical 16-QAM with MRC. The 1 dB penalty is due to using the differential receiver rather than the complex maximum likelihood detection (MLD) used for MRC 16-QAM [14, 94]. If we use coherent detection of 2-MAMSK then the performance should be identical for both systems. However, differential detection is attractive for practical application due to its simplicity.
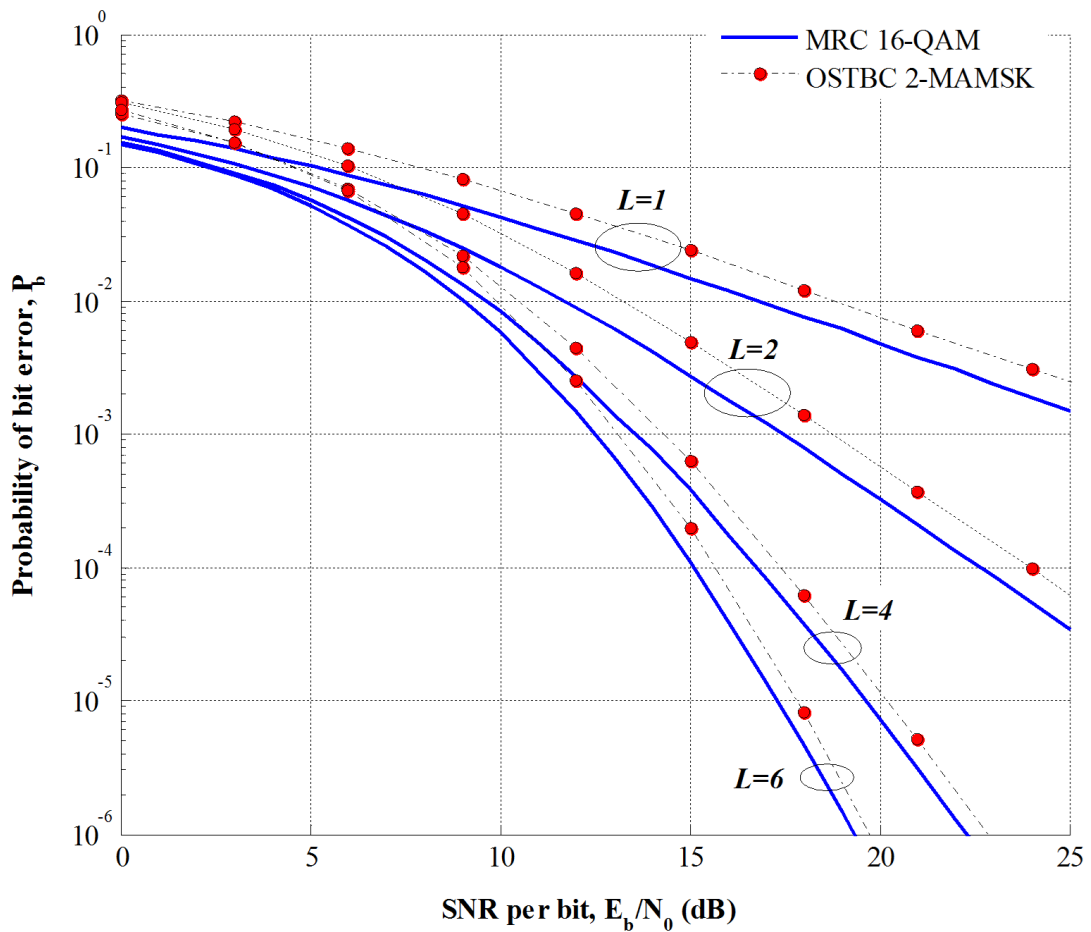
Figure 4-4 Average P_b for 16-QAM and 2-MAMSK in Rayleigh Fading with various diversity orders, 16-QAM are theoretical curves of [14, 94], $L=$ total diveristy

4.6   Summary

In this chapter, we have presented an orthogonal STBC MIMO system using 2-MAMSK signals. The proposed system provides high-capacity data transmission by carrying information not only in the phases but also in the amplitudes. The performance of the system is compared to that of SIMO MRC systems utilising 16-QAM signals. The system is simulated in a quasi-static Rayleigh flat fading channel for various transmit and receive antenna configurations. Simulation results show that the proposed differential receiver achieves performance within 1 dB of the coherent detection used for MRC 16-QAM system. The advantage is that the proposed system has low complexity and can be implemented using the existing orthogonal STBCs in conjunction with MSK modems.

Chapter 5

Cooperative Diversity Using Multi-Amplitude Minimum Shift Keying

5.1 Introduction

One of the most powerful techniques to mitigate the effects of multipath fading is diversity. The idea of diversity is to transmit and receive the same data over independent fading paths. As we have discussed previously, one possible way to achieve diversity is to deploy multiple antennas at one or both ends of the communication link. However, in some wireless networks it may not be practical or feasible to deploy multiple antennas, (e.g. wireless sensor networks). This is because low powered wireless and mobile devices are small in size and have limited processing power, memory and battery life. In these situations, a technique known as cooperative diversity [28-30, 66, 67] or cooperative communication may be used to achieve transmit diversity and to extend coverage. Throughout this chapter, we shall call wireless and mobile devices nodes.

In general, cooperative or relay assisted communication can be achieved using two main strategies: decode-and-forward (DF) [35, 66, 67] and amplify-and-forward (AF) [67]. In the first scheme, the relaying node(s) decode and re-encode the source's message and then transmit it to the destination. In the second case, the relay(s) simply amplify and forward the source's signal towards the destination. Each node's time slot may thus be considered as two sub-slots: one is for transmitting its own message and the other for relaying data. As discussed in chapter 1, each relaying protocol has its own advantages and disadvantages depending on the channel condition of the source-relay link and the relaying capabilities [36-38].

As mentioned, in the classical strategies each node only uses half the length of its available time slot to communicate new information which causes it to exhibit low bandwidth efficiency. To compensate for this, Larsson and Vojcic [68] proposed a new cooperative transmission scheme based on DF, which increases the throughput by using superposition modulation. In the work of [68] both the source and the relaying node employ binary phase shift keying (BPSK) modulation and the superimposed signal results in a 4 level pulse amplitude modulation (4-PAM). The idea has been extended to higher order modulation schemes [96-101] and resulted in further spectral efficiency. The performance of the superposition based cooperative diversity is analysed in [98, 99, 102-104].

In this chapter, we consider the relay channel [31] employing superposition modulation cooperative transmit diversity [68] utilising a 2-level multi-amplitude minimum shift keying (2-MAMSK) signal. Furthermore, we restrict our consideration to the DF strategy in a half-duplex environment, where a node cannot transmit and receive data packets simultaneously. The proposed cooperative diversity system employing 2-MAMSK (CD 2-MAMSK) has the lowest detection complexity among the proposed cooperative diversity with superposition modulation (CD-SM) schemes [68, 96-101, 105]. This is because the proposed system at the destination node uses the differential 2-MAMSK detector [43] rather than

the iterative maximum a posteriori (MAP) detection used for CD-SM schemes [68, 96-101, 104, 105].

Moreover, the transmitting node exploits the overall 2-MAMSK phase to differentially decode the relaying signal without knowledge of its own information which was transmitted two time slots ago. Consequently, the proposed CD 2-MAMSK achieves the same results as those presented in [68, 96-101, 105], but with one less operation and lower memory requirements. As mentioned, the point of using cooperative diversity is to provide wireless nodes, which are constrained in size, memory and processing capability, with diversity gains. Thus, MAMSK signal is an excellent choice for this type of cooperative communication since it provides the same diversity gain with less memory and lower computational complexity.

The rest of the chapter is organised as follows. In the next section, we describe the system model of the CD 2-MAMSK scheme. The transmission protocol and the detection process are described in the following section. Simulation results and a short summary are presented in the last two sections.

5.2   System Model

We consider a wireless relay network, which consists of three nodes labelled "A", "B" and "D". As illustrated in Figure 5-1, the system operates in half-duplex mode, such that only node A or B can transmit or receive in each interval. The nodes A and B are paired as partners and communicate data packets $\{A_k, B_k\}$ to a common destination D by taking turns. They collaborate in transmitting their data by acting as relays for each other. A transmitting node plays the roles of the source and relay simultaneously by superimposing its own "local" signal and the partner's "relay" signal onto a common signal.   In contrast, in more conventional strategies [35, 66, 67] a node can either be a source or a relay at any given time.
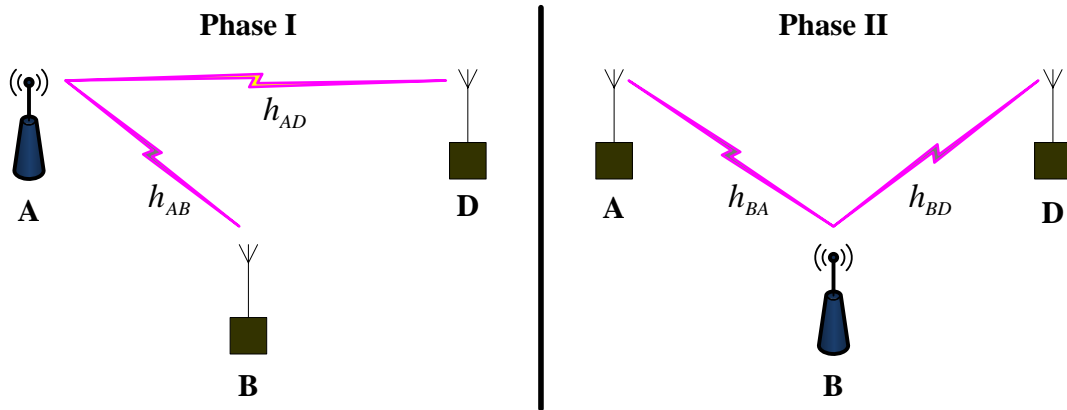
Figure 5-1   Channel model for the proposed CD 2-MAMAK scheme

In this chapter, we consider the DF relaying scheme, which requires the transmitting node to successfully decode the partner's message and then re-encode it before retransmitting. Once the message is successfully re-encoded, the transmitting node assigns a portion of its power to the relay signal and the remaining power for the local signal. The portion of the power dedicated to the relay signal, known as the superposition ratio, is crucial [68, 98, 99] in this superposition diversity scheme. This is because an insufficient or excessive amount of power allocation may reduce the cooperation success rate. We come back to this point later. Finally, the node transmits the algebraic superposition of the two signals. For our system, we assume that both transmitting nodes A and B are only capable of modulating information sequences using minimum shift keying (MSK) scheme. Therefore, the superimposed two MSK-modulated signals results in a 2-level multi-amplitude minimum shift keying signal, which carries both the local and relay information.

5.3   Cooperative 2-MAMSK Transmission Protocol

Assume that $\{A_k\}$ and $\{B_k\}$ for $k = 1, 2, \cdots, N$ are two independent binary information sequences of length N, to be transmitted by the nodes A and B to a common destination D. To demonstrate the scheme, let us assume that

117

data transmission initiates at node A (node B is similar). In the first time slot, node A modulates the data packet A_1 into s_{A1} and transmits s_{A1} to both B and D. In the second time slot, node B decodes packet A_1 which was received from node A in the previous time slot. Unlike a conventional DF scheme, instead of forwarding only the re-encoded version of A_1, node B transmits a superposition of its own signal s_{B2} with power $1 - \gamma^2$ and the remodulated version of s_{A1} with power γ^2, where γ is the superposition ratio. During the third time slot, node A transmits the local signal s_{A3} with power $1 - \gamma^2$ and the relay signal s_{B2} with power γ^2. This process is repeated until the transmission is complete. For more information, refer to the timing diagram shown in Figure 5-2. Note that the total emitted power is normalised to 1 in all cases.

Time	Slot 1	Slot 2	Slot 3	$\cdots$	Slot 2N-1	Slot 2N
Transmission at node A	s_{A1}		$\sqrt{1-\gamma^2}\,s_{A3}$ $+\sqrt{\gamma^2}s_{B2}$	$\cdots$	$\sqrt{1-\gamma^2}\,s_{A(2N-1)}$ $+\sqrt{\gamma^2}\,s_{B(2N-2)}$	
Transmission at node B		$\sqrt{1-\gamma^2}s_{B2}$ $+\sqrt{\gamma^2}s_{A1}$		$\cdots$		$\sqrt{1-\gamma^2}\,s_{B2N}$ $+\sqrt{\gamma^2}\,s_{A(2N-1)}$
Reception at node D	s_{A1}	$\sqrt{1-\gamma^2}\,s_{B2}$ $+\sqrt{\gamma^2}s_{A1}$	$\sqrt{1-\gamma^2}\,s_{A3}$ $+\sqrt{\gamma^2}s_{B2}$	$\cdots$	$\sqrt{1-\gamma^2}\,s_{A(2N-1)}$ $+\sqrt{\gamma^2}\,s_{B(2N-2)}$	$\sqrt{1-\gamma^2}\,s_{B2N}$ $+\sqrt{\gamma^2}\,s_{A(2N-1)}$

Figure 5-2 Transmission protocol of the cooperative 2-MAMSK system

Note that for the superposition scheme each data packet is modulated twice: once locally at the originating node and again as a relayed packet at the partner node. In this work, we assume that the message block is encoded with the same scheme at both the source and relay nodes. Assuming that the system is in continuous operation and neglecting the effect of the initial transmission, the transmitted superimposed signal, during k^{th} time slot can be written as

$$s_k = \sqrt{1 - \gamma^2}\, s_{ik} + \sqrt{\gamma^2}\, s_{j(k-1)} \tag{5.1}$$

where k is the kth time slot, s_{ik} is the local signal and $s_{j(k-1)}$ is the relay signal, for i and $j \in \{A, B\}$.

In our cooperative scheme both the local and the relay data packets are MSK modulated and we select the superposition ratio of $\gamma = \sqrt{0.2}$. Then, the transmitted superimposed signal becomes a 2-MAMSK signal with two different amplitudes. More specific, the amplitude of the local signal is twice that of the relay signal. That means that a node uses 80% of its power for its own signal and the remaining 20% for the signal which is relaying. Hence, the signal transmitted in each time slot is obtained by superimposing two MSK signals with a 6 dB difference in power. The constellation diagram for one possible combination of the local and the relay signals is illustrated in Figure 5-3a, whereas the signal trajectory for all possible combinations of s_{ik} and $s_{j(k-1)}$, $i,j \in \{A, B\}$ is shown in Figure 5-3b.

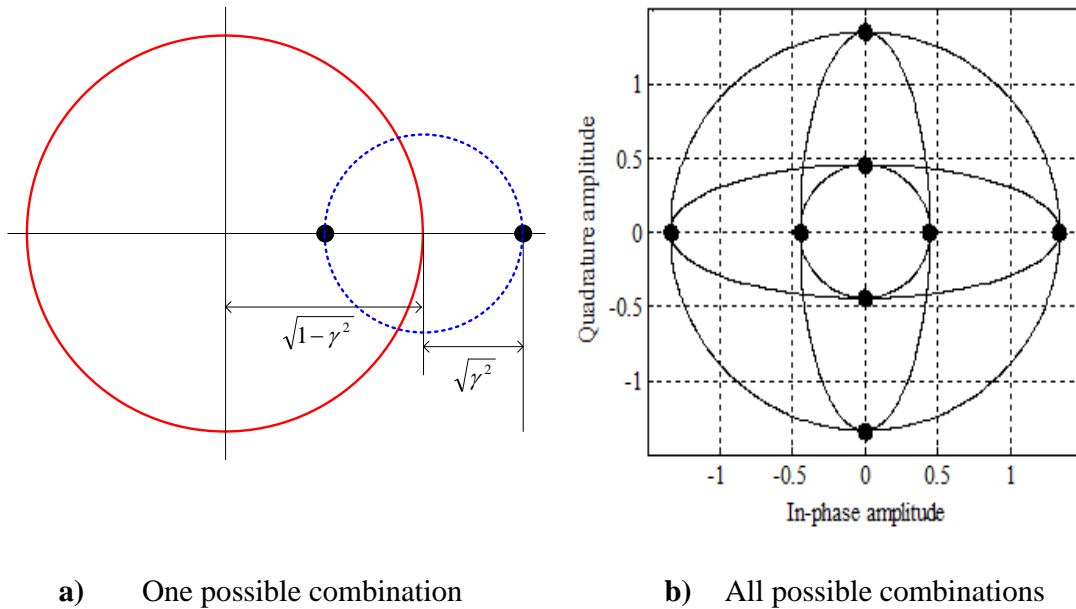**a)**   One possible combination   **b)**   All possible combinations

Figure 5-3 Signal trajectory for the cooperative superposition modulation

The circle of larger radius shown in Figure 5-3a represents the local signal and the smaller circle represents the relayed signal. The bold points shown

in Figure 5-3a and 5-3b represent the symbol transition times. From Figure 5-3, we observe that if the local and the relayed signal are in phase with each other at the symbol transition times, the transmitted 2-MAMSK signal would have an amplitude value of $\left(\sqrt{1-\gamma^2} + \sqrt{\gamma^2}\right)$ and if there is a phase difference of π between the two signals, the 2-MAMSK signal would have an amplitude level of $\left(\sqrt{1-\gamma^2} - \sqrt{\gamma^2}\right)$. In relating this to the 2-MAMSK modulator described in section 2.5, the local signal can be treated as the MSK component with the larger amplitude and the relayed signal can be treated as the MSK component with the smaller amplitude. For more details on 2-MAMSK signals, refer to chapter 3 and in particular section 3.5.

5.4 Signal Reception and Detection

In this section, we describe the detection of the data packets A_k and B_k at each node. As illustrated in Figure 5-1, the protocol of the superposition scheme is divided into two phases. During phase I, node A is the transmitter and B and D are the receivers. In phase II, B is the transmitter and the other two are receivers. Based on this protocol, the received signal in phase I, at the destination and node B respectively can be expressed as

$$r_{Dk} = h_{AD}\left(\sqrt{1-\gamma^2}\,s_{Ak} + \sqrt{\gamma^2}\,s_{B(k-1)}\right) + n_{Dk} \tag{5.2}$$

$$r_{Bk} = h_{AB}\left(\sqrt{1-\gamma^2}\,s_{Ak} + \sqrt{\gamma^2}\,s_{B(k-1)}\right) + n_{Bk} \tag{5.3}$$

Assuming that the decoding of s_{Ak} at node B was successful, the received signal in phase II, at the destination and node A respectively can be written

$$r_{Dk+1} = h_{BD}\left(\sqrt{1-\gamma^2}\,s_{B(k+1)} + \sqrt{\gamma^2}\,s_{Ak}\right) + n_{Dk+1} \tag{5.4}$$

$$r_{Ak+1} = h_{BD}\left(\sqrt{1-\gamma^2}\,s_{B(k+1)} + \sqrt{\gamma^2}\,s_{Ak}\right) + n_{Ak+1} \tag{5.5}$$

where s denotes transmitted signals, h stands for the channel gain, and n is the AWGN. The subscripts "A", "B", "D" indicate the nodes where signals are transmitted or received. The additional subscript $(\cdot)_{(\cdot k)}$ stands for "time slot k". Note that the resulting 2-MAMSK signals of (5.2)-(5.5) are combinations of the local (larger MSK) and the relay (smaller MSK) signals multiplied by their respective channel gains and degraded by noise at the receiver.

As mentioned earlier, each node decodes its partner's message from the signal which was received, in the previous time slot. Now, assume that at time slot $k + 1$, node B wants to decode A's message A_k received in the kth time slot. The received 2-MAMSK signal of (5.3) is used by node B to retrieve A_k. From Equation (5.3), we observe that A's message during k^{th} time slot is carried by the MSK component with the larger amplitude. In chapter 3, we established that the 2-MAMSK signal phase variation within a symbol interval depend primarily on the data sequence carried by the phase of the MSK component with the larger amplitude. In other words, the overall phase of a 2-MAMSK signal follows the phase of the larger MSK component. Thus, node B can exploit this property to differentially decode the information packet A_k from the received 2-MAMSK signal r_{Bk}. The receiver structure to decode A_k at B is shown in Figure 5-4.
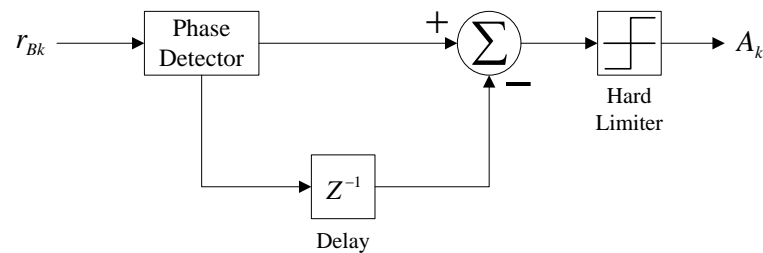

Figure 5-4 Receiver structure for decoding A_k at node B

The receiver shown in Figure 5-4 is differential and discussed in detail in section 2.8 and reference [87], thus we omit further discussion here. However, its operation is based on differentiating between the current phase value of the received 2-MAMSK signal and the one delayed by a symbol

interval. A decision is made based on the calculated difference value. The complexity of the above receiver is low as it does not require carrier phase recovery and there is no need to subtract $\sqrt{\gamma^2}\, s_{B(k-1)}$ from r_{Bk}, but instead it exploits the overall phase of the received 2-MAMSK signal. Thus, node B decodes A_k directly from the superimposed received signal without knowledge of its previously transmitted information.

In contrast, in the cooperative superposition schemes presented in the literature [68, 96-101, 105], assuming that during the kth interval, node B receives the superposition data $A_k + B_{k-1}$ from A. At time slot $k+1$, node B retrieves the information packet A_k by subtracting its own information B_{k-1} transmitted two times slots previously from the received superimposed data $A_k + B_{k-1}$. As a result, the detection of the A's message at node B requires knowledge of its own data packets from the previous slots in addition to the received signals. The detection of the B's message at node A is analogous. This requires additional memory to store previously transmitted information as well as an extra operation of subtraction. Therefore, in this respect the 2-MAMSK scheme can be considered as the best choice for the cooperative diversity based on superposition modulation, as the detection process of the partner's message requires significantly less computation and memory compared to those proposed in the literature.

In the same manner as for node B, in time slot $k+2$, node A can decode the information digits from the received 2-MAMSK signal r_{Ak+1} by employing the receiver shown in Figure 5-4. Hence, each node treats its partner's signal received in the previous time slot as the MSK component with larger amplitude and in the current time slot retransmits it as the MSK component with smaller amplitude. Finally, at destination node D, from both phases the receiver has two versions of s_{Ak} from Equation (5.2) and (5.4) and thus the diversity order is 2, assuming in phase I, node B decoded A's message successfully. The 2-MAMSK differential decoder [43] discussed in section 2.8 is used at the destination node to decode the information sequences $\{A_k, B_k\}$ from the received 2-MAMSK signals. The proposed

schemes in the literature, at node D employ iterative MAP detectors to decode A_k and B_k. Again the 2-MAMSK differential detector is of much lower complexity than MAP decoders. As a result, the overall decoding complexity of our scheme is significantly less than those presented in the literature [68, 96-101, 105].

Superposition based cooperative diversity system operation reduces to that of a non-cooperative scheme if data packets originating at node A are not received correctly at node B. This is also true if node A fails to successfully decode B's packets. In this case, a transmitting node modulates only its own information bits and transmits the resulting signal with full power. In other words, a node transmits an MSK signal rather than the 2-MAMSK signal described by Equation (5.1). A transmitting node can use flag bits to indicate whether its partner's data packet is decoded successfully or not. This requires the use of a cyclic redundancy check (CRC) to detect decoding errors. The diversity order at the destination node is reduced to one if any of the transmitting nodes are unable to send an acknowledgment of success. However, the detection process is the same during success or failure since the phase trellis of 2-MAMSK is identical to that of MSK.

5.5 Simulation Results

In this section, we present the bit error probability of our scheme to demonstrate its gain over the non-cooperative system. The probabilities of bit error with no cooperation and with cooperative transmit diversity at the destination nodes are shown in Figure 5-5. For the cooperative case two different values of superposition ratios are used (i.e. $\gamma^2 = 0.2$ and $\gamma^2 = 0.4$). In all simulations, the channels h_{AB}, h_{AD}, h_{BA} and h_{BD} are Rayleigh random variables with unit variance. In our model, we have assumed that both transmitting nodes A and B can decode each other's information without error. Therefore, cooperative transmission is always used and hence a diversity order of 2 is always achieved.

From Figure 5-5, we observe that a power allocation of $\gamma^2 = 0.2$ provides lower decoding error than the value of $\gamma^2 = 0.4$. In fact, the superposition ratio of $\gamma^2 = 0.2$ gives the best performance for our system. This result is consistent with the finding of [106] where it is shown that the minimum distance between signal points $d^2_{\min}$ is maximised when the power of the larger MSK component is four times that of the smaller MSK component. Using our analytical approach as in section 3.8, it is easy to show that $d^2_{\min}$ is maximised for $\gamma^2 = 0.2$. Note also that choosing $\gamma^2 = 0.5$ causes the scheme to breakdown as the MSK signals then have equal amplitude and the resulting 2-MAMSK signal reaches zero signal energy when the two MSK signals are out of phase by π with each other. Similarly, selecting $\gamma^2 = 0$ we would only be transmitting an MSK signal and hence, we must select $0 < \gamma^2 < 0.5$. For comparison, for the schemes presented in the literature [68, 100] the optimum value of γ^2 is 0.15.
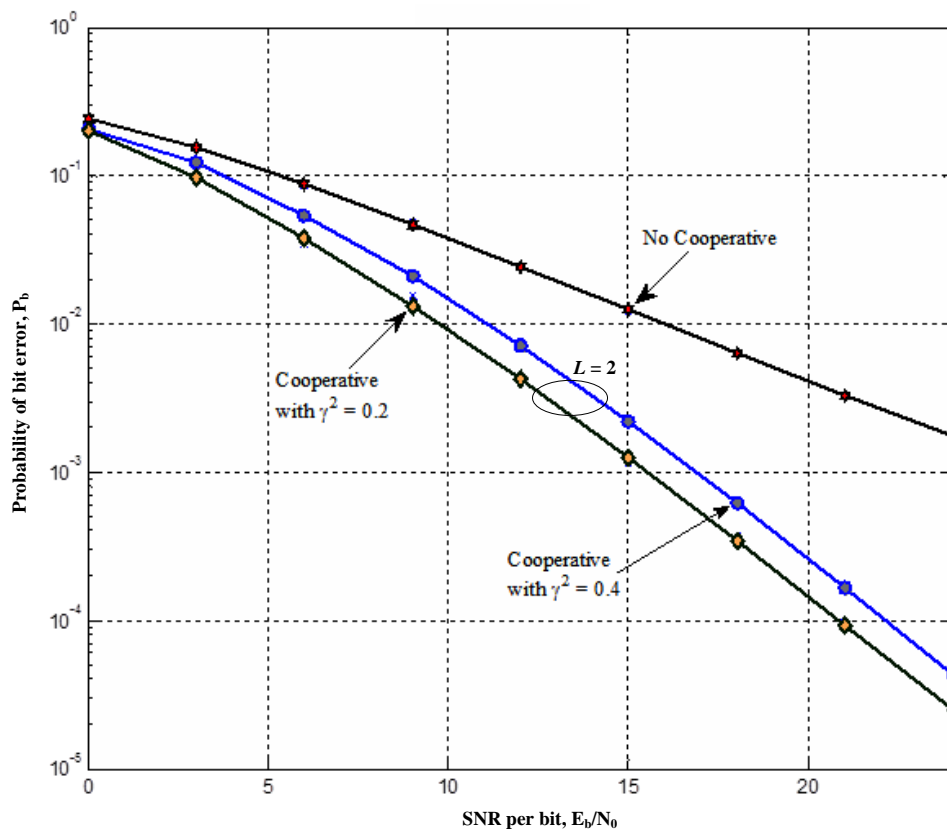

Figure 5-5 Probability of error for the cooperative system, *L*= total diversity

124

5.6   Summary

In this chapter, we have developed a scheme to use 2-MAMSK signals in a cooperative diversity system based on superposition modulation with DF strategy in a half-duplex environment. The spectral efficiency of the proposed system is twice higher than that of a classical DF scheme, as it superimposes both the local and the relayed signals onto a common signal. Simulation results show that our system can significantly outperform a non-cooperative system. The proposed cooperative system exploits the overall phase of a 2-MAMSK signal which allows differential detection and as a result it provides the lowest decoding complexity and memory requirements among the existing superposition based cooperation schemes. The optimum power allocation to be assigned to the partner's signal is 20 percent of the total power.

Chapter 6

Conclusions

In this thesis, a form of modulation referred to as multi-amplitude minimum shift keying (MAMSK) is analysed in term of its phase variation, spectral and error probability performance. We have explicitly shown that the phase values of a MAMSK signal at the symbol transition times are identical to that of minimum shift keying (MSK). Unlike MSK, the phase evolution with time is either linear or nonlinear, and thus, paths in the phase trellis are straight or curved lines with a slope of $\pm\pi/2T$. The overall phase change in a MAMSK signal is determined by the phase of the largest MSK component and the nonlinear behaviour is caused by the remaining MSK components. This characteristic is very useful as it allows low-complexity differential detection of an MAMSK signal. The spectral shape of MAMSK is identical to that of MSK, but for a fixed data rate, the MAMSK power spectrum is M times narrower because it encodes $2M$ bits per symbol. The theoretical bit error rate (BER) performance analysis of the optimal maximum likelihood receiver for MAMSK in AWGN channel is presented. The results of our analysis show that the theoretical BER of MAMSK is essentially identical to that of square quadrature amplitude modulation (QAM) for the same average transmit power.

The design and implementation of a space-time block coded (STBC) MIMO system using MAMSK signal is described. The STBC MAMSK system achieves high throughput as it uses both the phase and amplitude to encode the information bits. The proposed system combines the benefits of both orthogonal space-time block coding and differential detection. As a result, the proposed system is attractive for practical applications due to its simple linear decoding, low complexity receiver and robustness to carrier phase variation. The system is simulated in a quasi-static Rayleigh fading channel for various transmit and receive antenna configurations. Simulation results show that the system achieves a diversity order of $N_t \times N_r$ where N_t and N_r are the number of transmit and receive antennas, respectively. The proposed MAMSK differential receiver achieves performance within 1 dB of coherent detection and can be constructed from the existing orthogonal STBC combiners and MSK modems.

A MAMSK signal is adapted into a multiuser cooperative diversity based on superposition modulation with a DF strategy. In the proposed cooperative scheme, two nodes collaborate with each other to transmit their information to a common destination. We have shown that the overall phase of MAMSK can be well-exploited at each transmitting node, where a node can differentially extract the partner's data packets directly from the received MAMSK signal without the knowledge of its previously stored packets. Moreover, the destination node retrieves the data from both nodes using the low-complexity MAMSK differential detector. As a result, the cooperative MAMSK system provides the lowest decoding complexity and memory requirements among the existing cooperation schemes based on superposition. A significant improvement in the decoding error probability of the proposed scheme compared to that of a non-cooperative system is shown. The spectral efficiency is doubled compared to that of a classical DF scheme, since each node transmits its own data and the partner's data simultaneously. A node allocates a fraction of its power to the relayed signal and the remaining power for its own signal; the optimum power allocation for our scheme is one-fifth of the total transmitted power.

6.1   Future work

In this section, we suggest possible future directions for research based on the work presented in this thesis. Such research directions include, but are not limited to:

➢ The analysis of MAMSK characteristics accomplished in chapter 3 can be extended to multi-amplitude continuous modulation (MACPM).

➢ The performance of the differential MAMSK detector is evaluated only by simulation results; hence a closed-form expression of the error probability is of interest. The BER analysis of differential MSK detection [86, 87] can be adapted into differential MAMSK detection.

➢ Designing non-orthogonal STBC-based or perhaps STTC-based MIMO system using MAMSK or MACPM signals via the method described here.

➢ A quasi-static Rayleigh flat fading channel is assumed throughout this thesis. The work should be extended to examine the effects of different fading environments.

➢ In this thesis, MAMSK signal was examined based on the simplest case of cooperative communication. However, we have demonstrated its potential in superposition based cooperative diversity. For this reason, the MAMSK cooperative scheme should be extended to a bigger relaying system with more nodes.

➢ The performance of the MAMSK cooperative system was based on simulation results; hence an analytical result is of interest to fully understand the superiority of the system.

References

[1]   M. Simon, "An MSK Approach to Offset QASK," *Communications, IEEE Transactions on,* vol. 24, pp. 921-923, 1976.

[2]   W. Weber, P. Stanton, and J. Sumida, "A Bandwidth Compressive Modulation System Using Multi-Amplitude Minimum Shift Keying (MAMSK)," *Communications, IEEE Transactions on,* vol. 26, pp. 543-551, 1978.

[3]   G. J. Foschini and M. J. Gans, "On Limits of Wireless Communications in a Fading Environment when Using Multiple Antennas," *Wireless Personal Communications,* vol. 6, pp. 311-335, 1998.

[4]   E. Telatar, "Capacity of Multi-antenna Gaussian Channels," *European Transactions on Telecommunications,* vol. 10, pp. 585-595, 1999.

[5]   V. Tarokh, H. Jafarkhani, and A. R. Calderbank, "Space-time block codes from orthogonal designs," *Information Theory, IEEE Transactions on,* vol. 45, pp. 1456-1467, 1999.

[6]   S. M. Alamouti, "A simple transmit diversity technique for wireless communications," *Selected Areas in Communications, IEEE Journal on,* vol. 16, pp. 1451-1458, 1998.

[7]   J. G. Proakis, *Digital Communications*, 4th ed. New York: McGraw-Hill, 2001.

[8]   F. Xiong, *Digital modulation techniques*: Artech House, 2006.

[9]   T. T. Ha, *Theory and Design of Digital Communication Systems*: Cambridge University Press, 2010.

[10]   K. Wesolowski, *Introduction to Digital Communication Systems*: John Wiley & Sons, 2009.

[11]   A. Goldsmith, *Wireless communications*: Cambridge University Press, 2005.

[12]   T. S. Rappaport, *Wireless communications: principles and practice*, 2nd ed.: Prentice Hall PTR, 2002.

[13]   J. G. Proakis and M. Salehi, *Communication systems engineering*: Prentice Hall, 2002.

[14]   M. K. Simon and M. S. Alouini, *Digital communication over fading channels: a unified approach to performance analysis*: John Wiley & Sons, 2000.

[15]   M. C. Jeruchim, P. Balaban, and K. S. Shanmugan, *Simulation of Communication Systems: Modeling, Methodology and Techniques*, 2nd ed.: Springer, 2000.

[16]   J. Boccuzzi, *Signal processing for wireless communications*: McGraw-Hill, 2008.

[17]   J. Ziv, "Probability of decoding error for random phase and Rayleigh fading channels," *Information Theory, IEEE Transactions on,* vol. 11, pp. 53-61, 1965.

[18]   W. C. Jakes, *Microwave mobile communications*: Wiley, 1974.

[19]   M. J. Gans, "A power-spectral theory of propagation in the mobile-radio environment," *Vehicular Technology, IEEE Transactions on,* vol. 21, pp. 27-38, 1972.

[20] T. Aulin, "A modified model for the fading signal at a mobile radio channel," *Vehicular Technology, IEEE Transactions on,* vol. 28, pp. 182-203, 1979.

[21] X. Chengshan, Y. R. Zheng, and N. C. Beaulieu, "Second-order statistical properties of the WSS Jakes' fading channel simulator," *Communications, IEEE Transactions on,* vol. 50, pp. 888-891, 2002.

[22] G. M. Vitetta, U. Mengali, and D. P. Taylor, "Blind detection of CPM signals transmitted over frequency-flat fading channels," *Vehicular Technology, IEEE Transactions on,* vol. 47, pp. 961-968, 1998.

[23] H. Jafarkhani, *Space-Time Coding: Theory and Practice*: Cambridge University Press, 2005.

[24] E. Sha, S. K. Han, C. Z. Xu, M. H. Kim, L. T. Yang, and B. Xiao, *Embedded and Ubiquitous Computing: International Conference, EUC 2006, Seoul, Korea, August 1-4, 2006, Proceedings*: Springer, 2006.

[25] E. Biglieri, R. Calderbank, A. Constantinides, A. Goldsmith, A. Paulraj, and H. V. Poor, *MIMO wireless communications*: Cambridge University Press, 2007.

[26] V. Kühn, *Wireless communications over MIMO channels: applications to CDMA and multiple antenna systems*: John Wiley & Sons, 2006.

[27] J. Winters, "On the Capacity of Radio Communication Systems with Diversity in a Rayleigh Fading Environment," *Selected Areas in Communications, IEEE Journal on,* vol. 5, pp. 871-878, 1987.

[28] J. N. Laneman and G. W. Wornell, "Energy-efficient antenna sharing and relaying for wireless networks," in *Wireless Communications and Networking Confernce, 2000. WCNC. 2000 IEEE*, 2000, pp. 7-12 vol.1.

[29] Z. Hongtao and K. Geng-Sheng, "Cooperative Diversity for Virtual MIMO System in Geometry-Based Stochastic Channel Model," in *Communications, 2007. ICC '07. IEEE International Conference on*, 2007, pp. 6091-6096.

[30] M. Di Renzo, F. Graziosi, and F. Santucci, "On the Performance of CSI-Assisted Cooperative Communications over Generalized Fading Channels," in *Communications, 2008. ICC '08. IEEE International Conference on*, 2008, pp. 1001-1007.

[31] E. V. D. Meulen, "Three-terminal communication channels," *Advances in Applied Probability,* vol. 3, pp. 120-154, 1971.

[32] T. Cover and A. E. Gamal, "Capacity theorems for the relay channel," *Information Theory, IEEE Transactions on,* vol. 25, pp. 572-584, 1979.

[33] A. Nosratinia, T. E. Hunter, and A. Hedayat, "Cooperative communication in wireless networks," *Communications Magazine, IEEE,* vol. 42, pp. 74-80, 2004.

[34] Y. W. P. Hong, W. J. Huang, and C. C. J. Kuo, *Cooperative Communications and Networking: Technologies and System Design*: Springer, 2010.

[35] A. Sendonaris, E. Erkip, and B. Aazhang, "User cooperation diversity. Part I. System description," *Communications, IEEE Transactions on,* vol. 51, pp. 1927-1938, 2003.

[36] Y. Meng and L. Jing, "Is amplify-and-forward practically better than decode-and-forward or vice versa?," in *Acoustics, Speech, and Signal Processing, 2005. Proceedings. (ICASSP '05). IEEE International Conference on*, 2005, pp. iii/365-iii/368 Vol. 3.

[37] N. Truman Chiu-Yam and Y. Wei, "Joint optimization of relay strategies and resource allocations in cooperative cellular networks,"

Selected Areas in Communications, IEEE Journal on, vol. 25, pp. 328-339, 2007.

[38]   V. Sreng, H. Yanikomeroglu, and D. D. Falconer, "Relayer selection strategies in cellular networks with peer-to-peer relaying," in *Vehicular Technology Conference, 2003. VTC 2003-Fall. 2003 IEEE 58th*, 2003, pp. 1949-1953 Vol.3.

[39]   S. Glisic and B. Lorenzo, *Advanced Wireless Networks: Cognitive, Cooperative & Opportunistic 4G Technology*: Wiley, 2009.

[40]   X. Yong, L. Shaoyang, W. Jibo, A. Burr, and D. Grace, "Asymptotic performance analysis of packet cooperative relaying system over quasi-static fading channel," in *Personal Indoor and Mobile Radio Communications (PIMRC), 2010 IEEE 21st International Symposium on*, 2010, pp. 2204-2209.

[41]   Y. Nasser and J. F. Helard, "Coded BER Based Algorithm for Decode and Forward in Cooperative OFDM Systems," in *Vehicular Technology Conference Fall (VTC 2009-Fall), 2009 IEEE 70th*, 2009, pp. 1-5.

[42]   V. Goncalves, A. Gusmao, and N. Esteves, "Coherent detection of multiamplitude MSK under imperfect phase synchronisation," *Electronics Letters,* vol. 27, pp. 623-625, 1991.

[43]   T. Javornik and G. Kandus, "A 2MSK receiver based on the regeneration of the larger MSK signal component," *Elektrotehniški vestnik,* vol. 69, pp. 34-39, 2002.

[44]   A. A. Eltholth, A. R. Mikhail, A. Elsherbini, M. I. Dessouky, and A. I. Abdelfattah, "Performance of Multi-Amplitude Minimum Shift Keying (N-MSK) with Orthogonal Frequency Division Multiplexing (OFDM)," in *EUROCON, 2007. The International Conference on Computer as a Tool*, 2007, pp. 1057-1060.

[45] X. Liang, R. Punnoose, and L. Huaping, "Space-Time Block Coded GMSK With Low-Complexity Linear Receiver," in *Communications, 2006. ICC '06. IEEE International Conference on*, 2006, pp. 4876-4881.

[46] S. Ogose, K. Murota, and K. Hirade, "A transmitter diversity for MSK with two-bit differential detection," *Vehicular Technology, IEEE Transactions on,* vol. 33, pp. 37-43, 1984.

[47] Z. Xiaoxia and M. P. Fitz, "Space-time code design with continuous phase modulation," *Selected Areas in Communications, IEEE Journal on,* vol. 21, pp. 783-792, 2003.

[48] R. L. Maw and D. P. Taylor, "Space-time coded systems with continuous phase frequency shift keying," in *Global Telecommunications Conference, 2005. GLOBECOM '05. IEEE*, 2005, p. 6 pp.

[49] J. K. Cavers, "Space-time coding using MSK," *Wireless Communications, IEEE Transactions on,* vol. 4, pp. 185-191, 2005.

[50] Y. Yi and M. K. Howlader, "Serial concatenated MSK modulated space-time block coding," in *Communications, 2004 IEEE International Conference on*, 2004, pp. 3015-3019 Vol.5.

[51] Ü. Aygölü and M. E. Çelebi, "Space-time MSK Codes for Quasi-Static Fading Channels," *AEU - International Journal of Electronics and Communications,* vol. 58, pp. 268-273, 2004.

[52] M. K. Simon and H. Jafarkhani, "Performance evaluation of super-orthogonal space-time trellis codes using a moment generating function-based approach," *Signal Processing, IEEE Transactions on,* vol. 51, pp. 2739-2751, 2003.

[53] H. Jafarkhani and N. Seshadri, "Super-orthogonal space-time trellis codes," *Information Theory, IEEE Transactions on,* vol. 49, pp. 937-950, 2003.

[54] M. L. B. Riediger and P. K. M. Ho, "A Space-Time MSK Code and its Detection," in *Information, Communications and Signal Processing, 2005 Fifth International Conference on*, 2005, pp. 208-212.

[55] C. Chih-Chung and L. Chung-Chin, "Space-time code design for CPFSK modulation over frequency-nonselective fading channels," *Communications, IEEE Transactions on,* vol. 53, pp. 1477-1489, 2005.

[56] R. L. Maw and D. P. Taylor, "Space-Time Coded Systems using Continuous Phase Modulation," *Communications, IEEE Transactions on,* vol. 55, pp. 2047-2051, 2007.

[57] A. G. Zajic and G. L. Stuber, "A Space-Time Code Design for CPM: Diversity Order and Coding Gain," *Information Theory, IEEE Transactions on,* vol. 55, pp. 3781-3798, 2009.

[58] F. Pancaldi, A. Barbieri, and G. Vitetta, "Space-time block codes for noncoherent CPFSK," *Wireless Communications, IEEE Transactions on,* vol. 9, pp. 1729-1737, 2010.

[59] R. H. H. Yang and D. P. Taylor, "Trellis-coded continuous-phase frequency-shift keying with ring convolutional codes," *Information Theory, IEEE Transactions on,* vol. 40, pp. 1057-1067, 1994.

[60] Z. Wanlun and G. B. Giannakis, "Reduced complexity receivers for layered space-time CPM," *Wireless Communications, IEEE Transactions on,* vol. 4, pp. 574-582, 2005.

[61]   X. Liang, R. Punnoose, and L. Huaping, "Simplified receiver design for STBC binary continuous phase modulation," *Wireless Communications, IEEE Transactions on,* vol. 7, pp. 452-457, 2008.

[62]   A. M. Silvester, L. Lampe, and R. Schober, "Space-Time Continuous Phase Modulation for Non-Coherent Detection," *Wireless Communications, IEEE Transactions on,* vol. 7, pp. 1264-1275, 2008.

[63]   A. Griffin and D. P. Taylor, "Coding CPFSK for differential demodulation," *Communications, IEEE Transactions on,* vol. 48, pp. 721-724, 2000.

[64]   T. Javornik and G. Kandus, "N-MSK adaptive modulation techniques in a slow Rayleigh fading channel," in *Personal, Indoor and Mobile Radio Communications, 2000. PIMRC 2000. The 11th IEEE International Symposium on*, 2000, pp. 138-142 vol.1.

[65]   G. Kandus, D. Lazic, and V. Senk, "Transmitter and receiver structures for multi-amplitude CPM," in *Electrotechnical Conference, 1989. Proceedings. 'Integrating Research, Industry and Education in Energy and Communication Engineering', MELECON '89., Mediterranean*, 1989, pp. 433-435, 437.

[66]   A. Sendonaris, E. Erkip, and B. Aazhang, "User cooperation diversity. Part II. Implementation aspects and performance analysis," *Communications, IEEE Transactions on,* vol. 51, pp. 1939-1948, 2003.

[67]   J. N. Laneman, D. N. C. Tse, and G. W. Wornell, "Cooperative diversity in wireless networks: Efficient protocols and outage behavior," *Information Theory, IEEE Transactions on,* vol. 50, pp. 3062-3080, 2004.

[68]   E. G. Larsson and B. R. Vojcic, "Cooperative transmit diversity based on superposition modulation," *Communications Letters, IEEE,* vol. 9, pp. 778-780, 2005.

[69]   T. S. Rappaport, *Wireless communications: principles and practice*: Prentice Hall PTR, 1996.

[70]   M. L. Doelz, Heald, Earl T., "Minimum-shift data communication system," United States Patent, 1961.

[71]   S. Pasupathy, "Minimum shift keying: A spectrally efficient modulation," *Communications Magazine, IEEE,* vol. 17, pp. 14-22, 1979.

[72]   J. B. Anderson, T. Aulin, and C. E. Sundberg, *Digital phase modulation*: Plenum Press, 1986.

[73]   T. Javornik, G. Kandus, and F. Vejrazka, "Modulation Schemes for Wireless Access," *Radioengineering,* vol. 9, pp. 8-14, 2000.

[74]   S. A. Gronemeyer and A. L. McBride, "MSK and Offset QPSK Modulation," *Communications, IEEE Transactions on,* vol. 24, pp. 809-820, 1976.

[75]   R. de Buda, "Coherent Demodulation of Frequency-Shift Keying with Low Deviation Ratio," *Communications, IEEE Transactions on,* vol. 20, pp. 429-435, 1972.

[76]   M. K. Simon, *Bandwidth-efficient digital modulation with application to deep-space communications*: Wiley-Interscience, 2003.

[77]   R. De Buda, "The Fast FSK Modulation System," *Communications, International Conference on,* pp. 41-25 to 45-27, June 14-16 1971.

[78]   G. L. Stüber, *Principles of Mobile Communication*: Springer, 2011.

[79] X. Fuqin, "Modem techniques in satellite communications," *Communications Magazine, IEEE,* vol. 32, pp. 84-98, 1994.

[80] R. De Buda, "About Optimal Properties of Fast Frequency-Shift Keying," *Communications, IEEE Transactions on,* vol. 22, pp. 1726-1727, 1974.

[81] H. Mathwich, J. Balcewicz, and M. Hecht, "The Effect of Tandem Band and Amplitude Limiting on the Eb/No Performance of Minimum (Frequency) Shift Keying (MSK)," *Communications, IEEE Transactions on,* vol. 22, pp. 1525-1540, 1974.

[82] D. Morais and K. Feher, "Bandwidth Efficiency and Probability of Error Performance of MSK and Offset QPSK Systems," *Communications, IEEE Transactions on,* vol. 27, pp. 1794-1801, 1979.

[83] I. Altunbas and U. Aygolu, "Multiple multiamplitude minimum shift keying trellis codes for AWGN and fading mobile satellite channels," in *Universal Personal Communications, 1994. Record., 1994 Third Annual International Conference on*, 1994, pp. 199-203.

[84] Z. Lijia, X. Xiangjun, L. Bo, Z. Qi, Y. Jianjun, C. Nan, and Y. Chongxiu, "A Novel MAMSK-OFDM Technology for Next-Generation Optical Access Networks," *Photonics Technology Letters, IEEE,* vol. 23, pp. 60-62, 2011.

[85] D. Morais and K. Feher, "NLA-QAM: A Method for Generating High-Power QAM Signals Through Nonlinear Amplification," *Communications, IEEE Transactions on,* vol. 30, pp. 517-522, 1982.

[86] M. K. Simon and C. C. Wang, "Differential detection of Gaussian MSK in a mobile radio environment," *Vehicular Technology, IEEE Transactions on,* vol. 33, pp. 307-320, 1984.

[87]   N. A. B. Svensson and C. E. W. Sundberg, "Performance evaluation of differential and discriminator detection of continuous phase modulation," *Vehicular Technology, IEEE Transactions on,* vol. 35, pp. 106-117, 1986.

[88]   J. M. Wozencraft and I. M. Jacobs, *Principles of communication engineering*: Wiley, 1965.

[89]   A. Paulraj, R. Nabar, and D. Gore, *Introduction to Space-Time Wireless Communications*: Cambridge University Press, 2003.

[90]   L. Jiao, L. Wang, X. Gao, J. Liu, and F. Wu, *Advances in Natural Computation: Second International Conference, ICNC 2006, Xi'an, China, September 24-28, 2006, Proceedings*: Springer, 2006.

[91]   E. G. Larsson, P. Stoica, E. Lindskog, and J. Li, "Space-time block coding for frequency-selective channels," in *Acoustics, Speech, and Signal Processing (ICASSP), 2002 IEEE International Conference on*, 2002, pp. III-2405-III-2408.

[92]   J. Anderson and D. Taylor, "A bandwidth-efficient class of signal-space codes," *Information Theory, IEEE Transactions on,* vol. 24, pp. 703-712, 1978.

[93]   K. Feher, *Advanced digital communications: systems and signal processing techniques*: Prentice-Hall, 1987.

[94]   C. Kyongkuk and Y. Dongweon, "On the general BER expression of one- and two-dimensional amplitude modulations," *Communications, IEEE Transactions on,* vol. 50, pp. 1074-1080, 2002.

[95]   G. Ganesan and P. Stoica, "Space-time block codes: a maximum SNR approach," *Information Theory, IEEE Transactions on,* vol. 47, pp. 1650-1656, 2001.

[96] C. Mingwei, GuangguoBi, and J. Xiufeng, "Bandwidth efficient cooperative diversity scheme based on relaying superposition symbols," in *Communication Systems, 2008. ICCS 2008. 11th IEEE Singapore International Conference on*, 2008, pp. 1249-1253.

[97] H. Shuang, F. Zesong, H. Li, and K. Jingming, "Cooperative Transmission Utilizing High Order Superposition Modulation with Iterative Detection," in *Wireless Communications, Networking and Mobile Computing, 2009. WiCom '09. 5th International Conference on*, 2009, pp. 1-5.

[98] K. Ishii, "Cooperative Transmit Diversity Utilizing Superposition Modulation," in *Radio and Wireless Symposium, 2007 IEEE*, 2007, pp. 337-340.

[99] X. Lei, T. E. Fuja, J. Kliewer, and D. J. Costello, "Signal Superposition Coded Cooperative Diversity: Analysis and Optimization," in *Information Theory Workshop, 2007. ITW '07. IEEE*, 2007, pp. 614-619.

[100] X. Lei, T. E. Fuja, J. Kliewer, and D. J. Costello, "Error performance analysis of signal superposition coded cooperative diversity," *Communications, IEEE Transactions on,* vol. 57, pp. 3123-3131, 2009.

[101] K. Ishii, "Coded Cooperation Protocol Utilizing Superposition Modulation for Half-Duplex Scenario," in *Personal, Indoor and Mobile Radio Communications, 2007. PIMRC 2007. IEEE 18th International Symposium on*, 2007, pp. 1-5.

[102] D. Zhiguo, T. Ratnarajah, and C. Cowan, "On the Performance of Superposition Cooperative Diversity in Wireless Networks," in *Information Theory, 2006 IEEE International Symposium on*, 2006, pp. 2714-2718.

[103] C. Chun and R. S. K. Cheng, "Performance Analysis for Superposition Modulated Cooperative Relay HARQ Networks," *Vehicular Technology, IEEE Transactions on,* vol. 61, pp. 2978-2990, 2012.

[104] Y. Tao and Y. Jinhong, "Performance of iterative decoding for superposition modulation-based cooperative transmission," *Wireless Communications, IEEE Transactions on,* vol. 9, pp. 51-59, 2010.

[105] X. Lei, T. E. Fuja, J. Kliewer, and D. J. Costello, "A Network Coding Approach to Cooperative Diversity," *Information Theory, IEEE Transactions on,* vol. 53, pp. 3714-3722, 2007.

[106] J. P. Fonseka, E. M. Dowling, and C. C. Teng, "Quadrature multiplexed CPM," *Communications, IEEE Transactions on,* vol. 56, pp. 1487-1497, 2008.